An analysis of muon showers at large zenith angles

Holyoak, B.

AN ANALYSIS OF MUON SHOWERS AT LARGE ZENITH ANGLES

A Thesis submitted to the
University of Durham for the
Degree of Doctor of Philosophy

by

B. Holyoak, B.Sc.

September 1967

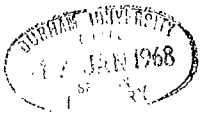

ABSTRACT

A theoretical model has been constructed in order to explain the known features of near vertical extensive air showers; the intention being to use this model to predict the features of showers at large zenith angles. The adopted model explains satisfactorily the longitudinal development of both the hard and soft components of the shower, but two discrepancies are found when comparison is made with the muon lateral distribution. The first is at small distances from the shower core where the model overestimates the muon density; a solution to this is found to be a reduction in the probability of transverse momentum transfers below 0.1 GeV/c. At large distances from the core and high threshold energies there is a considerable underestimate in the predicted muon densities. Many of the model parameters have been investigated in an effort to find a solution; apart from a drastic change in the model a fit between theory and experiment may be obtained by postulating an increase in the mean transverse momentum. The necessary values are $\langle p_t \rangle = 0.6 \pm 0.2$ GeV/c for pion interactions of mean energy ~200 GeV and $\langle p_t \rangle = 1.0 \pm 0.3$ GeV/c for interactions of mean energy ~4000 GeV.

The Durham Horizontal Extensive Air Shower Array has been used to measure the zenith angle distribution of muon showers at large zenith angles ($\theta > 45^{\circ}$), and the muon number spectrum for $57.5^{\circ} < \theta < 90^{\circ}$ has also been determined. The former is satisfied by the adopted model with $\langle p_t \rangle \approx 0.8$ GeV/c; there is however a discrepancy between the expected frequency of >2 muon events and the observed rate. In order to find a solution to this problem changes are made in the primary flux; the best fit is obtained when the composition is such that protons are predominant for primary energies up to a few times 10^{15} eV, above this the effective mass of the primary flux increases with energy until 10^{17} eV is reached.

PREFACE

The work reported in this thesis was carried out while the author was a research student under the supervision of Professor A.W. Wolfendale, in the Cosmic Ray Group of the Physics Department of Durham University.

The thesis describes the determination of the muon zenith angle distribution and the muon number spectrum at large zenith angles using the Durham Horizontal Extensive Air Shower Array. In addition thorough theoretical investigations which have been made both for near vertical and large zenith angle showers are reported.

The responsibility for the construction of the array, its day to day operation and the analysis of the data has been shared by the author and his colleagues. The author has been solely responsible for the majority of the theoretical analyses presented in this thesis.

A report on the merits of plastic and liquid scintillation counters has been made by Ashton et al. (1965), this being an investigation carried out prior to the construction of the array. The preliminary results from the apparatus were presented to the International Conference on Cosmic Rays, Calgary, in a paper by Alexander et al. (1967). Interim reports on

the theoretical aspects of the present work have been made with special reference to near-vertical showers by Holyoak et al. (1966) and by de Beer et al. (1966, 1967a, 1967b). A paper giving details of the theoretical analysis of large zenith angle showers is to be submitted for publication in Proc. Phys. Soc. by the author of this thesis.

(Note - the author is a co-author of the publications mentioned above).

CONTENTS

CHAPTER 1

Introduction

1.1 The Origin of Cosmic Rays and the Nature of the Primary Flux

Although some of the low energy cosmic rays which arrive at the earth ($\lesssim$10 GeV) come from the sun, at higher energies sources further afield are certainly responsible for the observed particles. Supernovae are a likely source of many of the particles and at the highest energies extra-galactic sources are also possible.

Useful evidence about the composition of the primaries comes from the observation of a large percentage of L-group nuclei, $\sim 5\ 10^5$ times the cosmic abundance, these probably being due to the fragmentation of heavier nuclei during their passage through space. Many of the higher energy cosmic ray particles must therefore have a source which is anomalously rich in heavy nuclei. Such a condition exists in supernovae, dense old stars, which, having used up all their light nuclei, obtain energy by forming heavier nuclei until at some point they explode. During the explosion the very heavy nuclei are formed by neutron capture. One of the supernovae, the Crab nebula, has been extensively studied and its optical and radio

emissions are consistent with synchrotron radiation from electrons. This indicates that magnetic fields are present in a form capable of accelerating electrons and presumably protons and heavier nuclei up to high energies.

There is however, some evidence which may be in opposition to the supernovae theory; Mathieson et al. (1967) postulate an energetic source of iron nuclei which then fragment during their journey through $4\ g.cm^{-2}$ of interstellar space and they are able to reproduce the observed charge distribution. Nickel and heavier elements are not required in the proposed source with an abundance appreciably greater than that predicted by the cosmic abundances. Consequently the source material need not have experienced any appreciable amount of element building by neutron capture beyond iron, which is in contrast to the supernova mechanism. The alternative explanation is that the acceleration mechanism strongly favours iron nuclei. At present it is not possible to distinguish between these, and other theories.

The galactic magnetic field is not strong enough to contain particles with energies $\gtrsim 10^{17}$ eV and it is thought that the higher energy cosmic rays observed have an extra-galactic origin, perhaps one of the unusual objects such as M87.

An energy spectrum for the primary flux has been given by Linsley (1964), this is derived from E.A.S. data taken in conjunction with a model for shower propagation.

For $E_p < 10^{15}$ eV,

$$j(E_p) = 4\ 10^{-21}(E_p/10^{15})^{-2.6}\ m^{-2}sterad^{-1}sec^{-1}eV^{-1} \quad (1.1)$$

For $E_p > 10^{15}$ eV,

$$j(E_p) = 4\ 10^{-21}(E_p/10^{15})^{-3.0}\ m^{-2}sterad^{-1}sec^{-1}eV^{-1} \quad (1.2)$$

It must be pointed out, however, as will be seen later, that these spectra may not be applicable, depending as they do on the propagation models.

It has recently been proposed by Greisen (1966) that there should be a cut-off at $\sim 10^{20}$ eV in the primary energy spectrum. This arises because of the apparent existence of a black body radiation in space, corresponding to a temperature of $\sim 3^{\circ}K$, mean photon energy $\sim 7\ 10^{-4}$ eV, with which protons can interact. At $\sim 10^{20}$ eV proton energy the photon has sufficient energy in the C-system to generate a pion, with a corresponding retardation of the proton. Such a cut-off is on the present limit of measurement and has not yet been observed.

It appears that the chemical composition of the primary flux for energies up to ~ 10 GeV is roughly as given in Table 1.1.

Table 1.1

The composition of the primary flux (after Ginzburg and Syrovatsky (1964) for $E_p \lesssim 10$ GeV).

	Z	$\bar{A}$	Intensity $m^{-2}ster^{-1}sec^{-1}$	Abundance by number	Abundance in universe	Abundance by mass
p	1	1	1300	93%	91%	71.8%
	2	4	88	6.3%	9%	19.4%
L	3→5	10	1.9	0.14%	3×10^{-7}%	
M	5→9	14	5.7	0.41%	0.09%	8.8%
H	≥10	31	1.9	0.14%	0.03%	
VH*	≥20	51	0.53	0.04%	0.002%	

* included in H

These figures are in agreement with those reported by Waddington (1960).

For higher primary energies the picture of the chemical composition is not certain. One prominent theory is that for energies up to a few times 10^{15} eV the primary flux is composed almost entirely of protons. At this energy protons begin to leak from the galaxy due to the galactic magnetic field not being able to contain them. The rigidity (P/Z) of particles which may be contained within the galaxy is presumably constant, thus as the primary energy increases so the value of Z must

increase; this means that the mean mass of the primary particles will become greater, until at $\sim 10^{17}$ eV the field becomes incapable of containing even VH-nuclei within the galaxy. Above 10^{17} eV the primary flux is thought to revert to protons, these having an extra-galactic origin.

Hillas (1967) suggests that the necessary increase in slope of the primary energy spectrum in the energy range $\sim 3\ 10^{15}$ to 10^{17} eV may be a direct consequence of the most energetic cosmic ray protons having originated in powerful radio-galaxies. Radio-astronomical evidence suggests that such sources had a much greater output in the past than at present. If this is so it is proposed that the importance of interactions between the universal flux of microwaves and cosmic ray protons above $3\ 10^{15}$ eV is greatly increased because of "red shifts" in the energies of the protons and the microwaves, and changes in density. This would result in the microwaves taking a bite out of the energy spectrum, which, at production has an integral slope of -1.5 throughout, thus giving a steeper observed slope of -2.2 between $\sim 3\ 10^{15}$ and 10^{17} eV.

An alternative method of explaining the discontinuities in the sea-level size spectrum is to postulate a straight line primary spedtrum up to a primary energy of

at least a few times 10^{17} eV, with proton composition throughout; modifications are made to the nature of high energy nuclear interactions to bring about the required sea-level characteristics.

These three models of the high energy primary flux have been used in the present theoretical analyses and the results are presented in Chapter 7 where an attempt is made to distinguish between them.

1.2 The Importance of Extensive Air Showers

The name 'extensive air shower' (E.A.S.) is used to denote a chain of events initiated by a cosmic ray particle of ultra-relativistic energy interacting with an air-nucleus. The products of the primary interactions travel in practically the same direction as the parent particle and give rise to a cascade of interactions until, in the lower atmosphere, the number of particles in a near vertical shower may be many millions.

All the secondary particles arrive at sea-level within a time interval of $\sim$100 nanoseconds over a plane almost perpendicular to the direction of the original particle; this direction being known as the shower axis. During their traversal of many kilometres of atmosphere various processes cause the particles to be distributed about the axis. The result is that the shower covers

an area of many thousands of square metres the maximum density being in the central region, referred to as the core of the shower.

The primary cosmic rays which give rise to the largest showers in the lower atmosphere have energies up to $\sim 10^{20}$ eV and are the most energetic particles known to exist in nature. A knowledge of their properties and their behaviour in interactions with matter are consequently of the greatest interest. Whatever has been learned so far about the physics of energies $\gtrsim 10^{14}$ eV has been inferred from a study of air showers. At the moment there seems to be little hope of being able to study such ultra-relativistic particles by direct means. Even if measurements could be made at the top of the atmosphere, where these particles exist, the probability of detection would be extremely low due to the rapidly falling primary energy spectrum. In fact the frequency of arrival of a cosmic ray with energy $>10^{18}$ eV on 1 m^2 is only $\sim$1 per 3000 years. The atmosphere by its action of multiplying the original particle by millions and distributing them over a wide area thus makes it possible to detect the effects of such primaries at a not unreasonable rate. Even primaries of 10^{16} eV would be too rare for direct detection whilst their air showers

are easily detected at sea-level at a rate of many per hour. It should be stressed that the energies involved in even the small air showers are still several orders of magnitude higher than the maximum energies attainable by machine acceleration of particles. Present day machines produce beams of protons up to energies of 30 GeV. The U.S.S.R. hopes to commission the Serpukhov 70 GeV proton synchrotron in 1969, the U.S.A. have plans for a 200 GeV machine near Chicago and a European machine capable of attaining 300 GeV is under consideration at the moment.

1.3 The Mu-meson and its role in E.A.S.

Whilst measuring the absorption properties of cosmic rays, Rossi (1932) showed the existence of two components, the 'soft' or easily absorbed and the 'hard' or penetrating component. The use of cloud chambers allowed the soft component to be identified with electrons. Ionisation measurements and the existence of positively and negatively charged penetrating particles ruled out protons as being solely responsible for the hard component. Anderson and Neddermeyer (1936), and Street and Stevenson (1937), working independently, determined the mass of the particles forming the bulk of the hard flux as being ~200 m_e. Later work showed that each of these

particles, subsequently to be known as mu-mesons, decayed into an electron and two neutral particles, the lifetime being $\sim 2.2\ 10^{-6}$ second. It was natural at that time to identify this new particle with the particle proposed by Yukawa in order to explain the inter-nucleon force. However, the Yukawa particle should interact strongly with matter: the existence of mu-mesic atoms in which the mu-meson spends much of its time in the nucleus showed that mu-mesons are only weakly interacting. It is now known that the pi-meson is the particle predicted by Yukawa, and it is the pi-meson which, on decay, is the major source of mu-mesons.

The most important features of the mu-meson with regards to E.A.S. are its relatively long lifetime and the fact that it interacts weakly with matter. As a consequence muons are the predominant particles at large distances from the cores of near vertical showers. At large zenith angles, muons constitute nearly the whole of the shower observed at sea-level since the electron-photon cascade initiated by the decay of neutral pions will have died out long before sea-level.

1.4 E.A.S. at Large Zenith Angles

The object of the present investigation is to throw

some light on the nature of the primary flux and the characteristics of high energy interactions. As will be seen, much can be revealed by a study of near vertical showers, one reason for this being the vast amount of experimental data already collected about such showers. However, it is felt that a full investigation of high energy muons should give yet more information since these particles will, in general, have originated close to one of the early interactions of the primary particle, and it seems that the most fruitful investigation would be to look at the muons in large zenith angle showers.

At large zenith angles the first interaction of the primary particle will take place in less dense air than would be the case in the near vertical; the secondary pions will have an enhanced probability of decaying as opposed to interacting, consequently there should be a larger percentage of high energy muons than in near vertical showers. Because of the large thickness of atmosphere to be traversed, the lower energy muons will lose energy by ionisation to such an extent that, as a result, they will exhibit a preference for μ-e decay and the resultant shower at sea-level will be deficient in low energy muons. It will be shown that the mean

muon energy ($\bar{E}_{\mu}$) for showers at a zenith angle (θ) of 60° is ~15 GeV, at 75° it is ~27 GeV and at 84°,~60 GeV.

These facts, together with an expected lack of contamination by the soft component, provide the reasons for investigating muon showers at large zenith angles.

1.5 Mu-poor and Mu-rich Showers

The existence of near vertical showers in which the muon content is low ($\lesssim 1/30$ of the normal) has been established by many workers; recently reports have been made by the Łódź group (Gawin et al. (1966)), the B.A.S.J.E. group (Toyada et al. (1966)), and Matano et al. (1966). The theory has been developed by Wdowczyk (1966).

This phenomenon has been shown to be consistent with the initiation of a shower by a primary gamma ray; although it is just possible that it could be due to extreme fluctuations in the normal shower processes. For example, an upward fluctuation in the number of neutral pions emitted in the early interactions of the primary particle would give rise to a shower having an abnormally low μ to e ratio. It is unlikely that all the observed events are of this type of origin however.

In the primary energy range 10^{15}-10^{16} eV, mu-poor events contribute ~ $2\ 10^{-4}$ of the total; this must be

regarded as an upper limit to the ratio of primary gamma intensity to proton intensity.

The B.A.S.J.E. group do not find any low mu showers in the energy range 10^{16}-10^{17} eV, i.e. in the next higher decade of energy, and as a result of work by Penzias and Wilson (1965) and by Gould and Schréder (1966) a possible explanation has emerged. This involves the presence of the black body photon 'gas' at $\sim 3^{o}$K in the galaxy, as mentioned earlier, which is responsible for the absorption of high energy photons by means of electron-positron pair production as a result of photon-photon collisions in the required energy range.

At the other extreme, showers have been observed with an abnormally high muon content and these are thought to be produced by heavy primary particles.

Mu-poor and mu-rich showers are detected experimentally by demanding a certain number of electrons in unshielded detectors and the muon content is then determined by the examination of shielded detectors. Thus, fluctuations in the soft component play a vital role in the selection method; such fluctuations have been studied and the analysis will be presented in this report.

Since the soft component is almost completely absent in large zenith angle showers it is difficult to say

whether a shower which, for example, has relatively few muons has been initiated by a photon or whether it is simply due to a primary of lower energy. A similar argument may be put forward for mu-rich showers at large zenith angles, however, it is expected that heavy initiated showers will be reflected in a flatter lateral density distribution which, in turn, will give rise to a change in the predicted rate of observation of such showers. Furthermore, the absolute rate of detected events will depend on the primary mass composition.

1.6 Muon Bundles

Many authors (e.g. Vernov et al. (1962), Miyake et al. (1963)) have put forward experimental evidence for the existence of localised regions (a few cm^2 for near vertical showers) within the shower front having a high density of muons. The Japanese group rule out statistical fluctuations as being responsible and as a consequence need to interpret these events in terms of a special process in high energy interactions. Miyake et al. (1963) suggest that the phenomenon may be due to the decay of a particle of mass 1100 m_e which would give rise to a narrow beam of secondaries. Koshiba et al. (1967) propose that a new baryon, the Aleph baryon, is

produced in ultra-relativistic interactions. This particle has a mass of between 1960 and 2100 MeV, and a consequence of its properties is that a very narrow bundle of high energy $\mu^{\pm}$ mesons reach sea-level. Yet again, it has been conjectured that these muon bundles are due to heavy nuclei in the primary flux; however it is felt that such a primary would not be capable of producing the required high density of muons in a small region.

1.7 Conclusions

The preceding discussions show that a study of the muon component would be valuable in that it should throw light on several theories of high energy particle physics and some aspects of astrophysics. Some aspects seem to be more amenable to solution via the study of muons in near vertical showers, although large zenith angle showers may supply corroborative, but not conclusive, evidence. There are, however, further aspects where solution seems to lie in the study of large zenith angle showers.

Since facilities for observing near-vertical showers seem to be adequate, an array for the detection of large zenith angle showers has been installed in Durham; this report presents some preliminary results

of the apparatus and discusses their significance. Comparison is made with the results of other workers. In addition an extensive theoretical investigation has been made, first of all with respect to vertical showers in order to perfect a model and, secondly, large zenith angle showers are studied using the adopted model. Again the results are analysed with special reference to the mass composition of the primary flux and the nature of high energy nuclear interactions.

CHAPTER 2

Contemporary Experimental and Theoretical Studies of Large Zenith Angle Showers

2.1 Introduction

Up to the present time only two other experimental investigations of large zenith angle showers have been made. The apparatus are very different in character to each other, they are described in this section and details are given of the only previous attempt at a theoretical analysis of the muon component of large zenith angle showers.

2.2 The Experiment of Sekido et al. (1966)

The apparatus which is located in Nagoya, Japan, consists of two air Cerenkov counters each having an effective area of 10 m^2 and viewing a total solid angle of 0.05 steradian. Each counter utilises a parabolic mirror to focus the very narrow Cerenkov light cone ($\sim 1.3^{o}$ semi-vertical angle) onto an array of nineteen photomultipliers, see Figure 2.1. The two units are aimed in the same direction and a coincidence between them is used to denote the passage of one or more muons through each unit; in order to test that these are

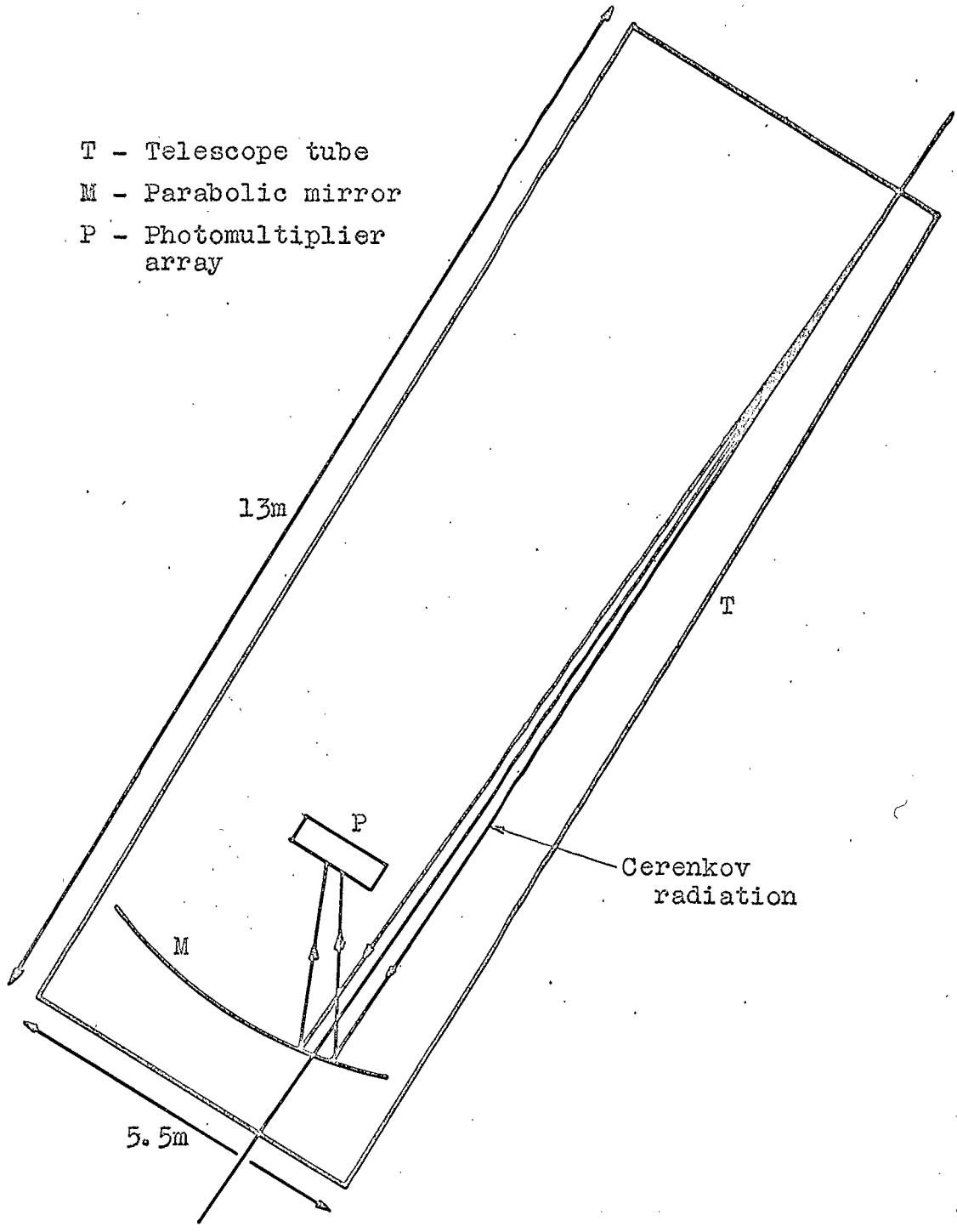

Fig. 2.1 A Nagoya Cerenkov Telescope.

parallel a hodoscope record of the photomultiplier tubes is checked. Sekido et al. quote the muon threshold energy for the device as being 10 GeV, this being made up of the energy loss in traversing 5 cm of lead shielding and the energy threshold necessary for the emission of Cerenkov radiation in air.

Geiger-Mueller counter trays of 2 m^2 are located at the sides of both Cerenkov tubes to eliminate spurious coincidences caused by near vertical E.A.S.; this is essential because although few electrons are expected at large zenith angles the apparatus would otherwise be sensitive to electrons of $\gtrsim$200 MeV which are present in near vertical showers.

There will be some divergence, $\Delta\theta$, between the parallel muons which define a muon shower, due to scattering; in order to estimate the magnitude of this parameter the authors considered the probability distribution of obtaining various patterns of photomultipliers giving simultaneous pulses, as a function of $\Delta\theta$. The observed distribution was found to be consistent with that calculated for $\Delta\theta \sim 3^\circ$ and as a consequence pairs of muons with $\Delta\theta \lesssim 3^\circ$ are accepted as parallel.

The experimental results, which will be discussed later, are based on 2351 events obtained over a period

of 50 days, observations being made at azimuthal angles of 72^{o} and 288^{o} from north and various zenith angles.

2.3 The Theoretical Studies of Sekido et al.

In an attempt to compare their experimental results with theory these workers formulate the following model.

It is assumed that the muons are simply produced at a depth of 400 $g.cm^{-2}$ measured from the top of the atmosphere along the trajectory, and that they are spread within a cone of constant opening angle 0.028^{c}, which is based on a mean transverse momentum of 0.4 GeV/c.

The effective area A(E) for the detection of a muon shower, initiated by a primary of energy E, is given by:-

$$A(E) = 2\pi \int_{o}^{r_{max}} r(1-e^{-\Delta S})^{2} dr \ m^{2} \qquad (2.1)$$

where S is the area of each detector (10 m^{2}), Δ is the muon density which is a function of E at a distance r from the core

$$\Delta = \frac{CE}{h^{2}} \left(\frac{r}{h} \right)^{-\alpha} \text{ for } r < r_{max} \qquad (2.2)$$

C and α being empirical constants, r_{max} is given by $r_{max} = 0.028h$ where h is the linear path length along the shower axis from the 400 $g.cm^{-2}$ level to the obser-

vation level.

Using the primary spectrum j(E) as given by Linsley (1964) the counting rate is given by the following integration

$$\text{Rate} = \int_0^\infty j(E)\ A(E)\ dE\ \text{st.}^{-1}\text{sec.}^{-1} \qquad (2.3)$$

C is assumed to be $6.7\ 10^{-11}\ eV^{-1}$ and $\alpha = +\frac{1}{2}$.

The theory does not, it appears, take into account Coulomb scattering or geomagnetic deflection. Further criticism is made of this model after its predictions have been compared with experimental results, §7.7.4.

2.4 The Utah Experiment

Schematic side and plan views of the prototype neutrino detector are shown in Figure 2.2, the columns marked 1,2,3, ... 7 are cylindrical spark counters, as described by Parker (1967). The axis labelled 'delay' may be converted to distance by use of the fact that the speed of sound is 0.311 metres/m.sec. The apparatus has a maximum detecting area of ~20 m^2 and events in the following angular ranges are accepted for analysis, $45^\circ < \theta < 90^\circ$ and $0^\circ < \phi < 45^\circ$; the energy threshold for muons is ~2 GeV.

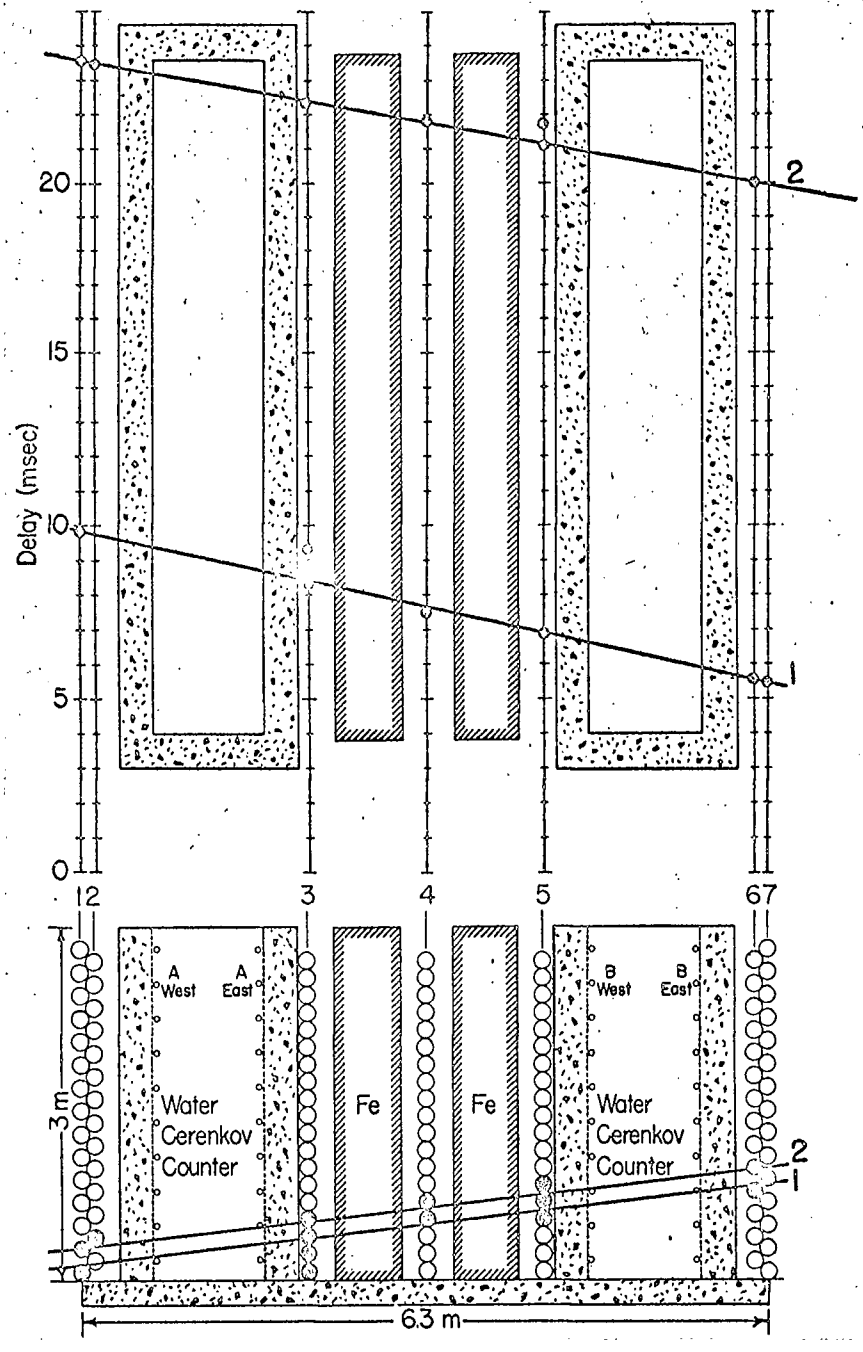

Fig. 2.2 Schematic diagram of the prototype Utah neutrino detector.

The coincidence requirements were such that any single fast muon passing through both Cerenkov tanks would be accepted, the trigger rate being ~ 25 sec^{-1}, recording delays reduced the useful rate to ~ 2.5 sec^{-1}. In order to locate muon showers these events were scanned by computer and those selected in which there were two or more muons crossing spark counter columns 3 and 5, the muon tracks being within 4^{o} of each other. This resulted in the selection of 1200 multiple events corresponding to a rate of $6.8^{+1.0}_{-0.5}$ hr^{-1}. The raw data has been processed to allow for changing effective area with zenith and azimuthal angles, also, the possibility of an event being lost due to a muon triggering an 'anti-wall' of a Cerenkov tank or having failed to trigger a coincidence wall has been considered.

At $\theta = 64^{o}$ the apparatus has an effective area of 10 m^2 and it may be shown that the probability of two particles traversing 10 m^2 is half of that for one particle through each of two areas of 10 m^2. Thus Parker's rates should be multiplied by two in order to compare them directly with Sekido et al.

2.5 Summary

The results of these two experiments are given in Figure 4.2 where they are compared with the zenith angle distribution derived from the Durham data; a discussion of the comparison is given in §4.5.2. The Durham theoretical predictions are compared with the experimental distributions and with the theory of Sekido et al. in §7.7.4 and the significance of the comparison is again discussed.

CHAPTER 3

The Horizontal Extensive Air Shower Array

3.1 Introduction

Basically, the experimental problem is to provide irrefutable evidence of muon showers travelling with axes highly inclined to the vertical, and to measure the density of particles in such showers as a function spectrum of zenith angle.

At large zenith angles, muons will typically have a mean depth of production of approximately 550 $g.cm^{-2}$; for $\theta = 60^{\circ}$ this corresponds to a height along the trajectory, $\bar{h}$, of ~10.5 kms, at $\theta = 75^{\circ}$, $\bar{h} \sim 17$ kms and for $\theta = 90^{\circ}$ $\bar{h} \sim 200$ kms. Thus, neglecting effects such as scattering and magnetic deflection the trajectories of the muons will be parallel at sea-level; inclusion of these effects means that the trajectories are 'parallel' to within a few degrees of each other. In order to classify an event as a muon shower it is clearly necessary to have at least two, and preferably more, 'parallel' tracks.

A complication arises because of electron showers produced by the electromagnetic interaction of muons a few tens of metres from the apparatus, these too would

appear to have parallel tracks. It is therefore essential to prevent these showers being recorded; this may be accomplished by the introduction of a layer of absorber. This is used to shield one side of the array only since the array may then be used to study both the soft and hard components. Bursts may be produced by nuclear interaction within the absorber; but such events are easily recognised because they give rise to highly diverging tracks.

Before considering the design of the array in detail, it should be mentioned that it must be capable of resolving many simultaneous particles and allow their zenith angles to be determined.

3.2 The Array

The steel framework which supports the detectors and from which the absorber is hung has the following dimensions: height 7.2 m, length 11.6 m and width 1.93 m. It is situated such that the plane of the detectors is vertical and the normal to this plane is 18° E of geographical north and 27° E of geomagnetic north. The absorber consists of steel plates and is hung on the north side of the array.

The first requirement is that there should be a continuously sensitive detection system which will record the passage of a shower and trigger the visual detectors. Four vertical scintillation counters, each having an area of 1 m^2, are available to be operated in coincidence with each other and in anti-coincidence with a further counter of similar area which is in a horizontal plane, the latter being necessary to reduce the rate of triggering of the array by near vertical showers. The visual detection system consists of twelve trays of neon flash tubes, each tray having an effective area of 2.82 m^2. The location of the detectors with respect to the frame is shown in Figure 3.1.

3.3 The Scintillation Counters

3.3.1 Design

As these counters are to be situated in rather inaccessible locations plastic scintillating material is used in preference to a liquid despite the higher cost of the former.

Brini et al. (1955) have analysed the class of counter in which the photomultiplier is in optical contact with the phosphor. They show that the conditions under which the uniformity is best and limited only by the absorption of the phosphor are:-

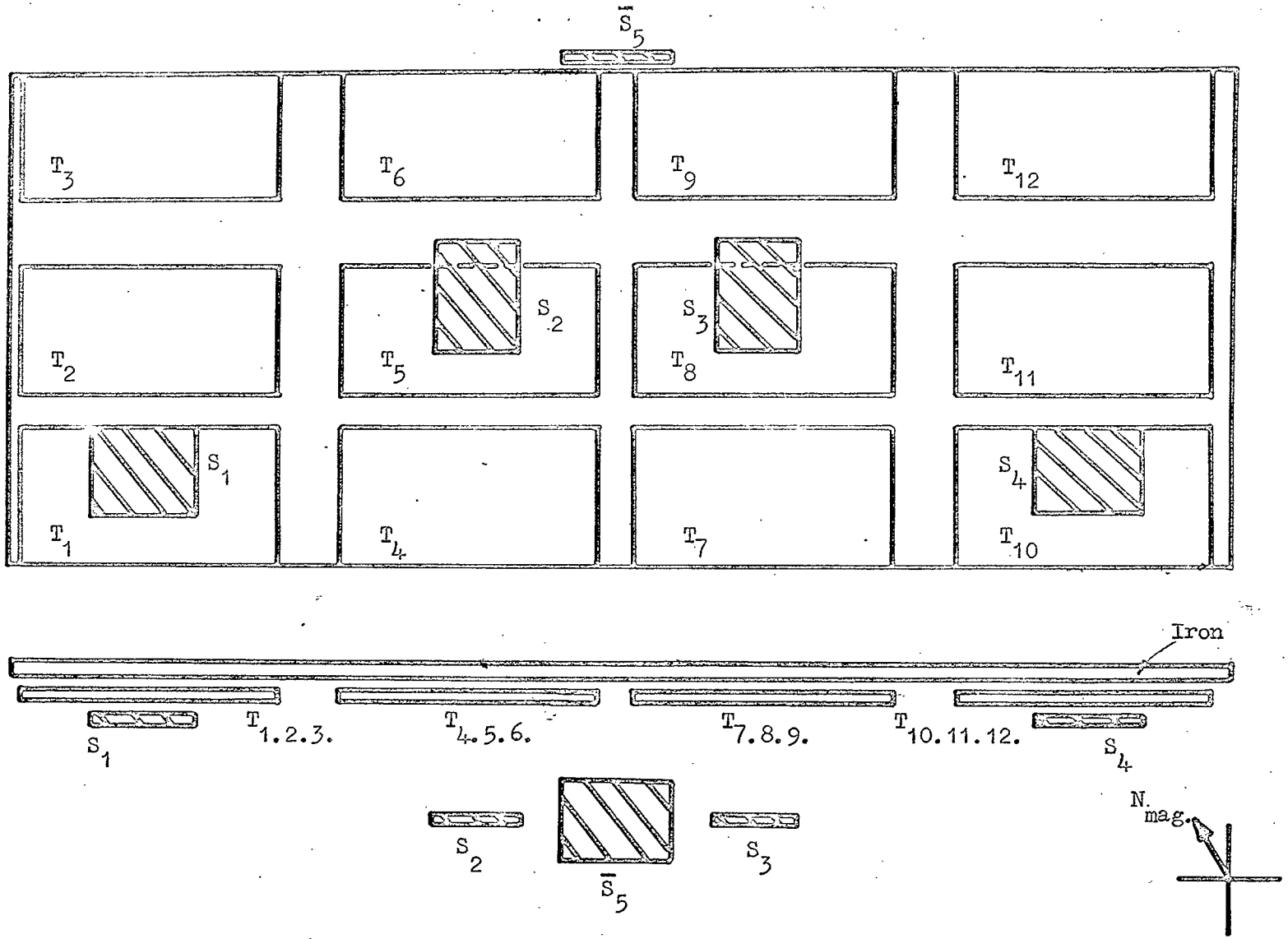

Fig. 3.1 Schematic plan and front view of the Durham array, S_1-S_5 are $1m^2$ scintillation counters and T_1-T_{12} are trays of neon flash tubes.

i) The phosphor must be rectangular.

ii) A short section of light guide should be included.

iii) The faces of the phosphor should be polished.

If these conditions are satisfied then light in only four of the escape cones will be lost.

Garwin (1952) has shown that of the total light output the fraction reaching the photomultiplier cathode will be $\Omega = 0.125\ S/A$ where A is the area of the phosphor face to which the light guide is attached and S is the area of the photocathode.

The plastic phosphor used is NE102A in the form of a rectangular slab 133 x 75 x 5 cm; this consists of scintillation chemicals in polyvinyltoluene, it has a decay constant of $3.5\ 10^{-9}$ sec, a refractive index of 1.58 and maximum light emission at 4300 Å. Perspex light guides, $\mu = 1.49$, are cemented to each end of the phosphor with Shell Epikote Resin 815. Mullard, 53 AVP, 11 stage photomultipliers with peak spectral response at 4200 ± 300 Å are attached to the light guides with NE580 optical cement. The useful cathode area is 15.2 cm^2, which means that $\Omega = 0.005$ for each end of the counter.

Because of stray magnetic fields in the laboratory, precautions have to be taken to prevent these affecting the performance of the photomultipliers. Each tube is surrounded by a mu-metal shield, and a length of $\frac{1}{4}$" thick steel tubing as well as the aluminium box which contains the whole counter. This arrangement has proved to be satisfactory in the flux encountered.

3.3.2 Operation

The pulses from the photomultiplier base are -ve and typically 250 mV high with a rise time of ~20 nsec and are ~1 μsec long. They are fed via individual head amplifier units to a coincidence and discrimination unit from which there is an added output and a discriminator output, this being a positive pulse of ~10v which indicates that the sum of the input pulses is greater than the discrimination level. It is therefore possible to gate the counter on itself and only look at the added output pulses which are above the noise level. The electronic units are transistorised and enclosed in earthed boxes of perforated brass sheet to prevent the pick up of electromagnetic radiation.

The photomultipliers are set up so that a particle passing through the mid-point of the phosphor produces the same output pulse height at each end of the counter.

Examination of the added pulse heights gives a distribution such as that in Figure 3.2. In order to detect single particles, the discrimination level is set such that most of the noise is eliminated; this variation of discrimination level may be achieved most easily by adjusting the E.H.T. to the photomultiplier bases. A small amount of noise is tolerable as it is unlikely to coincide with that in the other counters; if it is not included particles producing the initial rise of the single particle peak would not be accepted. Typically the operating voltage of the photomultipliers is in the range 1.3 to 1.7 kV, once set this should not vary otherwise the discrimination levels will drift.

3.3.3 Characteristics

In order to assess the performance of a counter and to compare it with other types we define two parameters:

i) Uniformity of response over the area of the counter - this is the percentage difference between the response at a given point and the response averaged over the whole area for particles traversing the phosphor normal to its area.

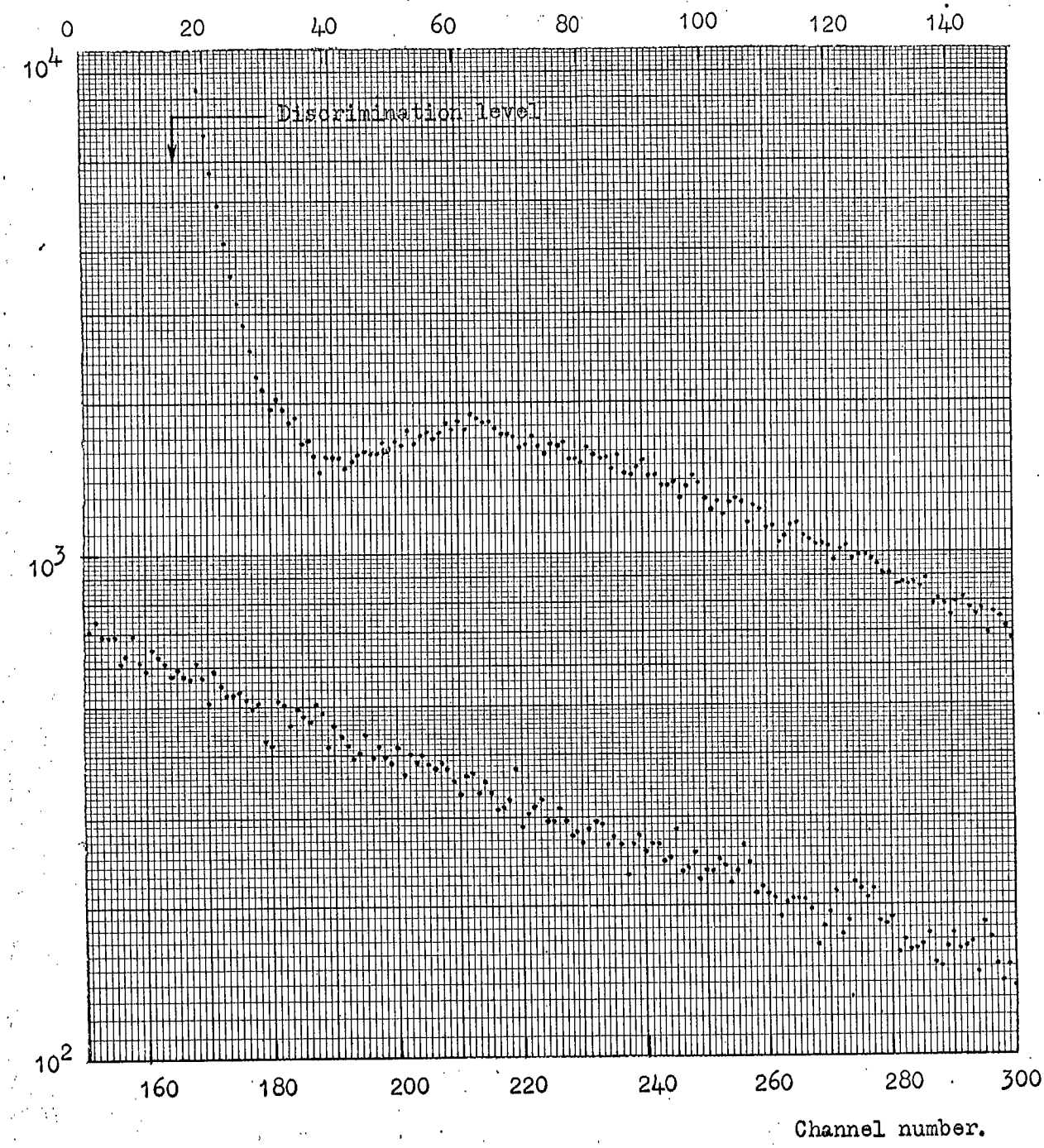

Fig. 3.2 A typical added output, ungated, from a coincidence scintillation counter.

ii) Resolution - this is the full width at half height, of the output pulse distribution, expressed as a percentage of the most probable value for relativistic particles traversing the mid-point of the phosphor normal to its largest face.

This work has been reported by Ashton et al. (1965); a summary of the results is given in Table 3.1.

Table 3.1

Comparison of the characteristics of liquid and plastic phosphors

Phosphor	Maximum non-uniformity (%)	Resolution (%)
Paraffin	18	80
NE102A	32	50
Paraffin + 10% Shellsol A	36	40

3.4 The Coincidence and Cycling System

The basic components of this system are illustrated in a block diagram Figure 3.3.

Pulses from each end of a scintillation counter are added and only those due to one or more particles traversing the phosphor pass through the discrimination unit.

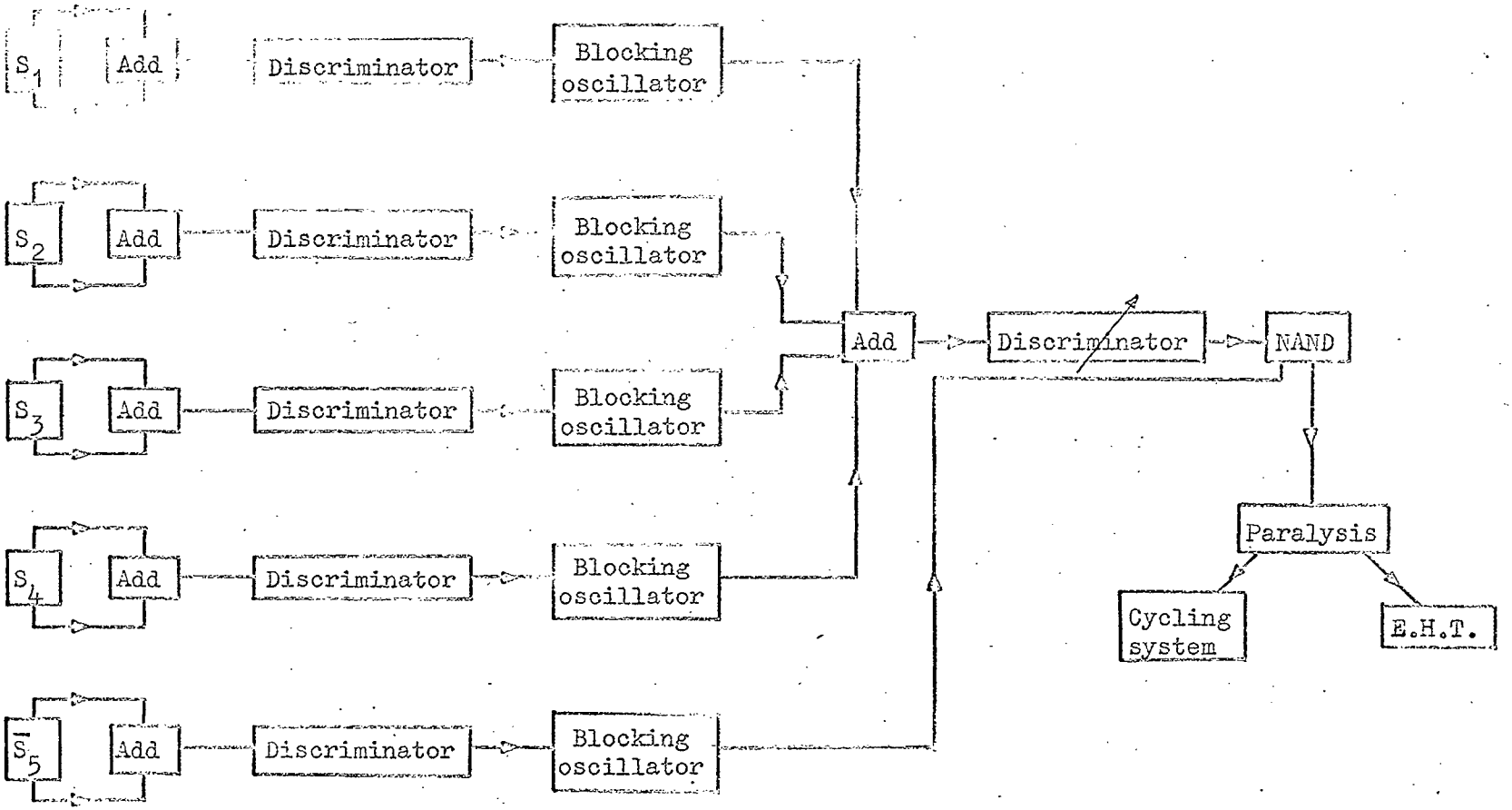

Fig. 3.3 — The coincidence system.

A blocking oscillator transforms these to square positive pulses of fixed height. The outputs from any desired combination of the four coincidence scintillation counters are added and a variable discriminator allows the triggering criteria to be varied. Assuming this to be satisfied the pulse is passed to an anti-coincidence gate which is closed only if there is a simultaneous pulse from the anti-coincidence counter. The trigger pulse after traversing a paralysis unit is split, one pulse going to the cycling system, the other to the E.H.T. section.

A paralysis unit is necessary because the cycling system takes ~ 8 seconds to operate, also, a certain time must be allowed for the E.H.T. unit to recover. The trigger pulse operates a flip-flop which applies a d.c. voltage to a diode so that further pulses which occur during the paralysis time are shorted to earth.

The cycling system consists of a set of microswitches operated by cams which are mounted on a shaft driven by a synchronous motor geared to 1 rev/8 sec. The trigger pulse is lengthened to 0.5 second and this pulse is used to operate a relay which applies mains voltage to the motor. During the 0.5 second the first microswitch is actuated thus keeping the mains voltage across the motor

for the desired length of time. Other microswitches operate the flash tube tray camera, illuminate the fiducial lights and the clock face. Finally, just before the motor is switched off, a pulse which is subsequently delayed by ~0.25 second is used to reset the flip-flop, thus allowing a further trigger pulse to pass.

3.5 The Neon Flash Tube Trays

3.5.1 The Neon Flash Tube

The flash tube was introduced by Conversi and Gozzini (1955). In its present form it consists of a glass tube filled with neon. The passage of a charged particle through such a tube will cause localised ionisation, and if a large potential difference is applied across the tube a visible discharge will take place. A number of these tubes suitably disposed will form an efficient track detector with good spatial resolution.

The specifications of the tubes used are as follows:-

length 2.25 m.

internal diameter 15 mm.

external diameter 17 mm.

gas filling - commercial neon,

Ne 98 ± 0.2%, He 2 ± 0.2%,

O_2 10v.p.m., N_2 100 v.p.m., A 0.5 v.p.m.

pressure, 60 cmHg.

Neon is used because it has comparatively good breakdown characteristics and the ensuing red glow is easily seen and photographed.

The characteristics of such tubes have been described and discussed by Gardener (1957) and Coxell and Wolfendale, (1960), the theory by Lloyd (1960) and the accuracy of track location in a stack of tubes by Ashton et al. (1958).

3.5.2 Design

Each tray is constructed as indicated in Figure 3.4a there being approximately 66 tubes in each of four layers. The tubes are interleaved with opaque 'Fablon' to prevent photon spread which would cause a discharge in tubes adjacent to those through which the ionising particle had passed. The walls of all tubes are painted white for 6" from the window in order to improve the light output.

The electrodes are aluminium sheet, the outer earthed plates are held rigidly in a steel frame and the inner electrode to which the pulse is applied is supported by 'Tufnol' formers which also insulate the electrode from the rest of the system. The electrodes are parallel to within less than 1 mm., obviously any misalignment would cause the field and therefore the tube efficiency to vary over the area of the tray. The twelve trays have a total effective particle detection area of 33.9 m^2.

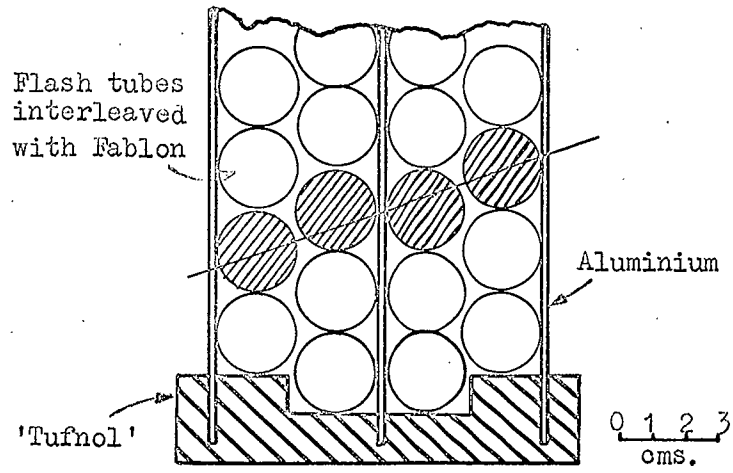

Fig. 3.4a Schematic section through a flash tube tray.

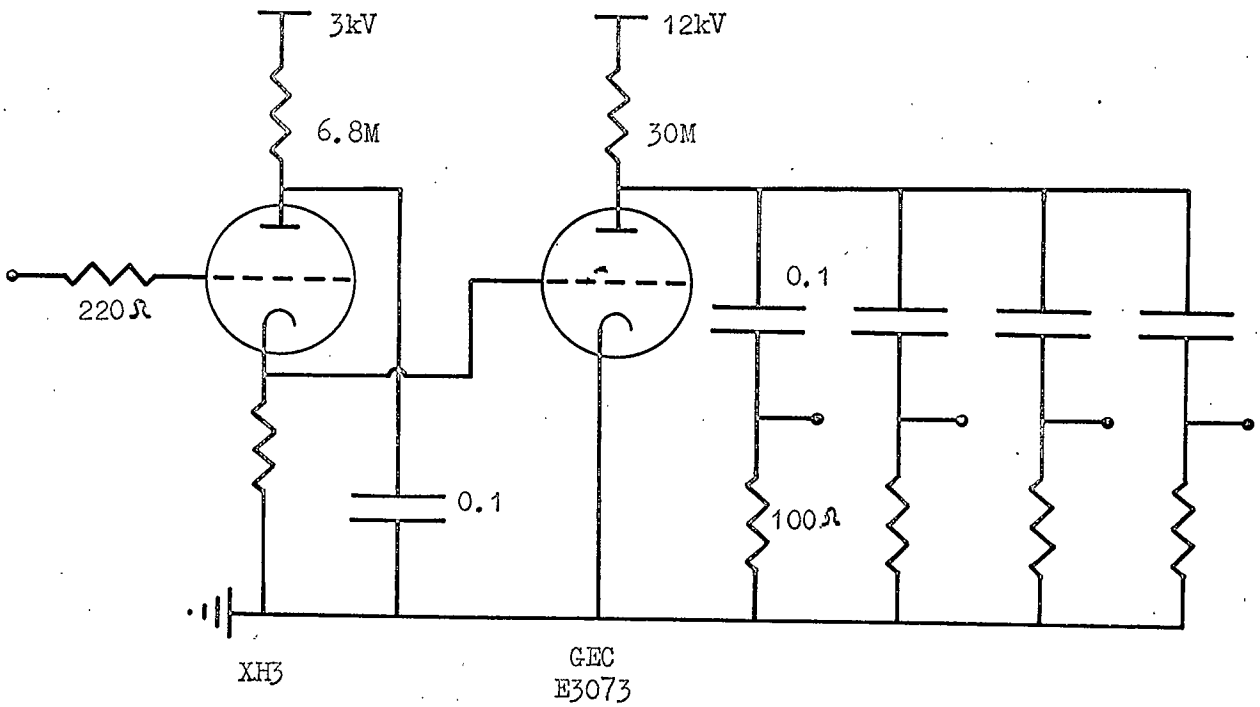

Fig. 3.4b The E.H.T. unit for the flash tube trays.

3.5.3 Operation

The trigger pulse from the coincidence circuit is amplified to ~200 v and applied to the grid of a hydrogen thyratron (Mullard XH3), Figure 3.4b. The output from the thyratron is used to trigger a surge diverter (GEC E3073) whose output is split, a pulse is applied to each of the four columns of trays. The pulses have the following characteristics, rise time ~2 μsec, delay time ~3 μsec, width ~10 μsec, height 13.5 kV thus giving a field of ~4.5 kV cm^{-1}.

Flashed tubes are recorded photographically on 'Ilford' H.P.S., red sensitive film, via a mirror system arranged so that the path length from the camera to the windows of all tubes to the same, ~23 m.

3.5.4 Characteristics

Two efficiencies may be defined for the trays:-

i) Layer efficiency (η_L) which is defined as the ratio of the number of single flashes observed in a layer to the number of particles having passed through that layer.

ii) Internal efficiency (η) which is determined from η_L by multiplying the latter by the ratio (R) of the separation of the tube centres to the internal diameter of the

tubes. This involves the assumption that only those particles traversing the gas in a tube can cause a flash in that tube.

$$\eta_L = 88\%$$

$$R = 1.13$$

$$\eta = 100\%$$

these efficiencies being assumed values.

3.5.5. The Accuracy of Zenith Angle Determination

The zenith angle had to be determined from tracks recorded in single trays of flash tubes, that is, each track had to be measured from four closely packed columns of flash tubes as shown in Figure 3.4a. A thorough analysis was made of the possible flash tube patterns for tracks at a specific zenith angle and the possible range of zenith angles which could give rise to each tube configuration. The outcome of this analysis is that the following limits to the error ($d\theta$) on a determination of zenith angle (θ) may be placed, Table 3.2.

CHAPTER 4

The Results of the Durham Apparatus

It has already been mentioned that only the north face of the array is covered with absorber, this means that events in which the shower is incident from the north may be used to examine the hard component and those from the south allow us to study the soft component of the shower. This is important since an analysis of the electron-photon component is interesting in itself and, in addition, it allows a correction to be applied to the 'muon' events for electron contamination.

4.1 The Operating Conditions

The apparatus has been operated as described in Table 4.1, which also shows the raw data obtained during each run.

During run C the southern side of the coincidence scintillators was shielded to reduce the rate of triggering of the array by S events.

4.2 Scanning Criteria

The filmed events are projected and those which have any possibility of satisfying the prevailing acceptance criteria are reproduced on a scale drawing of the flash tubes.

Table 4.1

The events recorded in experimental runs

Run	Absorber Thickness radiation lengths	Trigger mode	Running time hrs.	Events recorded in θ		
				θ	S	N
A	1.5	$S_1S_2S_3S_4\bar{S}_5$	801	42.5°-47.5°	148	36
				47.5°-52.5°	154	23
				52.5°-57.5°	133	45
				57.5°-77.5°	333	124
				77.5°-90°	24	19
B	4.5	$S_1S_2S_3S_4\bar{S}_5$	350	42.5°-47.5°		1
				47.5°-52.5°		1
				52.5°-57.5°		1
				57.5°-77.5°		13
				77.5°-90°		0
C	4.5	$S_1S_4\bar{S}_5$	153	< 20		13
				20°-42.5°		26
				42.5°-47.5°		14
				47.5°-52.5°		20
				52.5°-57.5°		22
				57.5°-77.5°		26
				77.5°-90°		5

The measured north and south number spectra are shown in Figure 4.1; the problem is to take the measured south spectrum and to derive from this the incident density spectrum.

The array triggering probability (ATP) is given by:-

$$ATP = (1-e^{-\Delta S})^{n} \; (e^{-\Delta S'})^{n'}$$

where Δ is the mean density of particles falling on the array,

S and S' are the projected areas on the shower plane of the n coincidence and n' anti-coincidence scintillation counters respectively.

The use of this expression alone will not lead to the correct result since fluctuations must be taken into account when translating from a density to a number of particles falling on a certain area. This is a consequence of the incident density spectrum being very steep and it follows that a shower of m particles through the array (of projected area A) is most probably due to a shower of mean density less than m/A, and is observed because of an upward fluctuation in the number of particles passing through that particular area.

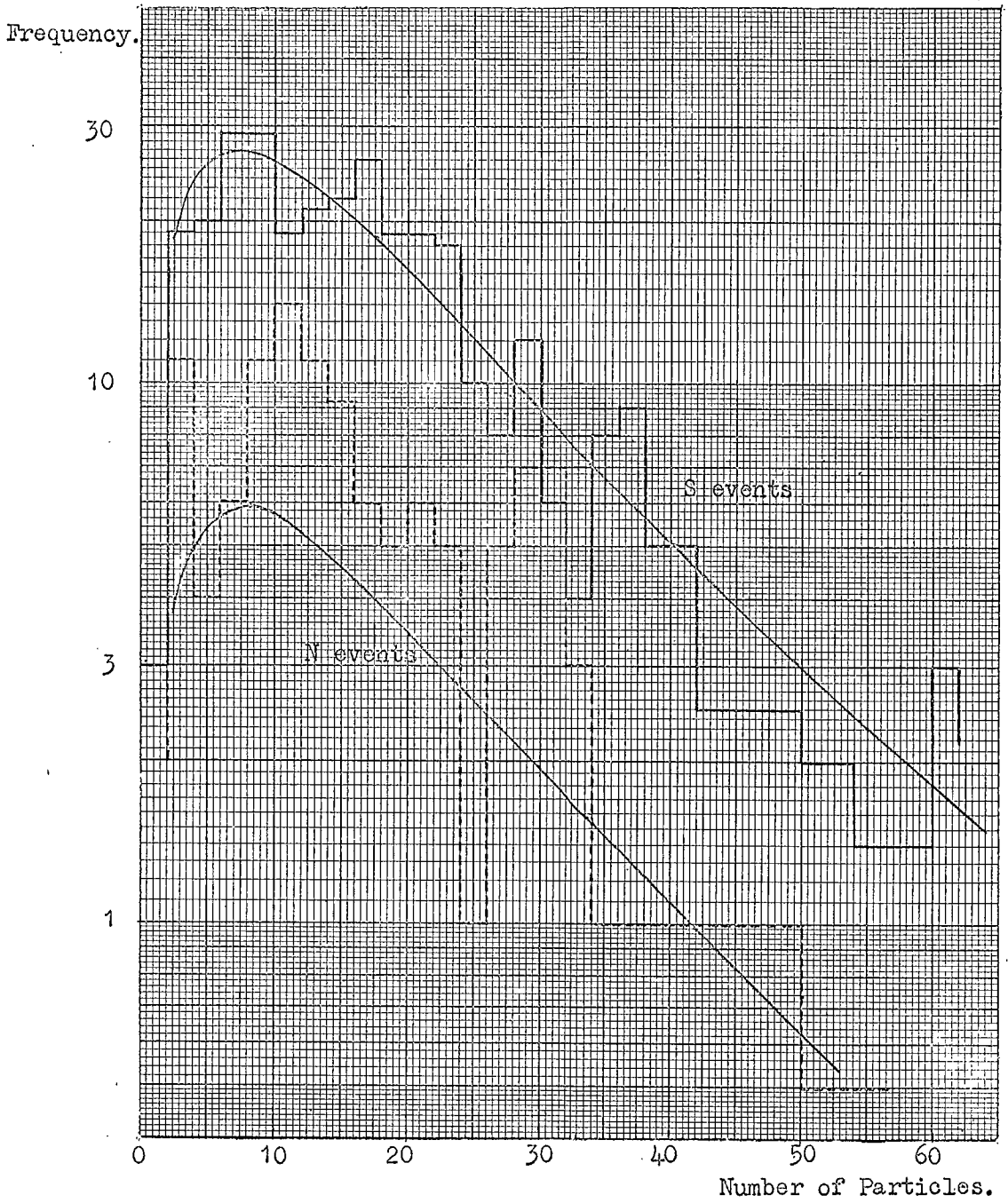

Fig. 4.1 The measured north and south number spectra with the best fitting theoretical south spectrum and the predicted north spectrum for 100MeV incident electrons, $57.5^{\circ} < \theta < 77.5^{\circ}$.

The adopted method was to assume an incident density spectrum and to fold in the array triggering probabilities to give an effective density spectrum. This is divided into cells; the mean number of particles ($\bar{m}$) passing through the projected area of the array is calculated by multiplying the mean density for that cell by the projected area. The number $\bar{m}$ is regarded as the mean of the Poisson distribution

$$P_m = \frac{e^{-\bar{m}} \bar{m}^m}{m!}$$

and each term P_m of the distribution when multiplied by the magnitude of the cell in the effective spectrum will give the contribution to the cell of magnitude m in the observed number spectrum. The total predicted number spectrum may be obtained by summing over all the cells in the effective incident spectrum. This predicted spectrum is then compared with experiment and the slope and magnitude of the incident spectrum adjusted until agreement is reached.

It is found that the shape of the predicted spectrum is independent of the magnitude of the incident spectrum, the best fit being given by:-

$$\text{Rate} = 2.56\ 10^3 \Delta^{-3.7\pm0.2}\ \text{sec}^{-1}\text{ster}^{-1}(\text{particle/m}^2)^{-1} \quad (4.1)$$

in the angular range $57.5^\circ < \theta < 77.5^\circ$, and this is

shown superimposed on the S event histogram of Figure 4.1.

4.3.2 Prediction of the Observed North Number Spectrum

The starting point for this calculation is the incident density spectrum and from this it is necessary to calculate the number spectrum of showers incident on the array. This is basically the same calculation as that detailed in the preceding section, the difference being that the probability of getting one or more particles through the area of the array is used instead of the array triggering probability.

From the results of Crawford and Messel (1965) the probability of one electron incident on the iron emerging as 0, 1, 2, ... was determined as a function of incident electron energy. Using a Monte Carlo treatment the probability of a shower of m incident electrons leaving the iron as m, m-1, m-2, ... was determined. This does not produce the spectrum observed by the array since not all of these showers would trigger the apparatus.

Various trial incident spectra were used in order to find one which would predict the number spectrum just derived. The array triggering probabilities applied to the adopted incident density spectrum give a number spectrum which can be compared with that obtained experimentally. This had the same slope as the observed

N spectrum, however it was a factor of two down in rate, Figure 4.1. The only explanation for this seems to be that the assumed mean energy of the incident electrons was too low, the alternative explanation would require the difference between theory and observation to be due to muon showers; theoretical studies have shown that virtually no muon showers would be recorded under the prevailing triggering conditions. Thus, in order to get agreement it is necessary to raise the assumed mean electron energy from 100 MeV to 140 MeV.

As a result of these studies it is now possible to predict the behaviour of electron showers for various array triggering criteria in conjunction with different thicknesses of absorber. It is therefore possible to make allowance for the effects of electron showers during studies of the hard component.

4.4 Run B

The triggering conditions were as in run A, but the thickness of absorber was increased to 4.5 radiation lengths. The apparatus was operated for a further 350 hours: 16 N events satisfied the scanning criteria, the S events were not analysed. Theory suggests that during the operating time approximately 5 N events due to muon showers would be recorded and the preceeding

work would lead us to expect not more than one event due to a penetrating electron shower with a mean incident energy of 140 MeV.

The conclusion from this run is that the preceding theory gives an underestimate due to upward fluctuations in the incident electron energies being neglected. However, as an order of magnitude calculation, it appears to be satisfactory.

4.5 Run C

Conclusive evidence for the existence of muon showers at large zenith angles came from the analysis of run C data. The array was operated with scintillation counters S_1 and S_4 in coincidence and S_5 in anti-coincidence; the thickness of absorber on the north face remaining at 4.5 radiation lengths. In addition the south sides of S_1 and S_4 were shielded by 6" of barytes laden concrete which amounts to approximately 4 radiation lengths, its purpose being to reduce the rate of triggering of the array by showers from the south.

The array was in operation for 153 hours using this triggering system; when all S events are rejected together with those N events obviously of a local nature, 145 N events remain, 126 of these are shown in table 4.2 the remaining 19 did not satisfy the scanning criteria.

Theory suggests that under these operating conditions ~0.1 event would be expected as a result of penetrating electron showers in 153 hours.

In order to compare the accepted events with those of other workers it is necessary to apply a further acceptance criterion, so that the showers finally accepted would have been capable of triggering the Nagoya apparatus. The condition that both triggering particles should be visible in flash tube trays T_1 and T_{10} reduces the number of acceptable events in the range $42.5^\circ < \theta < 90^\circ$ to 31 and these will be known as 'Sekido type' events.

The non-Sekido type events, that is to say, those events in which one or no tracks are seen in flash tube trays T_1 and T_{10}, may be ascribed to three possible causes. The most likely explanation is that one or both of the triggering particles have passed through gaps in the flash tube coverage. It is estimated, taking the zenith angle distribution of showers into account, that ~45% of particles which trigger either S_1 or S_4 would have missed a flash tube tray. Consequently, of the 87 N events of run C, in the angular range $42.5^\circ < \theta < 90^\circ$, an estimated 39 events would be rejected for this reason, thus leaving 48 events, a number which is

to be compared with the 31 accepted events. Another explanation, which is not very probable, is that there may be a coincidence between S_1 and S_4 due to a muon passing through one of the counters and a charged particle caused by a photo-nuclear interaction passing through the other; this would require an extremely high photo-nuclear cross section. Finally, the possibility of a coincidence with a noise pulse in either S_1 or S_4 must be considered; the probability of this occurring is thought to be small.

4.5.1 The Variation of Rate with Zenith Angle

Since comparison with other experimental work is necessary it is essential that only Sekido type events are used in this section of the analysis. The recorded events of the present experiment together with the triggering factors, necessary because the array triggering probability varies with θ as $\sin^2\theta$, and the area correction factors, which arise due to the gaps between trays of flash tubes, are given in Table 4.3. The final column of this table is plotted in Figure 4.2; in the region of $\theta = 70^\circ$ the results are consistent with a zenith angle variation of:-

$$\text{Rate } (\theta) \propto \cos^{(2.3 \pm 0.3)}\theta \qquad (4.2)$$

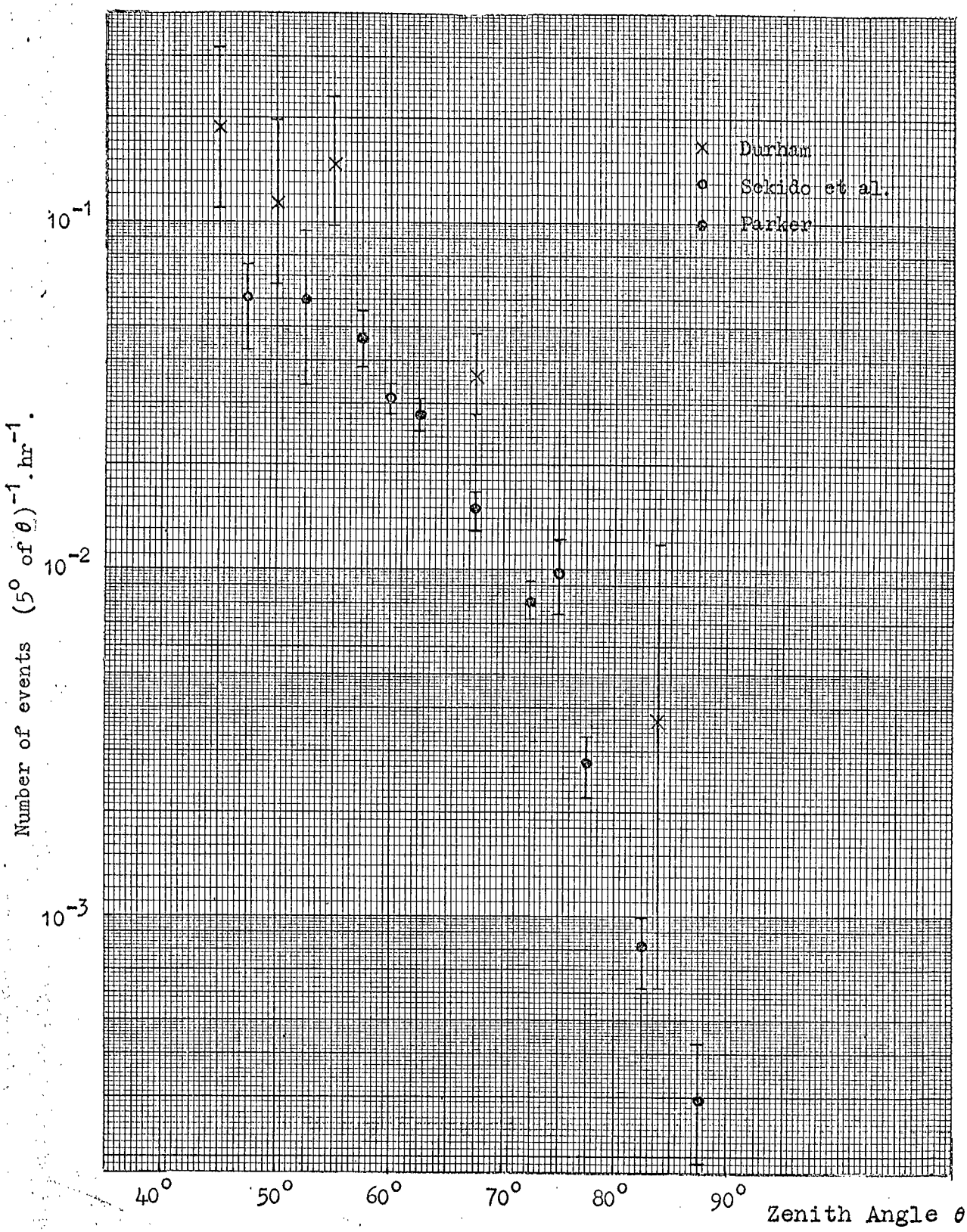

Fig. 4.2 The zenith angle distribution derived from the data of the present experiment compared with those of other workers.

Table 4.3

Events of run C having parallel tracks in T_1 and T_{10} and triggering S_1 and S_4

Angular Range	No. events	Trigger Factor	Area Factor	No. of events per $5^\circ\theta.hr^{-1}$
42.5°-47.5°	6	2.00	2.40	0.188
47.5°-52.5°	5	1.64	2.15	0.115
52.5°-57.5°	8	1.47	1.94	0.149
57.5°-77.5°	11	1.30	1.57	0.0367
77.5°-90°	1	1.00	1.35	0.00353

4.5.2 Comparison with Sekido et al. and Parker

The results of Sekido et al. and Parker are also plotted in Figure 4.2, after having been converted to the acceptance of the Durham array.

The angle over which particles are accepted by the Durham array is defined in zenith angle by the flash tubes, in azimuth it is undefined. The rate at which showers trigger the array is a function of azimuthal angle since the array triggering probability for this run is given by

$$ATP = (1-e^{-\Delta S})^2 \, e^{-\Delta S}$$

where the effective scintillator area (S) at θ and ϕ is related to the true area, S_o, by $S = S_o \sin\theta\cos\phi$. For

low densities we can approximate, $ATP \propto (\sin\theta \cos\phi)^2$, this is valid since the major contribution to the rate comes from showers having $\Delta \sim 10^{-3}$ p/m^2. Since the mean value of $\cos^2\phi$ occurs at $\phi = 24^\circ$ it may be assumed that all Durham observed showers are incident at $\phi = 24^\circ$ and triggering probabilities are based on this value.

The Durham acceptance may therefore be regarded as π in azimuth and $d\theta$ in zenith, for comparison to be made $d\theta$ is taken in steps of 5°; the acceptance per 5° in θ is 0.137 steradian.

Sekido's apparatus has an aperture of 0.05 ster., however the area of his detectors is 2 x 10 m^2, to be compared with our 2 x 1 m^2, thus his array triggering probability will be a factor of 10^2 greater (for small Δ). The net result is that Sekido's rates must be multiplied by $2.747\ 10^{-2}$; Parker states that the aperture of his apparatus is a factor of 2 down on that for Sekido, the scaling factor for Parker's rates will therefore be $5.494\ 10^{-2}$.

From Figure 4.2 it may be seen that the slope of the Durham distribution is in good agreement with that of Parker; the slight difference in absolute magnitude may, at this stage, be attributed to uncertainties in calculating the acceptance of the various experimental

arrangements. There is however a marked discrepancy between the slope of Sekido's distribution and the others; since the muon threshold is ~10 GeV compared with ~2 GeV for Parker and ~0.2 GeV for Durham it would be expected that Nagoya rates should be lower at all zenith angles. Parker suggests that the difference in slope may be attributed to the different threshold energies as there are more low energy muons in 60^{o} showers than in those nearer the horizontal. This has been investigated in the theoretical section of the present work and it is concluded that this will only explain part of the discrepancy. A second possibility, and one which may also help to explain the higher rate at large zenith angles, is the increasing sensitivity of the Cerenkov telescope measurement to contamination by vertical E.A.S. as the telescope is directed to larger zenith angles. Both the Utah and Durham experiments are immune to such contamination, and even if it were present it would be independent of zenith angle. A third factor is that the geomagnetic conditions at the three sites are different; preliminary theoretical considerations show that this will not explain the whole of the remaining discrepancy however.

The overall conclusion must therefore be that there is some factor, as yet unknown, which is responsible for the discrepancies between the Nagoya and other experimental distributions.

4.5.3 The Muon 'Number' Spectrum for $57.5^{\circ} < \theta < 90^{\circ}$

The Durham apparatus goes further than the other two in that it has a large area of detector in addition to the triggering counters, the respective areas being ~ 34 m^2 and 2 m^2. It is therefore possible to look at the muons accompanying the triggering particles. Table 4.4 shows all those events not rejected because of non-parallel tracks, for $\theta > 57.5^{\circ}$; that is, it includes the Sekido type events in this angular range as well as those considered to be of a type which Sekido would have rejected.

Table 4.4

The frequency of observation of multiple muons

No. of parallel muons (N)	2	3	4	5	6	11	14	20
Frequency	12	6	6	2	1	1	1	1

Parker quotes a two-muon to three-muon event ratio of 23:1, however this is not directly comparable with the Durham result of ~2:1 because of the vastly different acceptance conditions.

4.5.4 Muon Bundles

One possible candidate exists amongst the N events of run C, this has 27 visible parallel tracks at a zenith angle of 44^{o}, which means that the effective area of the array flash tube trays is $\sim 16.7\ m^2$ giving a density over the array of ~ 1.6 particles/m^2.

4.6 The Barometric Coefficient

During run A sufficient data were collected for a determination of the barometric coefficient (B). The observations of array triggering probability as a function of atmospheric pressure are shown in Figure 4.3. If $\Delta p = p - 760$ mm.Hg then the rate of triggering is given by:-

$$\text{Rate} = 6.17 \exp -0.186 \Delta p \text{ per hr.} \qquad (4.3)$$

and,

$$B = 19\% \text{ per cm.Hg.}$$

Previous experimental determinations give values of B ranging from 10% per cm.Hg for a shower of 10^4 particles to 14% per cm.Hg for 10^7 particles; these results being for near vertical showers. The reason for the much higher value of 19% per cm.Hg is not known at present.

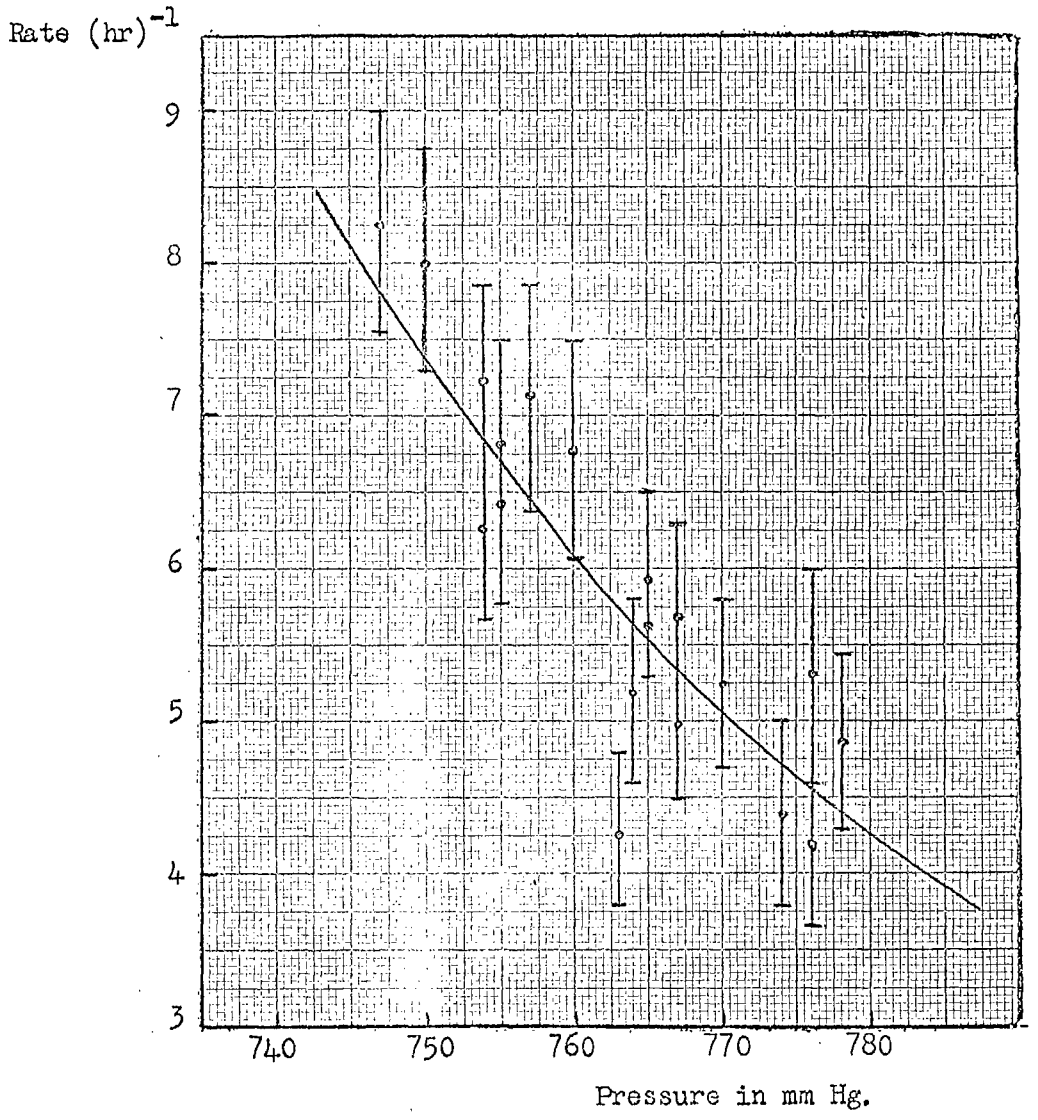

Fig. 4.3 The array triggering rate for two-fold coincidence (S_1, S_4, $\overline{S}_5$) as a function of the atmospheric pressure.

CHAPTER 5

High Energy Interactions - a Survey

5.1 Introduction

The ultimate aim of the present work is, as stated earlier, to throw light on two problems, the mass composition of the primary cosmic rays responsible for E.A.S., and those features of high energy collisions which are not accessible to examination by other means.

In order to understand the significance of experimental results it is necessary to have a model with which the effect of a change of, for example, some feature of high energy interactions on the sea-level characteristics of the shower may be examined. At the start of the present investigation there were no experimental results at large zenith angles to guide the development of a model. Consequently it has been necessary to perfect a model which will accurately predict the known features of near vertical showers and then to translate this to larger zenith angles.

The first step is to make a survey of all available results concerning high energy interactions from emulsion work, bubble and cloud chamber data. This means that the various spectra and the values assumed for parameters cannot be justified in themselves at the much higher

energies involved in E.A.S. However when these assumed values are used in conjunction with each other to form a shower model and the results concur with those observed experimentally, then there is, to some extent, justification for the individual parameters.

5.2 Interaction Length and Inelasticity

5.2.1 Nucleon-nucleus Collisions

There are two features to be discussed under this heading, the probability of such an interaction taking place and the elasticity of the interaction, these being inter-related.

It is important to note the difference between K_t and K_π, the former is the fraction of the incident particle energy given to all secondaries whereas K_π is the fraction taken by pions only. If λ_i is the interaction length for inelastic collisions and λ_a is the attenuation length then:-

$$\frac{\lambda_i}{\lambda_a} = 1 - (1 - K_t)^{\gamma - 1} \qquad (5.1)$$

where γ is the exponent of the differential primary spectrum.

There is some doubt as to the value of λ_i; experimental determinations by Walker et al. (1950) give $\lambda_i = 81 \pm 5$

$g.cm^{-2}$ whereas Bozoki et al. (1962) report a value of 73 ± 7 $g.cm^{-2}$. This parameter may also be calculated from a knowledge of the sizes of air nuclei and the magnitude of the elementary nucleon-nucleon cross section σ_i. Williams (1960) and Alexander and Yekutieli (1961, HFCRL-1089) have worked out the relation between λ_i and σ_i; using the inelastic cross section measured by Cocconi (1961) at 24 GeV, σ_i = 32 mb, λ_i is 93 $g.cm^{-2}$ for air. However, for the present work λ_i is required for much higher energies, it is thought that σ_i will approach 43 mb giving $\lambda_i \sim 80$ $g.cm^{-2}$. Udgaonkar and Gell-Mann (1962) using the Regge Pole hypothesis in the primary energy region $10\text{-}10^4$ GeV give λ_i = 70 $g.cm^{-2}$, however, they used a value of σ_i greater than the measured value, thus their value of λ_i is likely to be too short. Grigorov et al. (1966a) have measured the flux and energy of unaccompanied, charged, strongly interacting particles at mountain altitude by means of an ionisation calorimeter. This was compared with the flux of primary protons measured above the atmosphere by the satellite Proton I. They report $\lambda_i \lesssim 86 \pm 3$ $g.cm^{-2}$ for $E_p > 5\ 10^2$ GeV and falling smoothly with increasing energy until $\lambda_i \lesssim 64 \pm 4$ $g.cm^{-2}$ for $E_p \gtrsim 3\ 10^3$ GeV.

If we take a value of 80 g.cm^{-2} for λ_i, 120 g.cm^{-2} for λ_a and $\gamma = 2.58$ then substitution in equation (5.1) gives $K_t = 0.509$; Brooke et al. (1964) show that this is virtually energy independent. In a survey by these authors it is concluded that $K_t - K_\pi \sim 0.12$, that is, $K_\pi \sim 0.38$, and for the fluctuations in K_π, a distribution of the following form is assumed

$$F(K_\pi)dK_\pi = -(1+\alpha)^2 (1+K_\pi)^\alpha \ln(1-K_\pi)dK_\pi \qquad (5.2)$$

where $\alpha = 3.6$.

For K_t we replace K_π by K_t in the preceeding expression and put $\alpha = 1.43$.

5.2.2 Heavy nucleus-air-nucleus Collisions

The interaction cross section increases as the mass number of the incident nucleus increases, consequently, $\lambda_i = 15$ g.cm^{-2} for an iron nucleus. Bradt et al. (1966) suggest that only one of the 56 nucleons of an iron nucleus is involved in the first interaction and that the rest of the nucleons which are now fragmented continue with their original energy and have an interaction mean free path of 80 g.cm^{-2}.

Bradt and Rappaport (1967) have considered two cases:-

i) Complete fragmentation takes place in the first interaction.

ii) Alpha particles are produced in the first interaction and these fragment in a subsequent interaction.

They conclude that the change induced in the muon flux at sea-level is not significant.

5.2.3 Pion-air-nucleus Collisions

Most authors, at the time that this survey was carried out, agreed that these collisions are completely inelastic, that is to say, $\eta = 1$, the incident pion does not survive the interaction. However, the assumed value for the interaction mean free path varies considerably. Dedenko (1964) takes $\lambda_\pi = 80$ g.cm^{-2}, Hillas (1966) 100 g.cm^{-2} and Cowsik (1966) a value of 120 g.cm^{-2}.

5.3 The Multiplicity of Secondary Particles

A survey has been made of the experimental determinations of this parameter, and the results are shown in Figure 5.1. The lower primary energy events are bubble chamber interactions initiated by machine accelerated particles whilst those towards the upper end of the energy scale are observed in emulsions flown at high altitudes and are initiated by cosmic rays. Also shown in the figure are the relationships between the number of charged secondaries (n_s) and incident particle energy (E_p) used by various authors.

Caption for Figure 5.1

The number of charged secondaries as a function of incident particle energy, as reported by the following authors.

1 von Lindern (1961).

2 As 1.

3 Lal et al. (1962).

4 Dobrotin et al. (1962).

5 As 4.

6 As 4.

7 Lohrman et al. (1961).

8 As 4.

9 Abraham et al. (1963).

10 I.C.E.F. (1963).

11 Malhotra et al. (1966).

12 As 10.

13 Aly et al. (1960).

14 As 10.

The lines are due to the authors given in the key to the diagram.

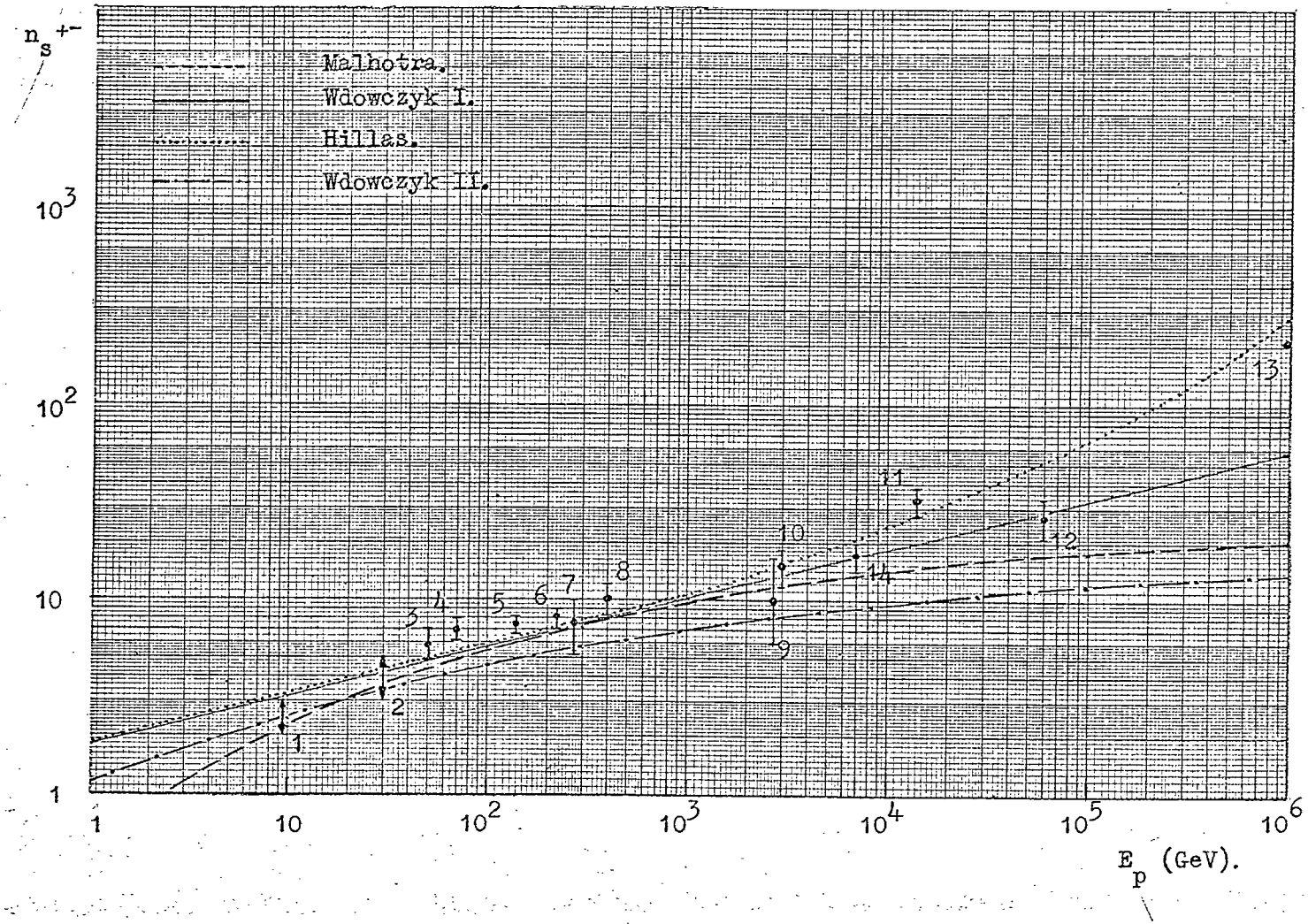
n_s^{+-}
Malhotra.
Wdowczyk I.
Hillas.
Wdowczyk II.
10^3
10^2
10
1
1
10
10^2
10^3
10^4
10^5
10^6
E_p (GeV).
1
2
3
4
5
6
7
8
9
10
11
12
13
14

Figure 5.1.

Some are simple power laws, for example, Wdowczyk I (1966),

$$n_s^{\pm} = 1.8\ E_p^{\frac{1}{4}} \qquad (5.3)$$

Others consist of compounded power laws, Hillas (1966)

$$n_s^{\pm} = 1.8\ E_p^{\frac{1}{4}} \quad \text{for} \quad E_p < 10^3 \text{ GeV}$$

$$n_s^{\pm} \propto E_p^{\frac{1}{2}} \quad \text{for} \quad E_p > 10^3 \text{ GeV} \qquad (5.4)$$

The other type of multiplicity law has a logarithmic form, for example,

Wdowczyk II (1966)

$$n_s^{\pm} = 1.0\ \ln(E_p+2) \qquad (5.5)$$

Malhotra (1964)

$$n_s^{\pm} = 1.6\ \ln \frac{E_p}{2.7} \qquad (5.6)$$

All of these relationships are in reasonable agreement with experiment for $E_p \lesssim 5\ 10^3$ GeV; above this energy they are at variance with each other and selection of the most suitable law is hindered by the dearth of experimental information.

5.4 The Energy Distribution of the Emitted Particles

5.4.1 Introduction

These may conveniently be divided into two groups, the 'one centre' and 'multi-centre' models. The former are exemplified by the theories of Fermi, Heisenberg and Landau in which the energy is confined in a small volume and then released in the form of created particles. In the multi-centre models, for example Kraushaar and Marks, Cocconi, Ciok et al. the collision leaves the nucleons in a highly excited state and there may be two or four regions moving with different velocities each capable of emitting mesons.

The fireball models emerged some eight or more years ago, from the study of cosmic rays in emulsions. Evidence to support the theories has been sparse and it is still not clear whether fireballs really exist. They may simply be a convenient way of describing peculiar angular distributions which may in fact have nothing to do with the formation of a massive body which subsequently decays isotropically into many lower energy secondaries.

5.4.2 The C.K.P. Model

This is an empirical model put forward by Cocconi et al. (1961) to account for the observed characteristics

of high energy interactions, in particular the observed energy spectrum of pions from the interaction of protons with light nuclei at machine energies. The relationship for the number of pions of one sign emitted in the forward direction in the C-system is:-

$$N(E_\pi)dE_\pi = \frac{A}{T} \exp\left(\frac{-E_\pi}{T}\right) dE_\pi \qquad (5.7)$$

where E_π is the energy of the pion in the L-system, A is the mean multiplicity of pions of one sign emitted in the forward direction in the C-system and T is the mean pion energy.

If E_p is the primary energy, then:-

$$A.T = \tfrac{1}{8} K_\pi . E_p \qquad (5.8)$$

They assume that the multiplicity follows the Fermi equation, $n \propto E_p^{\frac{1}{4}}$, where n is the total number of secondaries; if all of these are assumed to be pions, then $n = 6A$. The factor 6 is to allow for the three charge states of the pion and the 50% of pions emitted in the backward cone in the C-system, which they assume to have negligible energy in the L-system.

The transverse momentum distribution for pions follows, approximately, the Boltzman Law:-

$$f(p_t)dp_t = \frac{p_t}{p_o^2} \exp\left(\frac{-p_t}{p_o}\right)dp_t \qquad (5.9)$$

where the average value of p_t, $\langle p_t \rangle$, is equal to $2p_o$, they suggest that $\langle p_t \rangle$ should take a value in the range 0.4 - 0.45 GeV/c.

5.4.3 The Two-fireball Model

Huggett (1966) has re-examined the features of a symmetrical two-fireball model and compared its predictions with those of the C.K.P. model which is essentially a one centre model. The integral energy spectra of the secondaries in the L-system predicted by the two models are similar up to pion energies of ~600 GeV, ($E_p = 10^3$ GeV). Above this energy the two-fireball model has a tail which is higher than that of the C.K.P. model. Apart from this both models give similar features for many of the observable effects. The effect of the high energy tail would probably be to steepen the lateral muon density distribution and to decrease somewhat, at small zenith angles, the μ/e ratio, due to an increase in the number of sea-level electrons.

5.4.4 The Isobar Model

It has been suggested by many workers (e.g. Peters (1962)), that in high energy nucleon-nucleon collisions

the excitation of a baryon isobar may take place. This involves the production of massive excited bodies such as N^{*}, K^{*} and ρ mesons; the π mesons taking the role that β-particles and γ-rays play in nuclear interactions, namely the role of quanta emitted in subsequent transitions to a more stable state, for example, $N^{*} \rightarrow K + \bar{K} + N + n\pi$.

The properties of the model are best illustrated by reference to models of Cowsik (1966) and Pal and Peters (1964). They assume that the de-excitation proceeds via the emission of pions which carry away ~27% of the incident energy, these pions are emitted isotropically in the isobar rest frame, each having a unique energy, ~250 MeV in the C-system. The de-excitation leaves the nucleus with a flat energy spread of 35 → 70%, i.e. $\eta \sim 35 \rightarrow 70\%$, $\bar{\eta} = 53\%$. The remaining ~20% is taken up by a fireball which moves slowly in the C-system radiating nucleon-anti-nucleon pairs and pions isotropically. In pion-nucleon collisions, a fireball at rest in the C-system radiates as in an ordinary nucleon-nucleon collision.

At low energies they find that the major contribution to the muon component comes from the fireball or pionisation process, then the muons arising from the decay of the isobar take over.

However there is experimental evidence which is in disagreement. Grigorov et al. (1966b) have investigated showers with $E_p \gtrsim 2\ 10^3$ GeV using an ionisation calorimeter. They conclude that: direct investigation of interactions at particle energies $\sim 5\ 10^3$ GeV do not confirm the hypothesis of the production of high energy pions by isobar decay. Fowler and Perkins (1964) suggest that a further consequence of the model is that at very high energies the differential gamma-ray spectrum and the integral muon spectrum should both follow the differential primary spectrum, whereas, in fact, they are significantly steeper.

Thus it would seem that the probability of energetic pions being formed by the decay of a nucleon isobar is small.

5.4.5 The Persistent Baryon Model

Smorodin (1967) proposed that a number of inconsistencies in the experimental data on interactions between cosmic ray nucleons of >100 GeV and air nuclei could be removed if it is assumed that after interaction the nucleon goes to a passive state in which the cross-section for interaction is lower than normal. Analysis of experimental data suggests that the lifetime in the passive state should be in the order of 10^{-10} second and the interaction cross-section should be less than 0.1 to

0.2 of the normal value.

Erlykin et al. (1967) have reported investigations made with the Tien Shan ionisation calorimeter, situated at 20 m.w.e. underground, of the spectrum of ionisation bursts. The results show that the characteristics of the penetrating component do not differ from the properties of the muon component and do not give any indication of the existence of a passive baryon state.

5.5 The Charge Ratio

Spectrograph measurements of the charge ratio of muons in E.A.S. have been carried out by Bennett and Greisen (1961) and by Rochester et al. (1966). Both sets of measurements are consistent with a value which does not differ significantly from unity (at least for the bulk of the muons which come from pions emitted with rather small transverse momenta); this indicates the relative unimportance of K-meson production since these would give rise to a high plus to minus ratio.

5.6 Transverse Momentum

A survey of $\langle p_t \rangle$, the mean transverse momentum, of the secondary particles of an interaction is shown in Figure 5.2; this excludes the investigations to be discussed later in this section. It may be seen that all the values lie below ~0.7 GeV/c and that there is

Caption for Figure 5.2

The mean Transverse Momentum as a Function of Incident Particle Energy, as reported by the following authors.

1 Aly et al. (1959).
2 Blue et al. (1960).
3 Rajopadhye et al. (1960).
4 Grote et al. (1961).
5 Lukin et al. (1960).
6 Bozoki et al. (1962).
7 Peters (1962).
8 Fujioka (1961).
9 Hansen et al. (1960).
10 Dobrotin et al. (1962).
11 Edwards (1958).
12 Brisbout et al. (1961).
13 As 11.
14 As 11.
15 Schein et al. (1959).
16 As 11.
17 Minakawa et al. (1959).
18 Debenedetti et al. (1956).
19 Malhotra et al. (1966).
20 As 17.
21 As 11.
22 Awunor-Rennor et al. (1960).
23 Nishikawa (1959).
24 Akashi et al. (1966).
25 Hasagawa S. (1959).
26 Ciok et al. (1957).
27 Kazuno (1962).
28 Aly et al. (1960).

o refers to measurements on charged secondaries

□ refers to measurements on neutral secondaries which give rise to a e-γ cascade.

Figure 5.2.

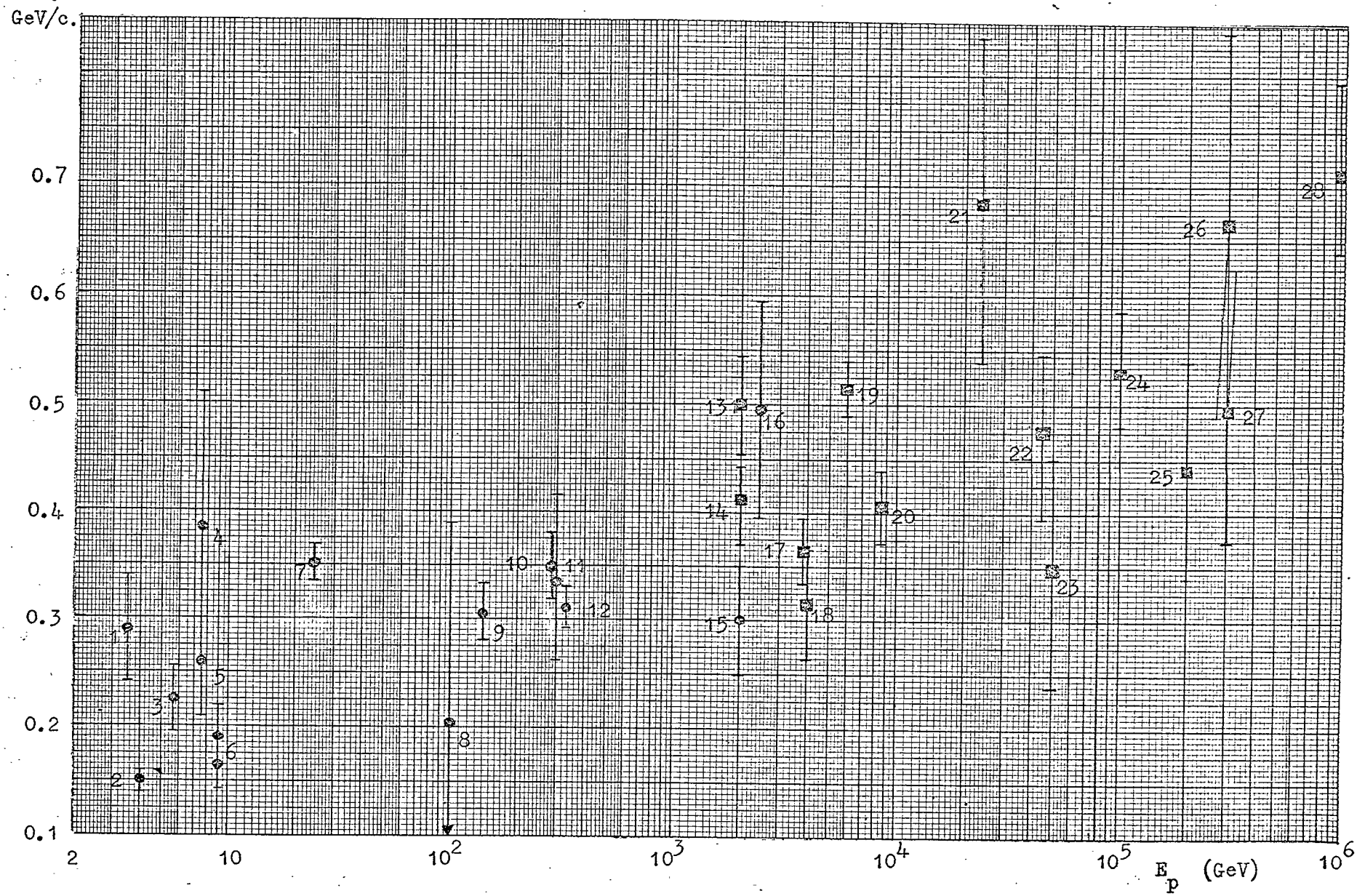

the suggestion of an increase of $\langle p_t \rangle$ with E_p.

The next consideration is the form of the transverse momentum distribution; three of these are illustrated in Figure 5.3 superimposed on, and normalised to the experimental histogram of Aly et al. (1964). The distributions, which are for pions, may be expressed mathematically as follows:-

C.K.P.

$$\text{I,} \quad N(p_t)dp_t = \frac{p_t}{p_o^2} \exp\left(-\frac{p_t}{p_o}\right) dp_t \qquad (5.10)$$

where $2p_o = \langle p_t \rangle = 0.4$ GeV/c.

Aly et al. (1964),

$$\text{II,} \quad N(p_t)dp_t = \frac{2p_t}{p_o} \exp\left(-\frac{p_t^2}{p_o}\right) dp_t \qquad (5.11)$$

where $2p_o = 0.43$ GeV/c.

Nikolskii (1963),

$$\text{III,} \quad N(p_t)dp_t = \frac{p_t^2}{2a^3} \exp\left(-\frac{p_t}{a}\right) dp_t \qquad (5.12)$$

where $a = 0.105$ GeV/c.

There is, however, evidence for the existence of higher values of $\langle p_t \rangle$ for pions although some results will be contaminated by nucleons. Hasegawa et al. (1966) have analysed bursts recorded in shielded scintillators, they report that a distribution of type I is consistent

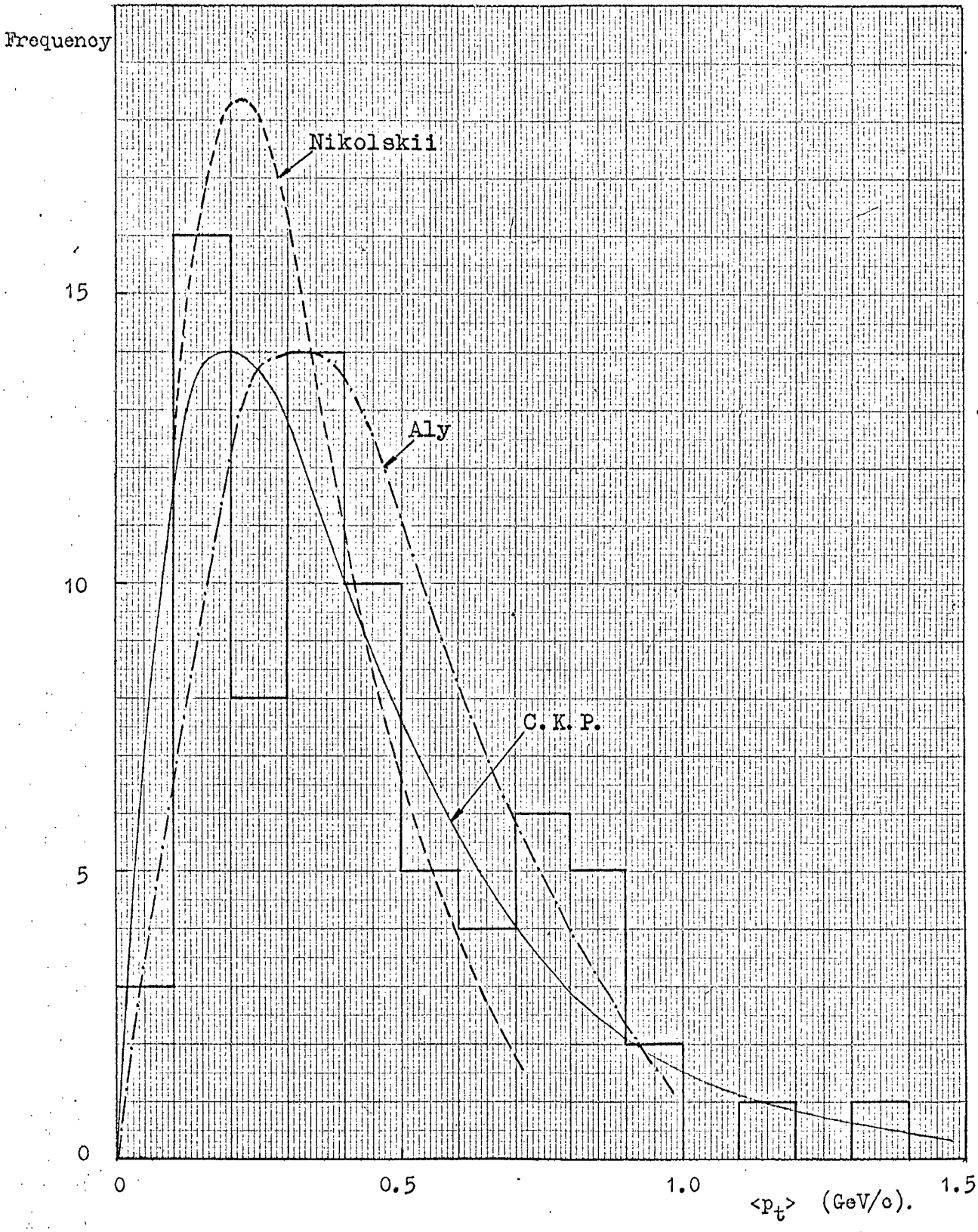

Fig. 5.3 Various transverse momentum distributions superimposed on and normalised to an experimental distribution due to Aly et al. (1964).

with their measurements for $\langle p_t \rangle \lesssim 1$ GeV/c. Among the 5000 showers with $N_e \gtrsim 5\ 10^6$ there were two large bursts with $\langle p_t \rangle$ values of 1.9 GeV/c and 1.4 GeV/c. The conclusion reached is that nuclear active particles with a value of $p_t \gtrsim 2$ GeV/c are 100 times more abundant than expected from a type I distribution. This is supported by Shibata et al. (1966) who have analysed double core events observed in a 20 m^2 spark chamber, they have events with $\langle p_t \rangle$ = 47, 21, 14 and 6.5 GeV/c. The authors estimate that the minimum probability of occurrence of large p_t ($\gtrsim$5 GeV/c) in interactions above 10^4 GeV is 10^{-3} which is to be compared with 10^{-8}, this being the probability derived from a type I distribution. Miyake et al. (1966) also report p_t values in the range 1 GeV/c to a few tens of GeV/c from their observations of shower cores.

A further discussion of this important question of the p_t-distribution will be given later.

5.7 Methods of Computation

There are basically two methods of computation which may be used to examine the propagation of extensive, cosmic ray initiated, air showers. These are the diffusion method and the step by step method, that is to say, analytical and numerical. Both of these methods have

been used in the present work and will be described in the following chapters. However, it might be advantageous at this stage to give a brief review of the models used by other authors over the last few years, and the features of E.A.S. which they have investigated. This will give some idea of the vast scope available when choosing the parameters of the model and in deciding how to manipulate these.

The problem of the nature of the primary particles has been studied by Bradt et al. (1966), using both the two-fireball and isobar models. The same problem has been examined by Thielheim and Karius (1966) using a Monte Carlo treatment, with fireball and isobar models, to investigate the production of multicore events. This model had only limited success due to lack of knowledge concerning the high energy tail of the production spectrum.

Turning to the muon component, Wdowczyk (1966), using an analytical method, has investigated the number of muons produced by primary photons. It is interesting to note that this author used both power law and logarithmic law for the multiplicity of secondaries and shows that the former gives a much wider muon density distribution with a mean density approximately three times that for the logarithmic dependence. Cowsik (1966) has examined the high energy muon and nuclear active particle component of E.A.S.

and developed an isobar model in which a large fraction of the non-pions produced in high energy interactions are assumed to be nucleon-anti-nucleon pairs. Khristiansen et al. (1966) have investigated the effect of a wide range of models by noting the sensitivity to changes in λ_π, the multiplicity law, energy spectrum of secondaries, inelasticity and allowing the possibility of isobar production. They have not compared their results with experiment and consequently do not make any conclusions regarding the values of the parameters.

Hillas (1966) has presented results obtained by employing the numerical method, he has derived the lateral distribution, energy spectrum and heights of origin of muons. The model employs fixed interaction points for the leading nucleon and a C.K.P. pion production spectrum. Multiplicity is proportional to $E_i^{\frac{1}{4}}$ for $E_i < 3\ 10^3$ GeV, where E_i is the incident particle energy, and proportional to $E_i^{\frac{1}{2}}$ above this value. Coulomb scattering and geomagnetic deflection have been examined and it is concluded that their effect is less than 2% for vertical showers, but it could be quite considerable at large zenith angles. An important feature of this model is that energy loss by the muon whilst traversing the atmosphere is taken into consideration, this means that the predictions of the model should be valid for muon threshold energies down to a few GeV.

CHAPTER 6

Theoretical Studies of Near Vertical E.A.S.

6.1 The Adopted Model Parameters

As mentioned in the previous chapter it is necessary to choose a model which will give consistency with observations made in the vertical direction.

Following the conclusions resulting from the survey of Chapter 5 the followingwere assumed initially, any deviation from these values being mentioned at the appropriate point in the text.

i) High energy nucleons lose, on average, 50% of their energy in each collision and have an interaction mean free path of 80 $g.cm^{-2}$, both of the quantities being energy independent.

ii) The secondary particles produced in the interaction of protons or pions are entirely pions and there are equal numbers of π^+, π^- and π^o mesons.

iii) These secondary pions have an energy distribution in the laboratory system given by the C.K.P. relationship, with allowance being made for pions emitted in the backward cone.

$$S(E_\pi, E_o) = \tfrac{1}{2}\left\{\frac{n(E_o)}{T}\exp\left(\frac{-E_\pi}{T}\right) + \frac{n(E_o)}{G}\exp\left(\frac{-E_\pi}{G}\right)\right\} \quad (6.1)$$

where $n(E_o)$ is the multiplicity of pions produced, E_o being the transferred energy. G is the average energy in the L-system of the backward cone pions and

$$T = 2\left[E_o - n(E_o)\frac{G}{2}\right]\left[n(E_o)\right]^{-1} \quad (6.2)$$

which is the average energy of those in the forward cone.

iv) The multiplicity of pions produced is given by:-

$$n_s = 2.7\ E_p^{\frac{1}{4}} \text{ with } E_p \text{ in GeV for } K = 0.5$$

$$\text{or } n_s = 2.7\ 2^{\frac{1}{4}}.(KE_p)^{\frac{1}{4}} \text{ for all K.} \quad (6.3)$$

The effects of variation of the coefficient and the index of the power law are considered.

v) The distribution in transverse momentum, p_t, of the produced pions is given by the expression suggested by Cocconi et al. (1961):-

$$N(p_t)dp_t = \frac{p_t}{{p_o}^2}\exp\left(\frac{-p_t}{p_o}\right)dp_t \quad (6.4)$$

The mean transverse momentum, $\langle p_t \rangle = 2p_o$, is assumed to be independent of energy and equal to 0.4 GeV/c. As will be seen later, p_o is regarded as a variable in interpreting the results.

vi) Pion interactions are assumed to differ from nucleon interactions in that they are catastrophic, with an interaction length of 120 $g.cm^{-2}$. The energy spectrum of pions produced in pion interactions is taken to be the same as that for proton interactions with K = 1, i.e., $n_s = 3.2\ E_p^{\frac{1}{4}}$.

vii) When fluctuations are allowed they may be in the depths and number of interactions of the leading particle and in some cases variations are allowed in the inelasticity of nucleon-air-nucleus collisions. The adopted form of the inelasticity distribution is:-

$$f(K) = -(1+\alpha)^2\ (1-K)^{\alpha}\ \ln(1-K) \qquad (6.5)$$

where $\alpha = 1.414$.

viii) In $\pi-\mu$ decay the energy of the muon is taken to be 0.76 of the pion energy.

ix) When considering heavy primaries of mass A and energy E_p, it is assumed that these produce A separate showers, each initiated by a primary nucleon of energy E_p/A, the first interaction being at the appropriate depth for a nucleus of mass A.

6.2 The Method of Computation Adopted

The properties of the atmosphere and the notation used in the calculations are described in Appendix B.

6.2.1 The Hard Component

Consider the charged pions, if it is assumed that none survive to sea-level then each must either interact with an air-nucleus or decay to a muon.

The probability (P_{π_I}) of a pion interacting in traversing 1 g.cm^{-2} of atmosphere is given by:-

$$P_{\pi_I} = \frac{1}{1 + \frac{B_\pi \lambda_\pi}{E_\pi x}} \qquad (6.6)$$

where x is the depth at which the pion is produced, the decay coefficient, B_π, is given by:-

$$B_\pi = \frac{M_\pi c\ h_o}{\tau_\pi} \qquad (6.7)$$

where the atmospheric scale height is:-

$$h_o = \frac{x}{\rho(x)} \qquad (6.8)$$

Substitution of numerical values in (6.6), and using $\lambda_\pi = 120$ g.cm^{-2}, gives:-

$$P_{\pi_I} = \frac{1}{1 + \frac{2.14\ 10^{-2}}{\rho(x) E_\pi}} \qquad (6.9)$$

The probability that a charged pion will decay, rather than interact is therefore given by:-

$$P_{\pi_D} = 1 - P_{\pi_I} \qquad (6.10)$$

In almost 100% of the cases the decay process is

$$\pi^{\pm} \rightarrow \mu^{\pm} + \nu(\bar{\nu})$$

The muons produced have a flat energy distribution from $r^2 E_\pi$ to E_π where $r = (M_\mu/M_\pi) \approx 0.76$.

In all problems involving the propagation of muons through the atmosphere, especially if we are interested in low energy muons, energy loss in traversing the atmosphere to sea-level must be allowed for.

For $E_\mu < 0.504/[\rho(x)]^{\frac{1}{2}}$ GeV

$$-\left(\frac{\partial E_\mu}{\partial x}\right) = 2.137\ 10^{-3} + 7.66\ 10^{-5}\left\{\ln E_m + 2\ln E_\mu + \tfrac{1}{4}\left[\frac{E_m}{E_\mu + 0.106}\right]^2\right\} + 2.73\ 10^{-6} E_\mu \text{ GeV g}^{-1}\text{cm}^2 \qquad (6.11)$$

otherwise,

$$-\left(\frac{\partial E_\mu}{\partial x}\right) = 2.109\ 10^{-3} + 7.66\ 10^{-5}\left\{\ln E_m + \tfrac{1}{4}\left[\frac{E_m}{E_\mu + 0.106}\right]^2 - \ln\rho(x) - \frac{0.2538}{E_\mu^2 \rho(x)}\right\} + 2.73\ 10^{-6} E_\mu \text{ GeV g}^{-1}\text{cm}^2 \qquad (6.12)$$

where,

$$E_m = E_\mu^2\left[E_\mu + \frac{M_\mu^2 c^2}{2m_e}\right]^{-1} \qquad (6.13)$$

is the maximum transferrable energy from a muon to an electron.

In addition to the energy loss it is essential to take into account the loss of muons via decay, the muon survival probability is given by:-

$$SP(x,E_o,\theta) = \exp\left[\frac{-M_\mu c^2}{c\tau_\mu}\int_o^{x_o} \frac{\sec\theta^*}{E_\mu(x',E_o,\theta)}\,\frac{dx'}{\rho(x')}\right] \quad (6.14)$$

where $\sec\theta^* dx' = dl$, the increment in atmospheric depth along the trajectory.

As an example, the muon survival probabilities for $\theta = 0^o$ are shown in Figure 6.1.

In the calculation the atmosphere is divided into cells of 12 $g.cm^{-2}$ starting at sea-level, the energy loss and survival probability for muons traversing each cell is determined. The total energy loss in going from the upper boundary of a cell to sea-level is the sum of the energy losses in the individual cells below the boundary. The survival probability is the product of the individual probabilities. A matrix is thus produced and the energy loss and survival probabilities for muons produced at intermediate depths may be obtained by a three point interpolation procedure.

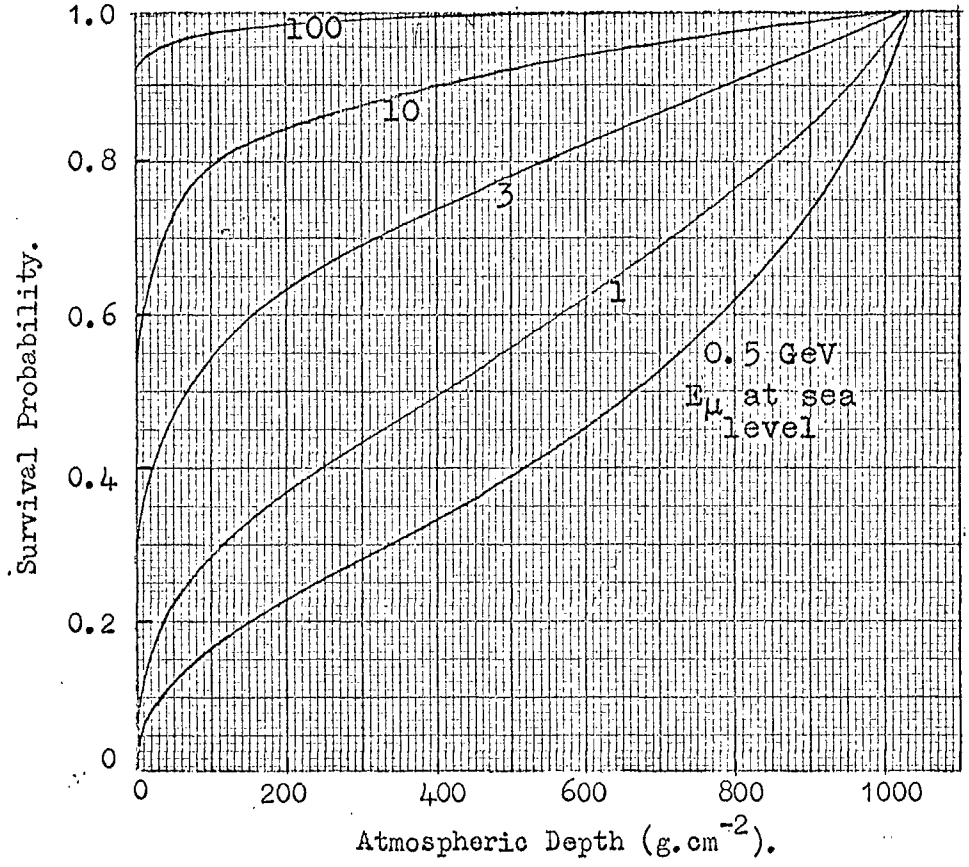

Fig. 6.1 The muon survival probability as function of threshold energy at sea-level and production depth, for $\theta = 0^\circ$.

6.2.2 The Soft Component

A contribution to the soft component is made by the decay of the uncharged pions produced in nucleon-nucleus and pion-nucleus interactions, in 98% of these decays the neutral pion goes to two gammas. It may be shown that an accurate result follows if it is assumed that one gamma-ray takes $\sim 0.8\ E_{\pi^0}$, and the other $\sim 0.2\ E_{\pi^0}$. The conversion from gamma ray energy to number of electrons at sea-level may be made via the formulae given by Snyder (1949):

$$N_e(t,E_\gamma) \simeq \frac{0.31}{\left[\ln(E_\gamma/\epsilon_c)\right]^{\frac{1}{2}}} \exp\left[t(1-3/2\ \ln S)\right] \qquad (6.15)$$

where ϵ_c is the critical energy in air, 84 MeV; t is the number of radiation lengths between the point at which the gamma was produced and sea-level, that is,

$$t = \frac{x_o(\theta)-x}{X_o} \qquad (6.16)$$

where X_o is one radiation length, in air $X_o = 37.7\ g.cm^{-2}$. The age parameter is:-

$$S = \frac{3t}{t+2\ln(E_\gamma/\epsilon_c)} \qquad (6.17)$$

Application of these formulae to all the gammas produced in a shower and summation of the resulting number of electrons will give the total number of

electrons at sea-level produced as a result of π^0 decay.

The electrons resulting from the decay of muons do not contribute significantly to the total flux as their energy at production is of the order of 50 MeV which is less than the critical energy. The contribution to the electron flux due to the electro-magnetic interaction of muons is neglected.

6.2.3 The Analytical Method of Calculation

The diffusion equations used are described in Appendix C; they are based on models of E.A.S. developed by various authors (e.g. Dedenko and Zatsepin, 1959) to evaluate the characteristics of the electromagnetic component.

The main feature of the model is the individual treatment of the cascades initiated by each interaction of the leading particle. Direct calculation of those features was not practicable because of the computing time involved. Consequently preliminary calculations were made in order to build up a lattice of 36 parameters as a function of the energy released and the depth at which this took place, the steps chosen were 0.5 in the logarithm of the primary energy and 180 $g.cm^{-2}$ in atmospheric depth. By means of third degree polynomial interpolation, the characteristics of any interaction

could be determined. The 36 parameters are, the total number of electrons and the total number and first six moments of the lateral distribution of muons for energy thresholds of 1, 3, 10, 30 and 100 GeV.

The effects of ionisation loss, μ-e decay and the variation of scale height with depth are allowed for, consequently the results should be valid down to muon threshold energies of a few GeV.

6.2.4. The Numerical Method of Calculation

Each interaction of the leading particle is again treated separately, the pions produced go to 'pion production levels', the first of these being at 80 g.cm^{-2} and succeeding ones at multiples of 120 g.cm^{-2} below this, see Figure 6.2. If a leading particle interaction level does not coincide with one of the pion production levels then an appropriate fraction of the pions go to each of the two nearest production levels, those being the one above and the one below the interaction level. Since λ_π = 120 g.cm^{-2} the pion interaction levels will always be in phase with the already established production levels, consequently no adjustment will be necessary. Ionisation loss and μ-e decay probability are again taken into account.

The computer output from the first stage of the calculation consists of the total number of electrons and

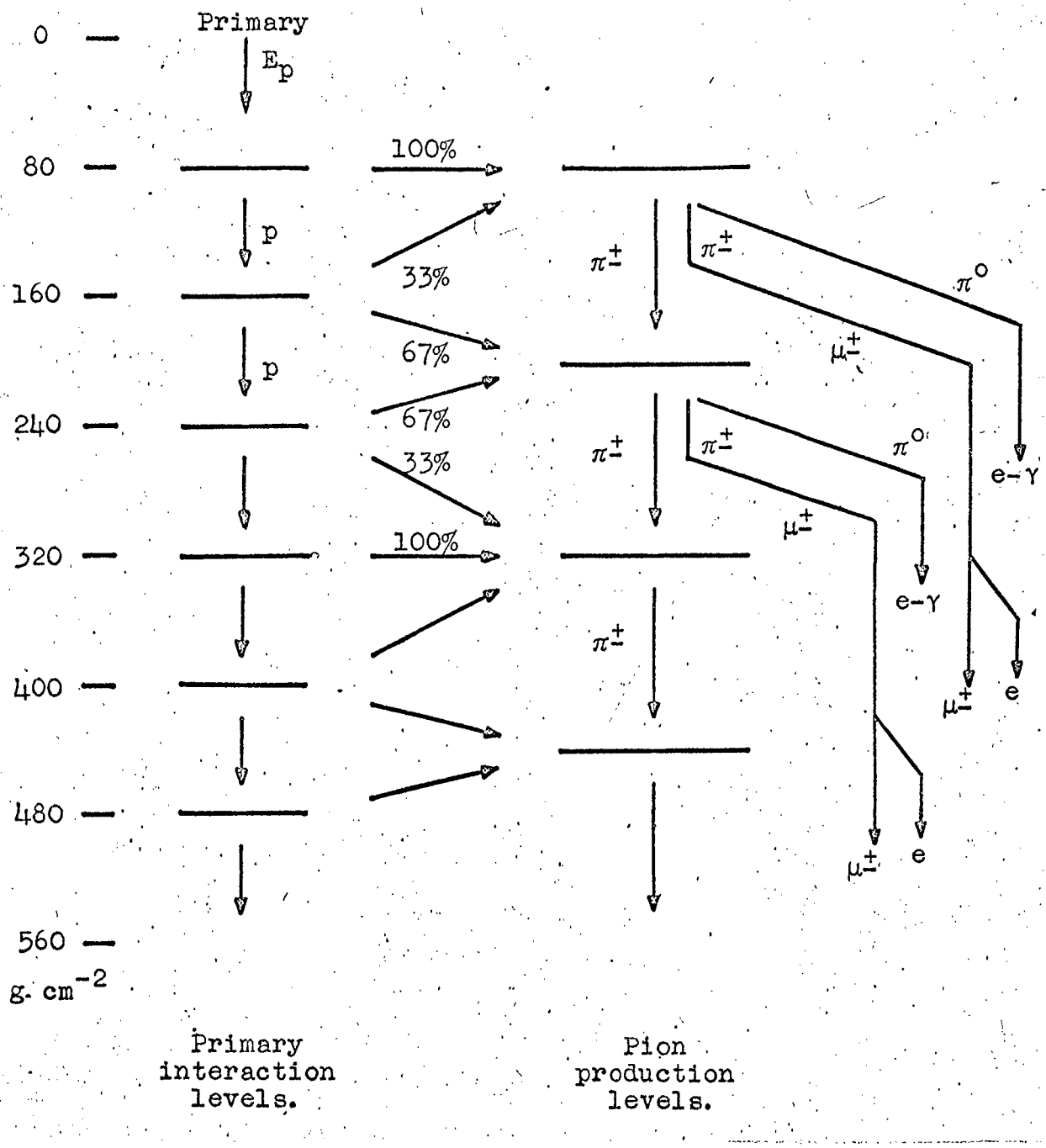

Fig. 6.2 The numerical method of calculation.

the number of muons from each production level as a function of energy. These results may then be processed by the introduction of a transverse momentum distribution to give the sea-level lateral density distribution for the desired threshold energies.

In order to calculate the lateral distribution, the muons from each production level are divided into energy cells whose widths increase as 0.1 in the logarithm of the primary energy. Each cell of muons has the C.K.P. transverse momentum impressed on it, the method of doing this is to consider annular rings at sea-level, about the core, having mean radii r_1, r_2, ... r_n. The probability of this cell of muons falling in the annulus denoted by r_1 is determined, similarly for r_2 ... r_n; the muons in the cell are than allocated to these annulii according to the determined probabilities. Their contribution to the particle density in the annulus is calculated by dividing the number by the area of the annulus. This procedure is repeated for all the energy cells from all production levels and the resulting densities are summed.

6.3 The Characteristics of Showers for Primaries of Unique Energy

The sensitivity of shower characteristics to the parameters of the model may be examined by studying the

average values of the muon and electron components at sea-level for primaries of unique energy. The parameter to which the total numbers of particles are particularly sensitive is the multiplicity law, accordingly calculations are made for the three following cases:-

I $n_s = 3.2\ (K.E_p)^{\frac{1}{4}}$

II $n_s = 2.72\ (K.E_p)^{\frac{1}{4}}$

III $n_s = 3.2\ (K.E_p)^{\frac{1}{4}}$ for $E_p \lesssim 2\ 10^3$ GeV and

$n_s = 0.57\ (K.E_p)^{\frac{1}{2}}$ at higher energies.

A property of many E.A.S. arrays is that they have an acceptance which leads to an average zenith angle of detected showers in the region of 30^o; consequently, calculations have been made both for vertical showers and for showers at 30^o to the zenith.

After the average shower properties have been examined the effect of fluctuations is considered.

6.3.1 The Total Number of Muons and Electrons for Primary Protons

The variations with primary energy of the total number of electrons, (N_e), and muons, (N_μ), for vertical showers and for $\theta = 30^o$ for primary protons and model I are shown in Figure 6.3.

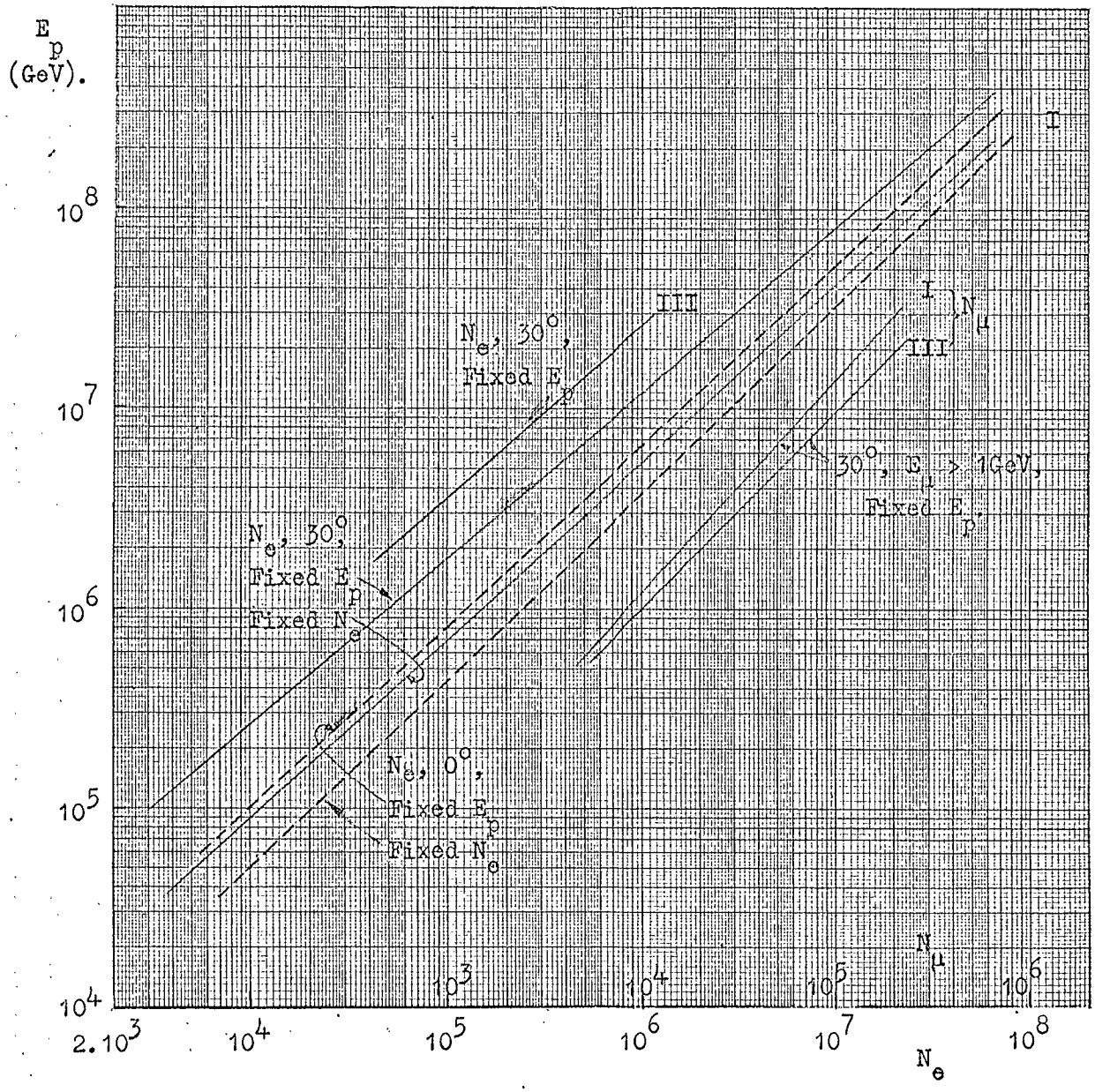

Fig. 6.3 The variation in the number of electrons, N_e, and number of muons, N_μ, with primary energy, E_p. The Roman numerals refer to the various models and the angles are the zenith angles of the showers. Results for the showers initiated by primaries of fixed energy are denoted by 'Fixed E_p' and the mean primary energies for showers of fixed size are denoted by 'Fixed N_e'.

Using model II, instead of model I, again with primary protons, and at $\theta = 30^{\circ}$, the effect is to increase N_e by 20%, to reduce N_μ by 20% at 1 GeV and leave N_μ unchanged at 100 GeV. Thus, the N_μ/N_e ratio for $E_\mu \geq 1$ GeV decreases by $\sim 40\%$. Model III produces much larger changes, for example, at $E_p = 10^7$ GeV and $\theta = 30^{\circ}$, the N_μ/N_e ratio for $E_\mu \geq 1$ GeV is 19% compared with 9.2% for model I.

Comparing these results it may be noticed that there is a reduction in the number of electrons at sea-level with increasing multiplicity. The reason for this is that higher multiplicity gives rise to a greater number of secondary pions with a corresponding lower mean energy. Two neutral pions with energy E are not as efficient as electron producers as one of energy 2E; consequently the e-γ cascade will be reduced by an amount which is not completely offset by the increased number of pions.

6.3.2 The Total Number of Muons and Electrons for Primary Heavy Nuclei

The ensuing shower may be considered as the superposition of A showers of energy E_p/A; the dependence on E_p of N_μ and N_e is such that N_e will be reduced and N increased. For example, for $E_p = 10^7$ GeV, $\theta = 30^{\circ}$ and A = 20, the N_μ/N_e ratio for $E_\mu \geq 1$ GeV is 27% compared with the 9.2% for protons, using model I in each case.

6.3.3 The Lateral Distribution of Muons for Primary Protons

The results on the lateral distribution at 30° are shown in Figure 6.4. Integrating over the lateral distribution for each threshold energy, the overall energy spectrum may be determined. It is found that the spectra for the three models are similar in shape; if the spectra are normalised at 1 GeV then only above 30 GeV do the intensities differ significantly, as may be seen in Table 6.1.

Table 6.1

The integral energy spectrum of muons for primary protons, $E_p = 2\ 10^7$ GeV, $\theta = 30^{\circ}$; the numbers in the body of the table are relative intensities.

Muon Energy	1 GeV	3 GeV	10 GeV	30 GeV	100 GeV
Model No					
I	1.00	0.62	0.28	0.092	0.017
II	1.00	0.63	0.30	0.125	0.027
III	1.00	0.62	0.29	0.099	0.021

6.3.4 The Lateral Distribution of Muons for Primary Heavy Nuclei

Table 6.2 shows that the muon lateral distribution is a little flatter for showers initiated by heavy primaries than it is for proton primaries. The reason for this is

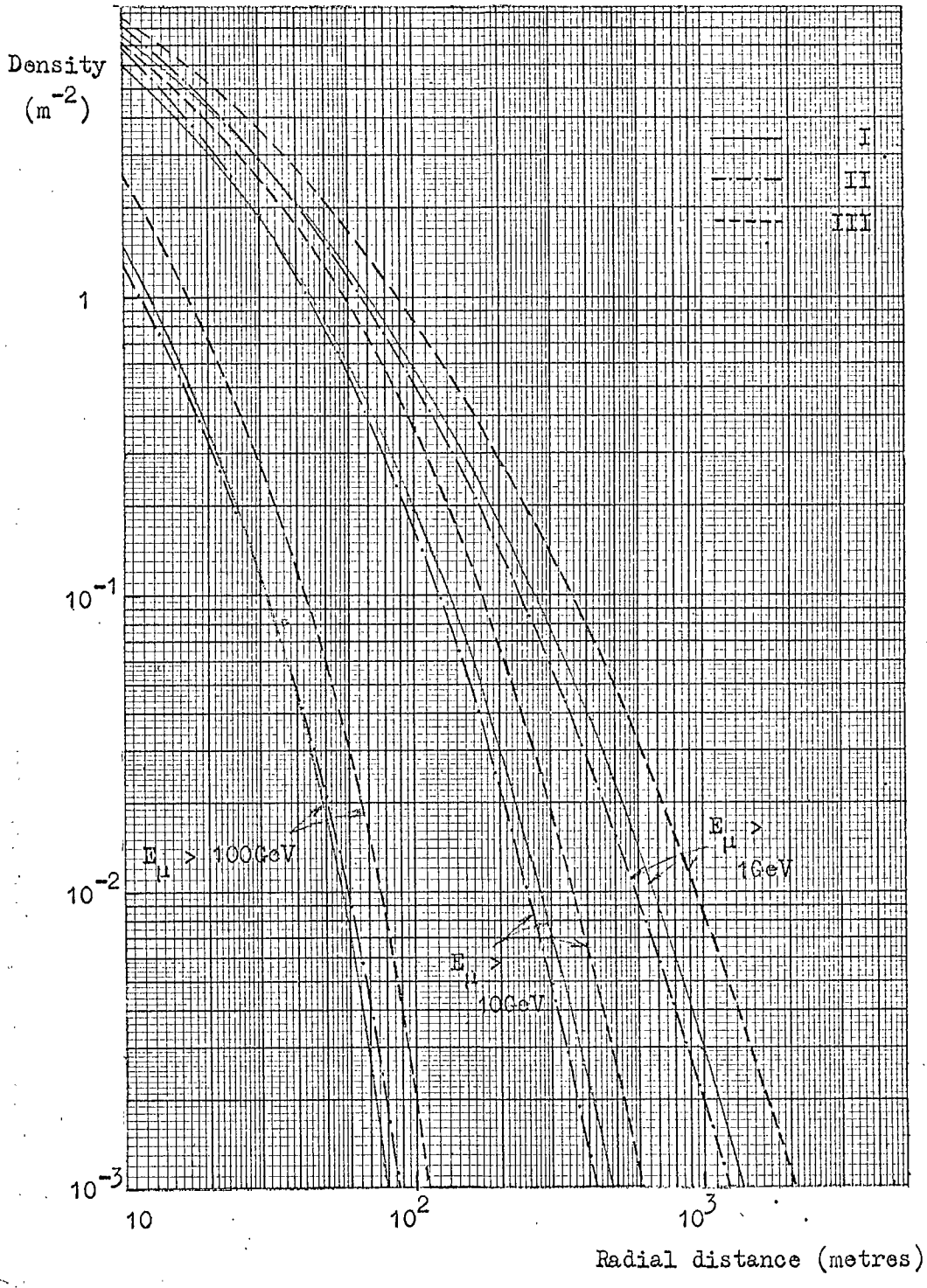

Fig. 6.4 The lateral distribution of muons in showers at 30° to the zenith initiated by primary protons of 2.10^7 GeV.

that the effective height of production is greater than for proton initiated showers due to the heavy nucleus traversing a much smaller thickness of atmosphere before making its initial interaction.

Table 6.2

Comparison of the lateral distributions for proton and heavy primary (A = 20) initiated showers, $E_p = 2\ 10^7$ GeV. $\theta = 30^o$. The total number of muons is normalised to unity.

Threshold Energy (GeV)	Number of muons per m^2 A = 1	A = 20	Distance from core (metres)
	$8.8\ 10^{-5}$	$7.9\ 10^{-5}$	10
	$2.7\ 10^{-5}$	$2.4\ 10^{-5}$	30
1	$4.5\ 10^{-6}$	$4.4\ 10^{-6}$	100
	$4.9\ 10^{-7}$	$5.2\ 10^{-7}$	300
	$1.2\ 10^{-8}$	$1.5\ 10^{-8}$	1000
	$2.7\ 10^{-4}$	$2.2\ 10^{-4}$	10
	$5.4\ 10^{-5}$	$5.4\ 10^{-5}$	30
10	$4.3\ 10^{-6}$	$5.0\ 10^{-6}$	100
	$1.1\ 10^{-7}$	$1.5\ 10^{-7}$	300
	$6.0\ 10^{-4}$	$6.4\ 10^{-4}$	10
100	$2.8\ 10^{-5}$	$4.0\ 10^{-5}$	30
	$8.5\ 10^{-8}$	$1.6\ 10^{-7}$	100

6.3.5 The Mean Height of Muon Production

Figure 6.5 shows the number of muons reaching sea-level from various production depths. It may be seen that the mean height of production increases with increasing muon threshold energy at sea-level.

6.3.6 The Distribution of N_e

It has been shown, de Beer et al. (1967a), that the largest contribution to the width of the N_e distribution for a fixed primary energy comes from fluctuations in the interaction depths of the primary. The profound effect of these fluctuations is well known and the significance of the depth of the first interaction has been realised. The next largest contribution arises from fluctuations in the inelasticity from one interaction to the next. Two distributions have been investigated, the preferred one of Brooke et al. (1964) and one with more violent fluctuations in which it is assumed that f(K) is constant from K = 0 to K = 1; the resulting distributions are not very different.

The results of a Monte-Carlo analysis, incorporating both types of fluctuations, for electrons at sea-level due to proton primaries for both vertical showers and showers at $\theta = 30^{\circ}$ are shown in Figure 6.6. An illustration of the basic data from which the smooth curves are

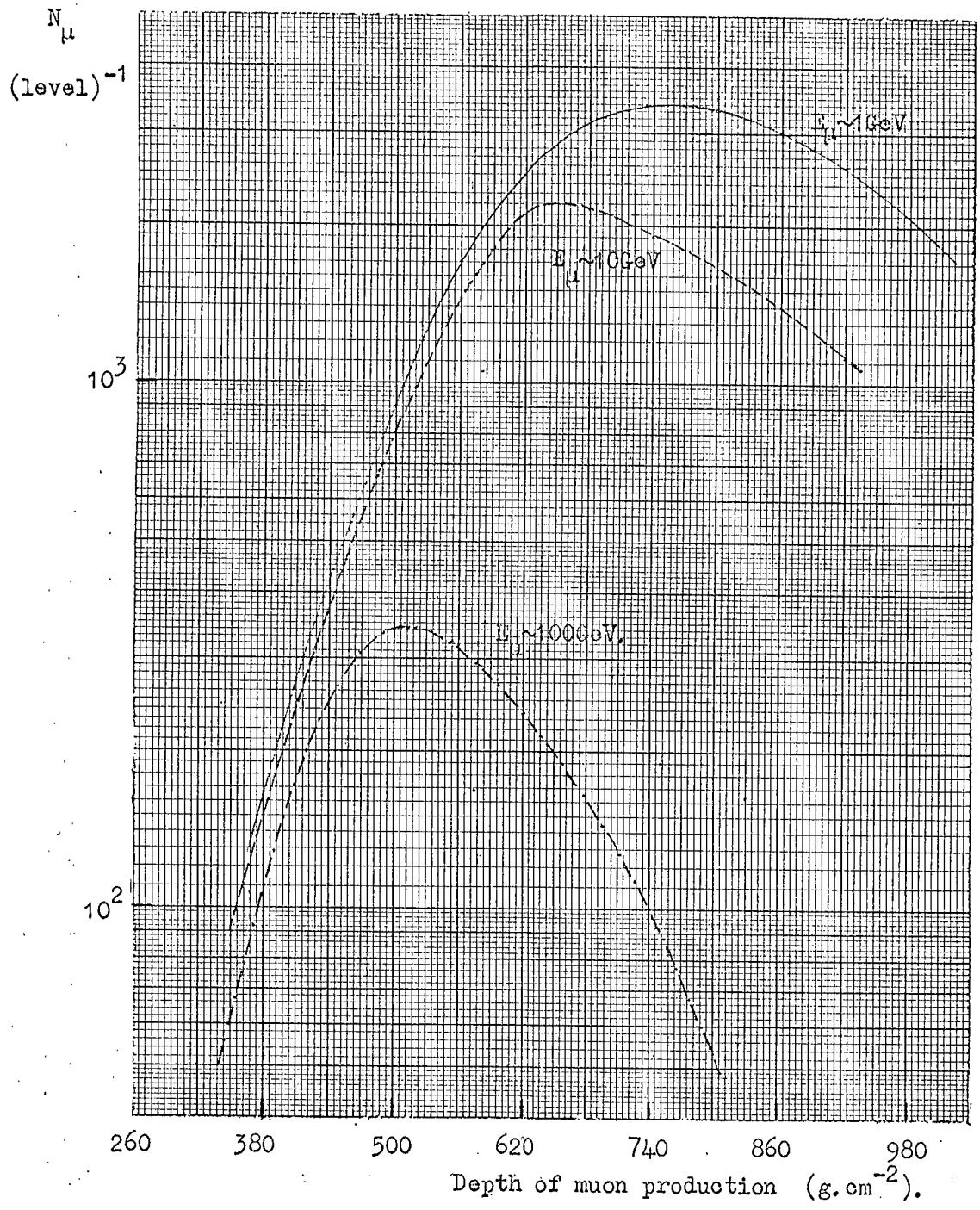

Fig. 6.5 The number of muons per production level for a shower initiated by a primary of 2.10^7GeV at a zenith angle of 0^o, for three threshold energies.

Caption for Figure 6.6

Frequency distributions of electron number, N_e, for fixed values of primary energy for vertical and 30^o showers. Smooth curves have been drawn through the predicted histograms, one histogram is shown in order to give an indication of the statistical accuracy of the calculations.

Figure 6.6.

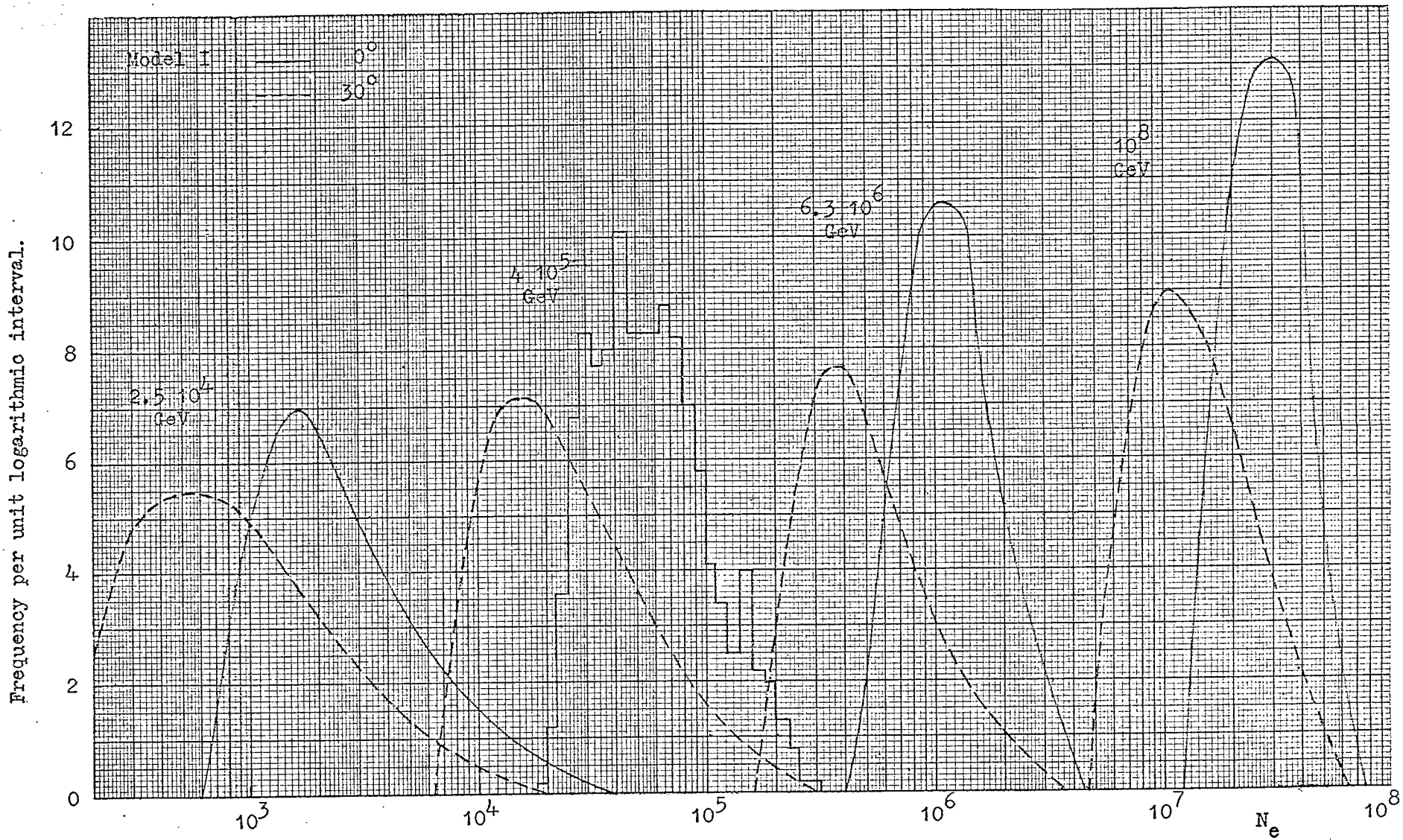
Model I
0°
30°
2.5 10^4 GeV
4 10^5 GeV
6.3 10^6 GeV
10^8 GeV
Frequency per unit logarithmic interval.
0
2
4
6
8
10
12
10^3
10^4
10^5
10^6
10^7
10^8
N_e

drawn is shown for one value of E_p. The reduction in width in going from $\theta = 30^\circ$ to 0° and on increasing the energy of the primary is very marked; both arise because these changes give closer proximity to the shower maximum, where fluctuations are a minimum.

If the primaries are heavy nuclei, instead of protons, the width of the distributions are reduced considerably. A measure of the magnitude of the fluctuations may be achieved by taking the width of the N_e distribution at one-tenth peak height on a logarithmic plot and dividing by N_e. Table 6.3 shows such values for three values of A for a primary energy of 10^6 GeV.

Table 6.3

The width of the electron size distribution for primaries of energy 10^6 GeV for showers at 30°.

A	Width at $\frac{1}{2}$ height	Width at $^1/_{10}$ height
1	5	20
4	2.5	8
20	1.2	3

This large reduction in width for heavier nuclei offers the prospect that experimental studies of fluctuations might give some information on the mass composition of primary cosmic rays.

6.3.7 The Distribution of N_μ

The fluctuation in the number of muons from shower to shower, for primaries of unique mass and energy, is very small. Distributions for three threshold energies at $\theta = 0^\circ$ and 30° are shown in Figure 6.7 for $E_p = 10^7$GeV. The widths are approximately a factor of 4 narrower than for electrons and fairly insensitive to zenith angle and threshold energy. For heavy primaries the distributions are even narrower and may be approximated to delta functions.

Although the variation in the total number of muons may not be very great, there are considerable fluctuations in the lateral distribution of muons. The significance of this is that in many experiments although the electrons are sampled by many detectors distributed over the shower front, the muons are detected only by a small number of detectors (often only one) and these are quite commonly close to the axis. In addition to calculating the total number, the mean distance ($\bar{r}$) of muons from the shower axis has been determined. Figures 6.8 and 6.9 show histograms of the frequency distribution for N_e/N_μ and $N_e\ \bar{r}^2/N_\mu$ for muon threshold energies of 1 and 10 GeV; the considerable reduction in width for $N_e\ \bar{r}^2/N_\mu$ is evident. The significance of $N_\mu/\bar{r}^2$ is that it is, approximately, proportional to the average density of

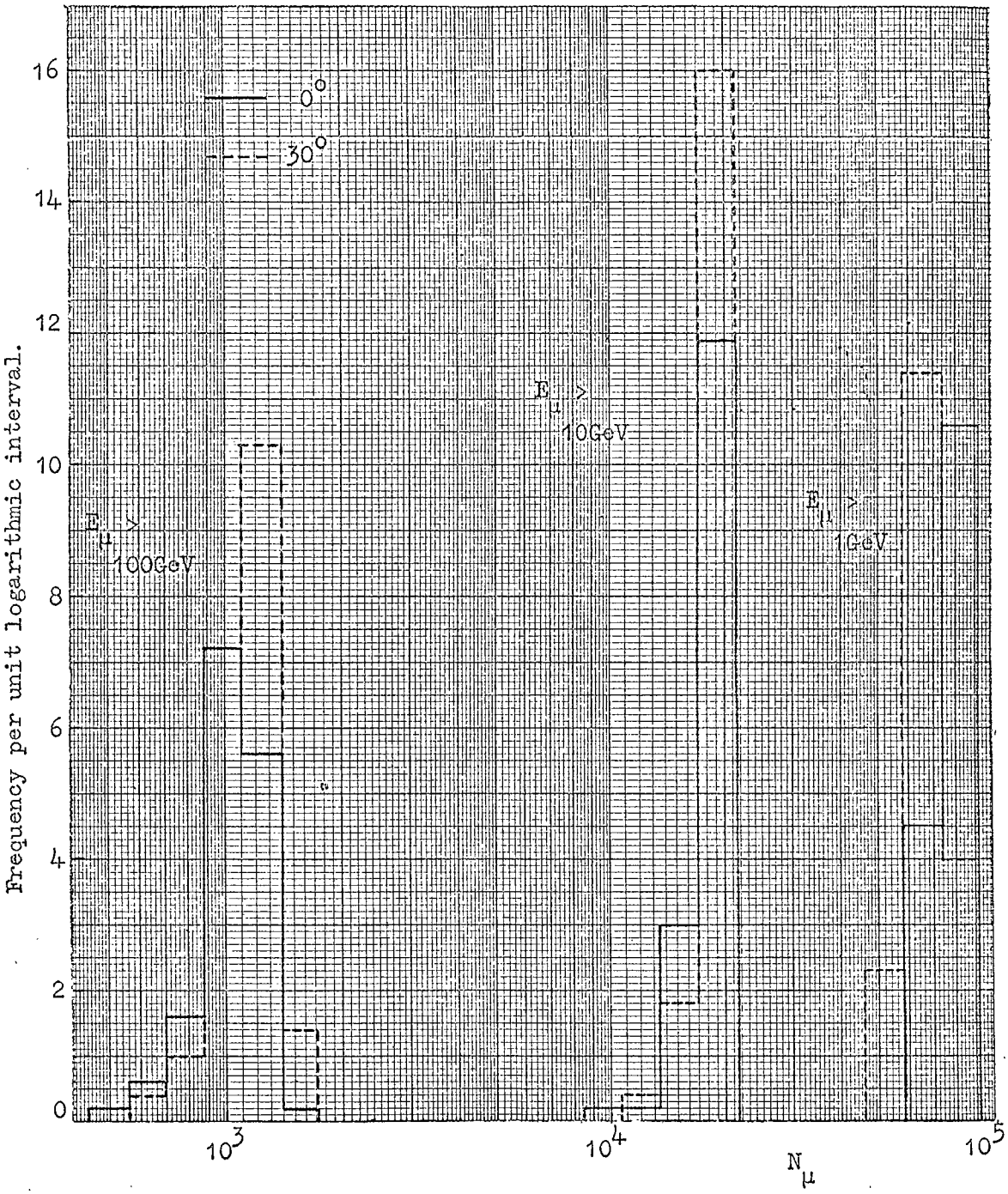

Fig. 6.7 Frequency distributions in muon number, N_μ, for primary protons of 10^7GeV, for three threshold energies and two zenith angles.

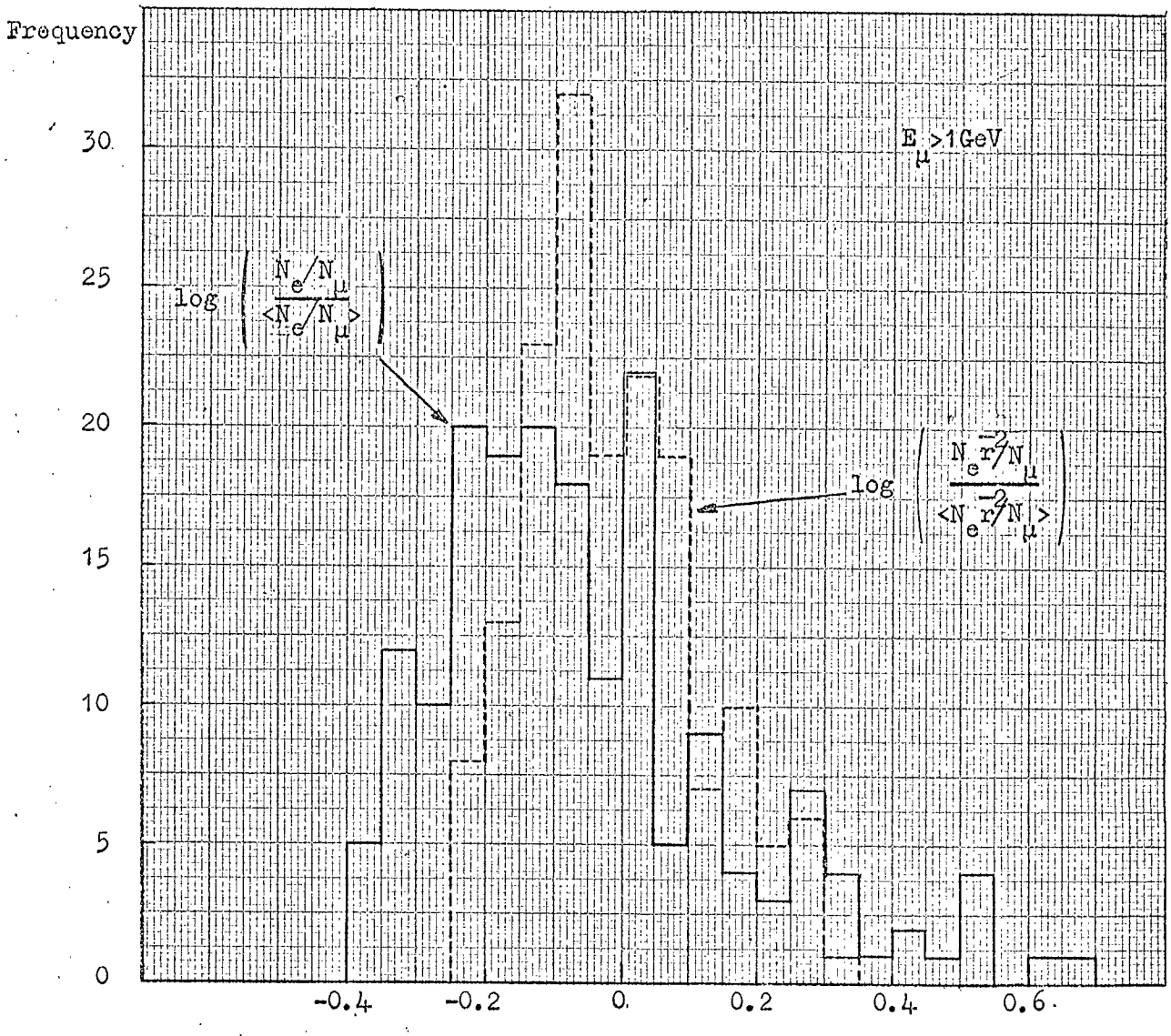

Fig. 6.8 Distributions of N_e/N_μ and $N_e r^{-2}/N_\mu$ for showers produced by primary protons of 10^7GeV, and for a sea-level muon threshold energy of 1GeV.

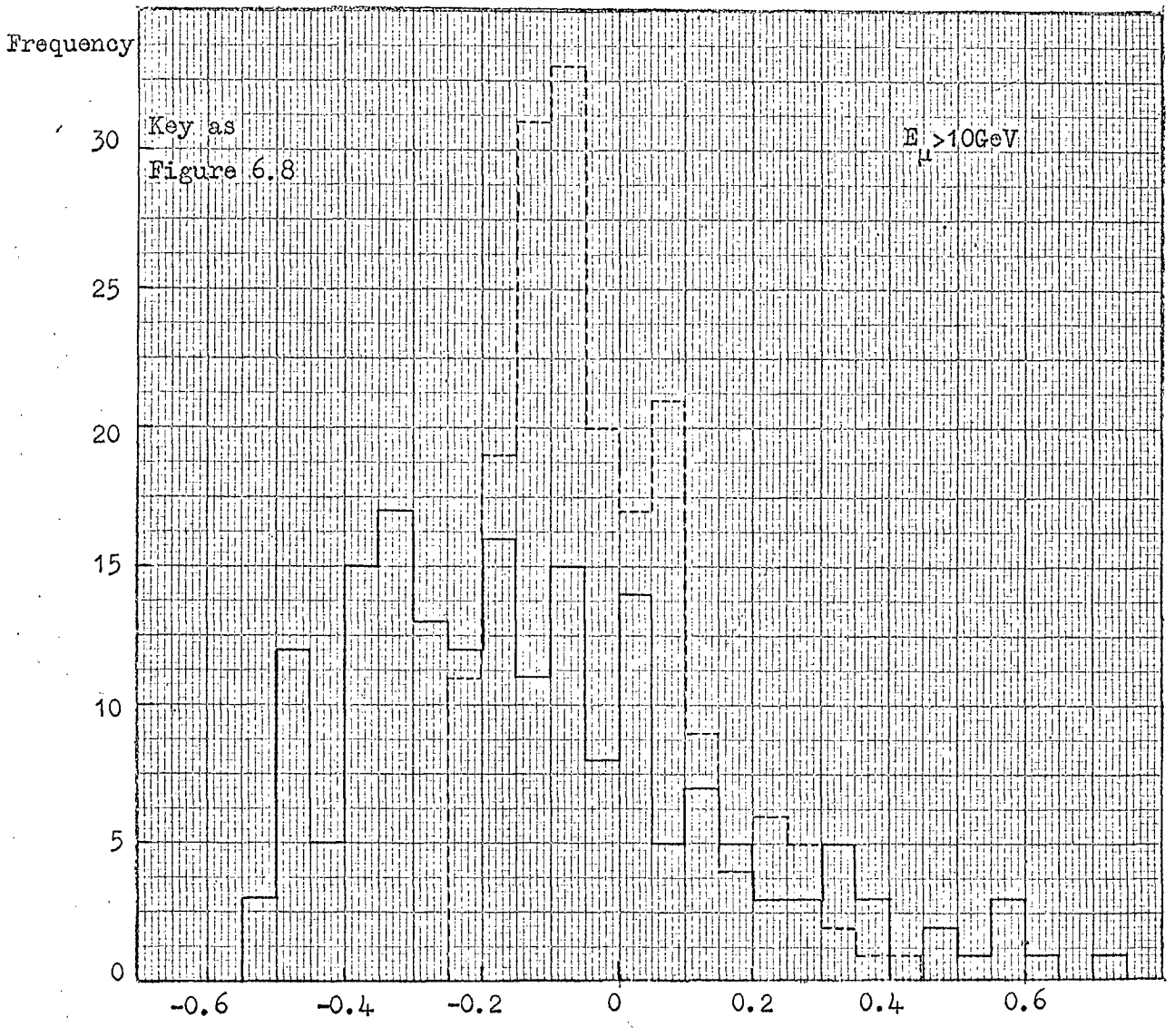

Fig. 6.9 Distributions of N_e/N_μ and $N_e r^{-2}/N_\mu$ for showers produced by primary protons of 10^7GeV, and for a sea-level muon threshold energy of 10GeV.

muons in the central region of the shower and it is clear that the fluctuations in the central density are smaller than in the total number. ~~That is to say, the fluctuations in the central density are greater than in the total number.~~ The effect of fluctuations with regards to the lateral distribution of muons will be discussed in a later section.

6.3.8 Discussion on the Predictions for Showers with Fixed Primary Energy

The most noticeable feature of the results is the fact that there are wide fluctuations in the number of electrons but only relatively small fluctuations in the number of muons. The fluctuations in N_e have several sources, notably the position of interaction of the primary particle and the energy released in such an interaction. The muons are comparatively unaffected because they are weakly interacting and as a consequence relatively insensitive to the point of origin.

6.4 The Characteristics of Showers of Constant Size

6.4.1 The Relationship between Shower Size and Primary Energy

Because electrons predominate in near vertical showers at sea-level, most experimental arrays are triggered by this component and the total number of electrons (N_e) is

taken as the datum. This quantity may be taken to represent the 'shower size' which is strictly the number of particles of all types; for $\theta \lesssim 45^{o}$ this will give rise to a negligible error. Other shower properties are then related to the shower size for the purpose of examining trends and to allow comparison to be made with other experimental results. As the preceeding section has shown, there are large fluctuations in N_e thus making it an unfortunate choice for the datum, even though it is easily measured.

The main effects of these fluctuations are to bias showers of a particular N_e to primary energies lower than those shown for 'fixed E_p' in Figure 6.3, in which, by chance, a large fraction of the initial energy is released low down in the atmosphere. The data of Figure 6.6 have been used in conjunction with an assumed primary spectrum ($N(>E_p) = AE_p^{-1.6}$) to give the mean primary energy for proton initiated showers having a constant number of electrons at sea-level. These are shown in Figure 6.3 denoted by 'Fixed N_e'.

The fluctuations in N_μ are small, however, since shower size is used as a datum there will be a decrease in the N_μ/N_e ratio for 'fixed N_e' and because of the bias towards showers which develop late, a steepening of the muon lateral distribution.

6.4.2 The Energy Spectrum of Muons in a Shower of Given Size

The results for model I for both proton and heavy primary initiated showers at $\theta = 30^{\circ}$ are shown in Figure 6.10 in the form of N_{μ} against shower size plotted with muon threshold energy as a parameter.

From Figure 6.10 the muon energy spectrum Figure 6.11 may be derived, it is plotted for $\theta = 20^{\circ}$ since measurements of high energy muons are usually made underground where the mean arrival angle is commonly $\sim 20^{\circ}$ to the zenith.

For proton primaries the sensitivity of the N_{μ}/N_{e} ratio to the model is clearly visible, particularly the large increase associated with the rapidly rising multiplicity of model III. When heavy primaries are considered the enhancement is even more marked. Comparing with the theoretical work of Hillas (1966), the shape of this author's energy spectrum lies between those of models I and II.

For a comparison between theory and experiment to be satisfactory it should be made over a wide range of shower sizes. However, many measurements have been made for showers in the order of 10^{6} particles, even here there are difficulties associated with the facts that

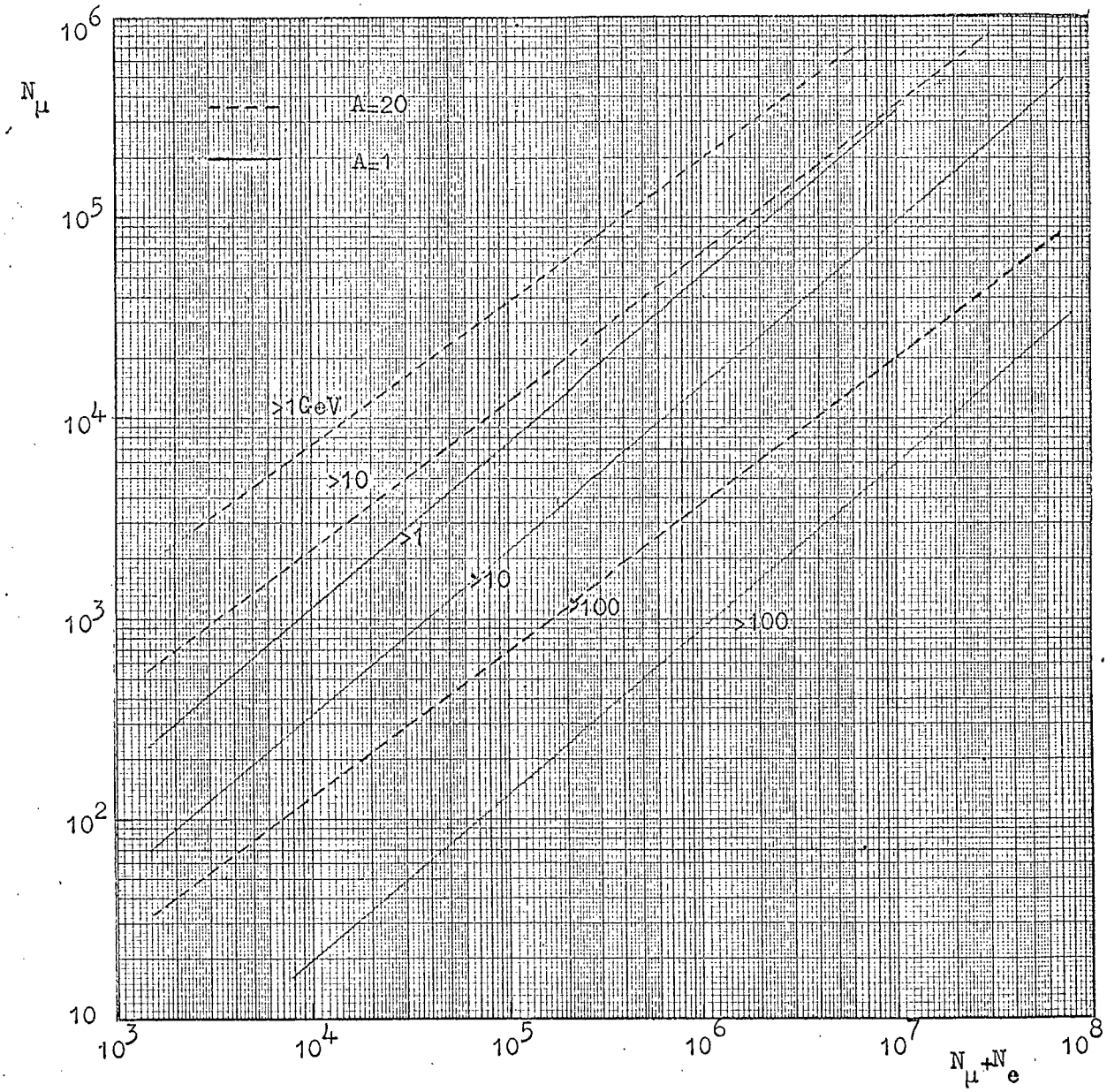

Fig. 6.10 The total number of muons as a function of shower size ($N_\mu + N_e$) for showers at 30° initiated by protons and heavy nuclei (A=20). The predicted values are valid only above a few times 10^3

i) The measurements have not been made for a unique zenith angle and in some cases the arrival direction is not known accurately, thus making it necessary to estimate the value.

ii) The apparatus usually accepts a range of shower sizes and in order to transform the muon densities to those for a unique shower size, a scaling law, which is not well known, is applied.

iii) The total number of muons is derived by integrating over the lateral distribution and this quantity is rarely measured accurately in those regions which make the major contribution to the total number.

The experimental results used in this analysis are indicated in the caption to Figure 6.11, conversion having been made, where necessary, to $\theta = 20^{\circ}$, sea-level and a shower size of 10^6 particles. It may be seen that the experimental values appear to lie on a smooth curve, which is similar in shape to those predicted.

It may be concluded from this comparison that the chosen features of the model concerning the longitudinal propagation of the shower through the atmosphere are acceptable. However, the predicted spectra are slightly

Caption for Figure 6.11

The energy spectrum of muons for showers of mean size 10^6 particles compared with experimental results.

Symbol	Authors	E_{μ}min (GeV)	Size	$\bar{\theta}^{\circ}$	Altitude
1	Bennett and Greisen 1961	1	10^6	20*	S.L.
1'	Greisen 1960		As 1.		
2	Chatterjee et al. 1966	220	10^6	20*	S.L., U.G.
3	Barnaveli et al. 1964	40	$6\ 10^5$	15	400m, U.G.
4	Khrenov 1965	10	10^6	30*	S.L., U.G.
5	Earl 1959 ($r < 900$ m)	1	$4\ 10^6$	25	S.L.
6	Vernov et al. 1964	10	10^6	20	S.L., U.G.
7	Hasegawa et al. 1962	4.5	10^5	10	S.L.
8	Porter et al. 1957	0.4	$6\ 10^6$	30*	S.L.
9	Abrosimov et al. 1958	0.5	$5\ 10^5$	30*	S.L.
	1960	0.5	$2\ 10^7$	30*	S.L.

* Value assumed

S.L. Sea level

U.G. Underground

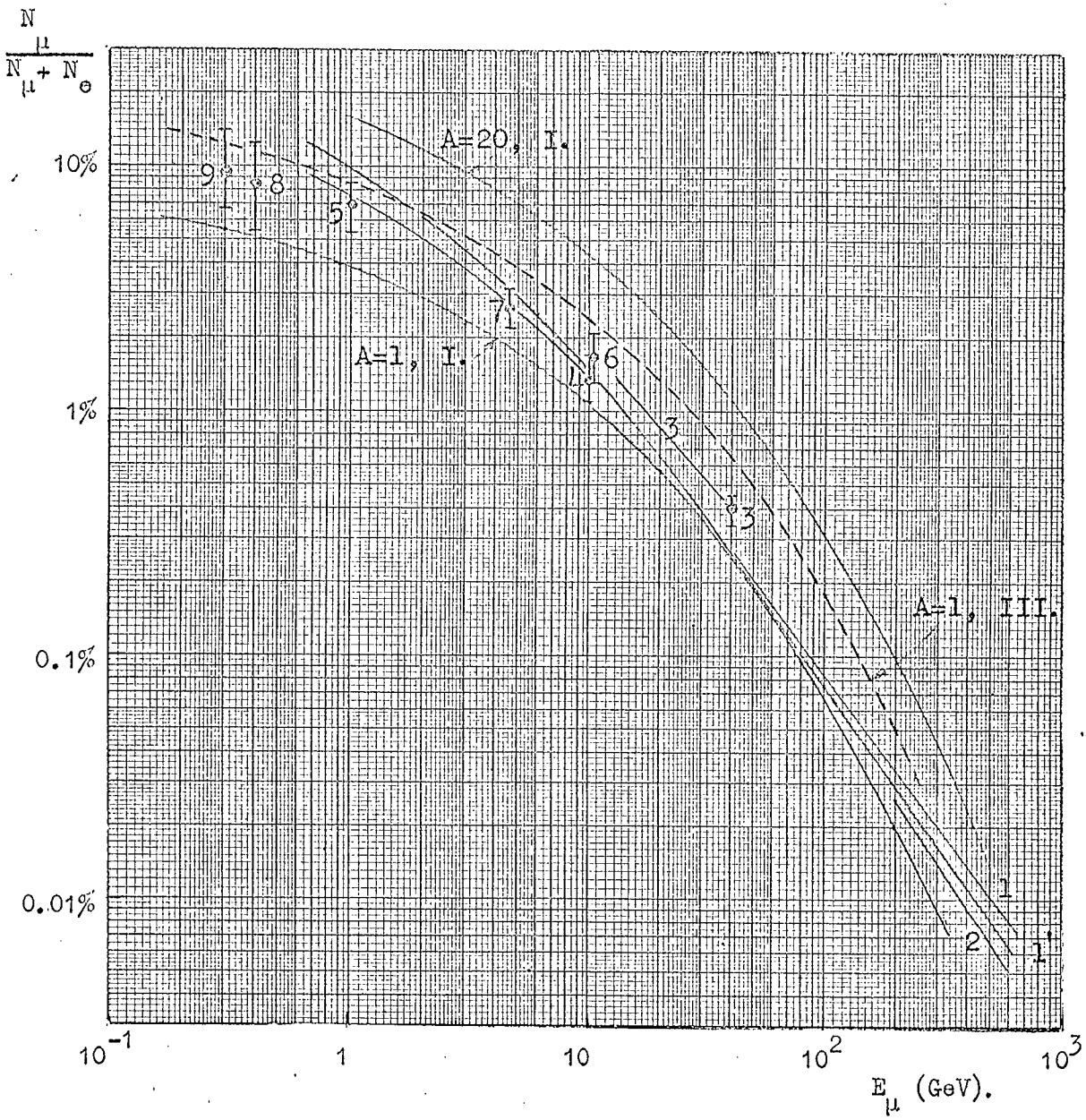
$\frac{N_\mu}{N_\mu + N_e}$
10%
1%
0.1%
0.01%
A=20, I.
A=1, I.
A=1, III.
9°
8
5°
7
6
5
4
3
2
1
1'
10^{-1}
1
10
10^2
10^3
E_μ (GeV).

Figure 6.11.

steeper above ~ 100 GeV, this may be due to the neglect of kaons amongst the secondaries. The neglect of non-pions will also introduce a small uncertainty into the vertical scale of the spectra, therefore, the predictions of this figure with respect to the mean mass of the primary cosmic rays will have a corresponding uncertainty. By interpolation it is possible to arrive at a value of $A_{eff} \sim 4$ for the preferred model - model I; although the uncertainty mentioned previously has now been enhanced by errors on the experimental points. Model II would predict $A_{eff} \sim 8$, and it is obvious that model III would require $A_{eff} < 1$, which is impossible.

Using the data on composition given by Ginzburg and Syrovatsky (1964) and assuming that the primary composition is the same for primary energies corresponding to a shower size of 10^6 as it is for lower energies, then A_{eff} would be ~2. One possible conclusion is that, assuming model I to apply, the present work lends support to the hypothesis that the fraction of heavy particles in the primary flux is greater at energies in question than at lower energies. Conversely if the hypothesis is true then this exercise has shown that model I is satisfactory, at least for the longitudinal development of showers.

6.5 The Lateral Development of the Shower

The muon energy spectrum allowed the longitudinal aspects of the model to be compared with experimental results. In order to carry out a comparison with those aspects which give rise to the lateral development of the shower the lateral distribution of muons at sea-level will be examined. It should be borne in mind that any changes to the model as a result of this comparison should have a minimal effect on the longitudinal development as this has already been shown to be in good agreement with experiment.

6.5.1 The Lateral Distribution of Muons

Figures 6.12, 6.13 and 6.14 show the muon lateral density distributions predicted by model I and slight variants on this model for a shower size of 10^6 at three threshold energies. These distributions have a shape which is almost indistinguishable from those predicted by Hillas (1966). A comparison is made with the experimental work listed in the caption to each figure; the difficulties mentioned as points (i) and (ii) of 6.4.2 are again operative. Corrections have been applied to the experimental data, where necessary, to convert them to a mean shower size of 10^6 particles, the ordinates were scaled according to $N_\mu \propto N_e^{0.83}$, a law which is derived from the present calculations. Further corrections have

Caption for Figure 6.12

The lateral distribution of muons for $E_\mu > 1$ GeV, $N_e = 10^6$. Comparison is made between predicted and the following experimental results normalized to E_μ min.

Symbol	Authors	E_μ min (GeV)	Size	$\bar{\theta}^o$	Altitude
■	Abrosimov et al. 1958	0.5	$5\ 10^5$	30*	S.L.
Δ	Abrosimov et al. 1960	0.5	$2\ 10^7$	30*	S.L.
o	Earl 1959	1	10^6-$3\ 10^7$	30	S.L.
×	Porter et al. 1957	0.4	$6\ 10^6$	30*	S.L.
▼	Lehane et al. 1958	1	$2\ 10^5$-$2\ 10^6$	30*	S.L.

* Value assumed

S.L. sea level

'All p_t' denotes the complete transverse momentum distribution.

'$p_t \not< 0.1$' denotes a cut-off applied so that particles with transverse momenta below 0.1 GeV/c are suppressed.

'corr' denotes correction for errors in core location.

Except where $\langle p_t \rangle = 0.6$, the distributions refer to a transverse momentum (with no cut-off) of 0.4 GeV/c.

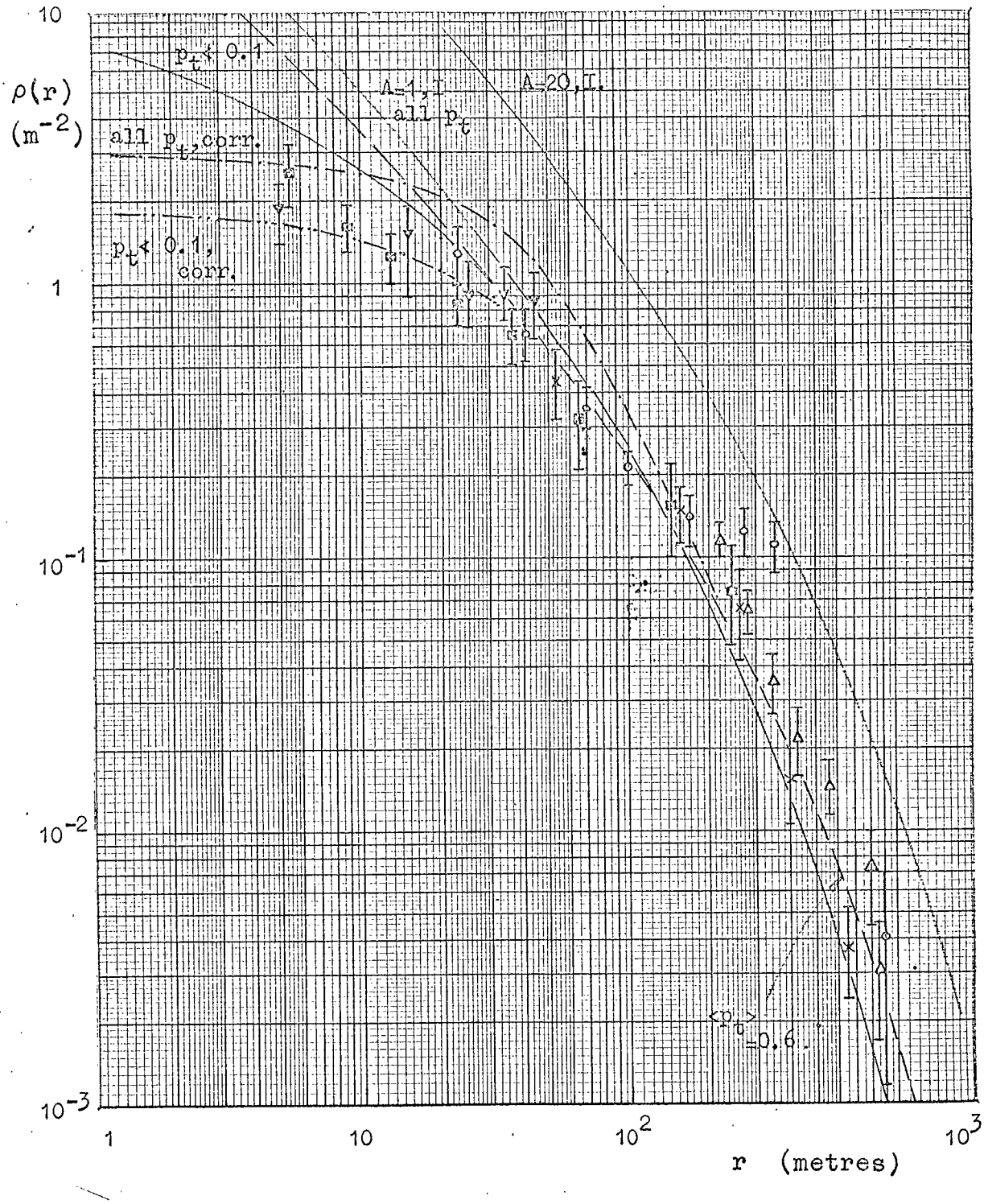
10
1
10^{-1}
10^{-2}
10^{-3}
$\rho(r)$
(m^{-2})
$p_t < 0.1$
A=1, T
all p_t
A=20, T.
all p_t, corr.
$p_t < 0.1$, corr.
$\langle p_t \rangle = 0.6$
1
10
10^2
10^3
r (metres)

Figure 6.12.

Caption for Figure 6.13

The lateral distribution of muons for $E_\mu > 10$ GeV in showers of mean size 10^6 particles. Comparison is made between prediction and the following experimental results.

Symbol	Authors	$E_\mu$min (GeV)	Size	$\bar{\theta}^\circ$	Altitude
o	Vernov et al. 1964	10	$5\ 10^6$	20	S.L., U.G.
■	Vernov et al. 1964	10	$5\ 10^5$	20	S.L., U.G.
Δ	Vernov et al. 1966 (after Khrenov)	10	10^6	30*	S.L., U.G.

Nomenclature as Fig. 6.12.

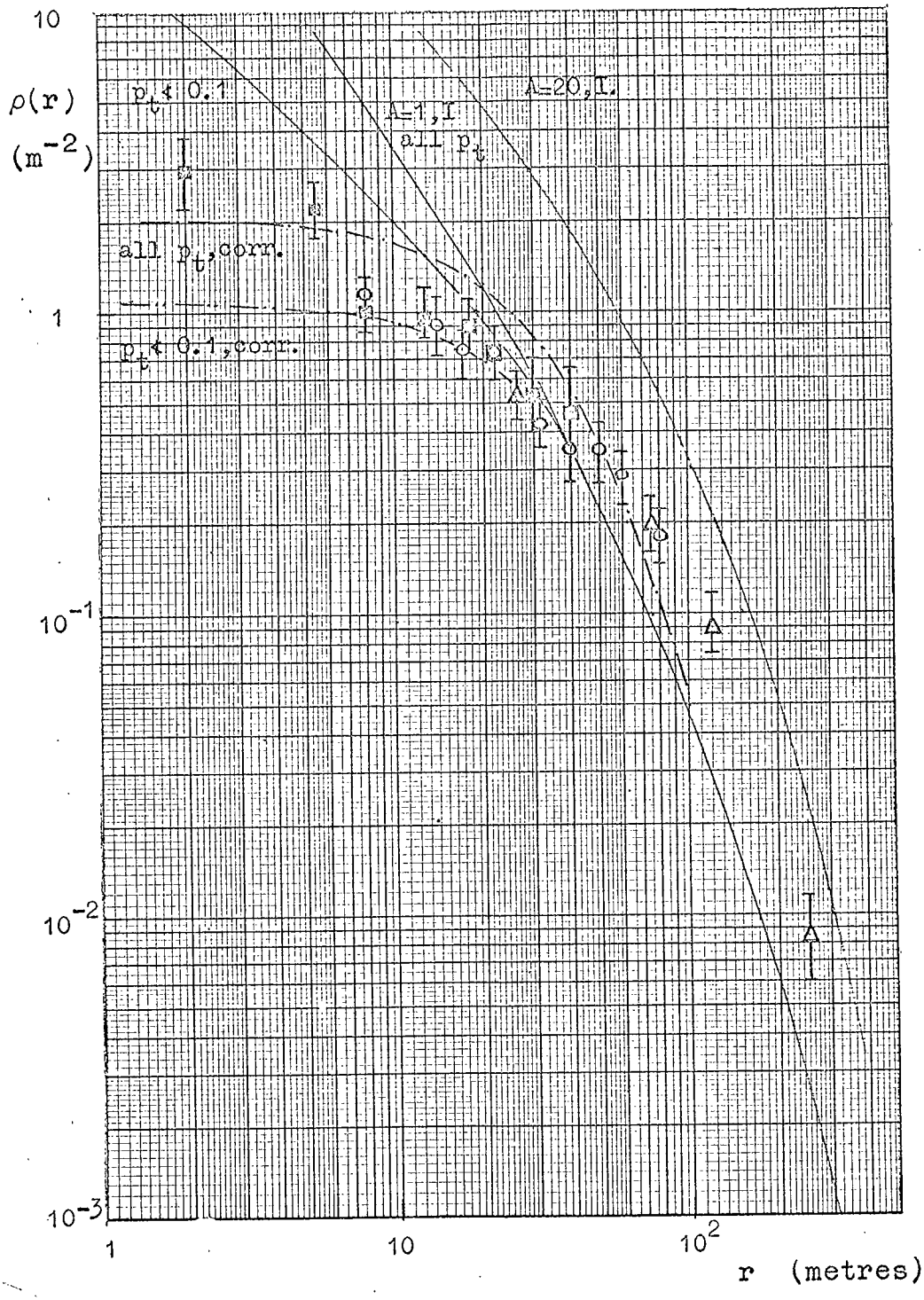
10
ρ(r)
(m⁻²)
p_t ≤ 0.1
A=1,1
all p_t
A=20,1.
all p_t,corr.
1
p_t ≤ 0.1,corr.
10⁻¹
10⁻²
10⁻³
1
10
10²
r (metres)

Figure 6.13.

Caption for Figure 6.14

The lateral distribution of muons for $E_\mu > 40$ GeV, $N_e = 10^6$. Comparison is made between predictions and the following experimental results.

Symbol	Authors	$E_\mu$min (GeV)	Size	$\bar{\theta}^\circ$	Altitude
●	Barnaveli et al. 1964	40	$6\ 10^5$	15	400m, U.G.

Nomenclature as Fig. 6.12.

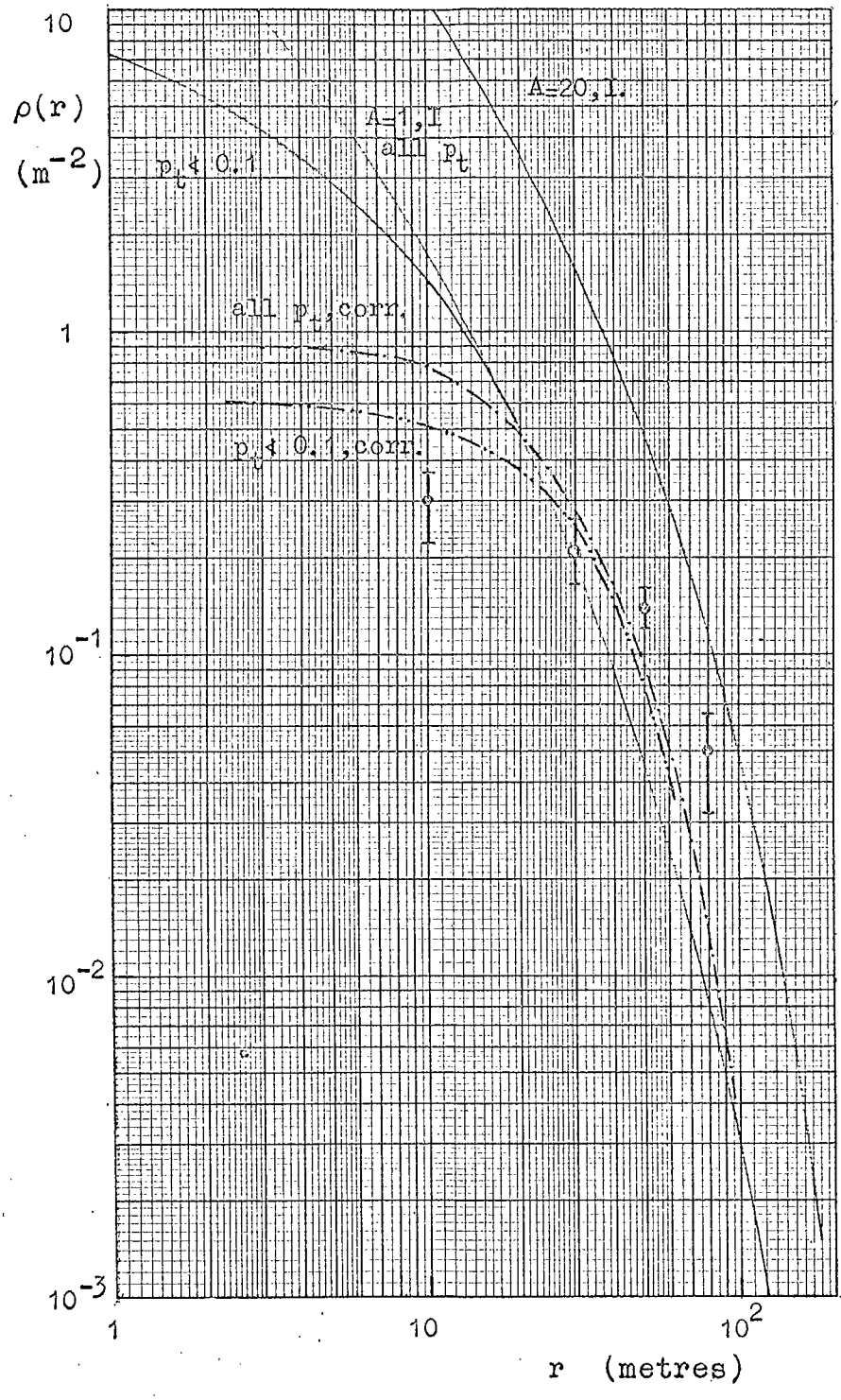
10
ρ(r)
(m⁻²)
1
10⁻¹
10⁻²
10⁻³
A=20, I.
A=1, I
all p_t
p_t ≤ 0.1
all p_t, corr.
p_t ≤ 0.1, corr.
1
10
10²
r (metres)

Figure 6.14.

been made to convert to a mean zenith angle of 30^{o}, and to sea-level assuming the electron number to vary with an attenuation length of 200 $g.cm^{-2}$. In the case of the figure for $E_{\mu} > 1$ GeV some of the data have been corrected to allow for the fact that their threshold energy is less than 1 GeV, this has been done using the energy spectrum as a function of radial distance, derived in the present work.

Comparing the curve marked 'A = 1, all p_t', which is the direct result of applying the Cocconi et al. transverse momentum distribution to model I for protons, it is obvious that it predicts excessive muon densities at small distances from the core for all threshold energies. Before attributing this to a defect in the model the accuracy of the experimental determinations of core location should be considered. The accuracy of core location will vary within each array and from array to array; in this study it is only possible to make a 'blanket' correction. The effect has been examined by taking what is thought to be a typical error of core location - a triangular distribution having a standard deviation of 25m - and folding this into the predicted lateral distribution. The resulting curve is denoted by 'All p_t - corr'.

The effect of errors in determination of shower size are mainly to change the absolute magnitudes of the muon densities, not the shape of the lateral distribution. Coulomb scattering and geomagnetic deflection would tend to flatten the distribution; Hillas (1966) states that the change for the former would be in the order of 2% and the latter should be of the same order.

Despite the improvement in fit between theory and experiment, the agreement is still not satisfactory and some modification to the model would appear to be necessary, although further experimental corrections are not entirely ruled out. This is also true for the tail of the distribution at the higher threshold energies, where, despite a slight enhancement due to the correction for core location, the predicted curve still lies below the experimental points.

6.5.2 Modifications to Transverse Momentum Distribution Necessary to give Agreement at Small Radial Distances

Since we require fewer muons to fall close to the core it would be beneficial to reduce the frequency of small transverse momentum transfers. An indication that this is the correct parameter to vary is the fact that, if the median transverse momenta are calculated for various muon

thresholds, as a function of radial distance, it is found that the departure of the experimental points from the predicted distribution occurs in each case at about the same value of p_t. Also such a modification would cause negligible change in the muon energy spectrum.

An estimate of the effect of reducing the frequency of low transverse momentum transfers has been made by introducing into the transverse momentum distribution a cut-off such that transverse momenta of less than 0.1 GeV/c are not allowed. The ensuing reduction factors are shown in Figure 6.15. The muon lateral distributions have been recalculated and error in core location has again been allowed for, the resulting curves are denoted by '$p_t \not< 0.1$, corr'. It appears that the reduction is sufficient to give agreement in Figures 6.12 and 6.13, and some improvement in Figure 6.14.

The justification for such a change is as follows:-

i) Von Dardel (1962) pointed out that the adopted transverse momentum distribution would predict a cusp at the origin, which is a physically unreasonable result, they suggest a Gaussian distribution which would be flatter near the origin.

ii) Lindendbaum and Sternheimer (1962) suggest that, on general theoretical grounds there should be a lower limit to the transverse momentum in the range 0.15 - 0.28 GeV/c.

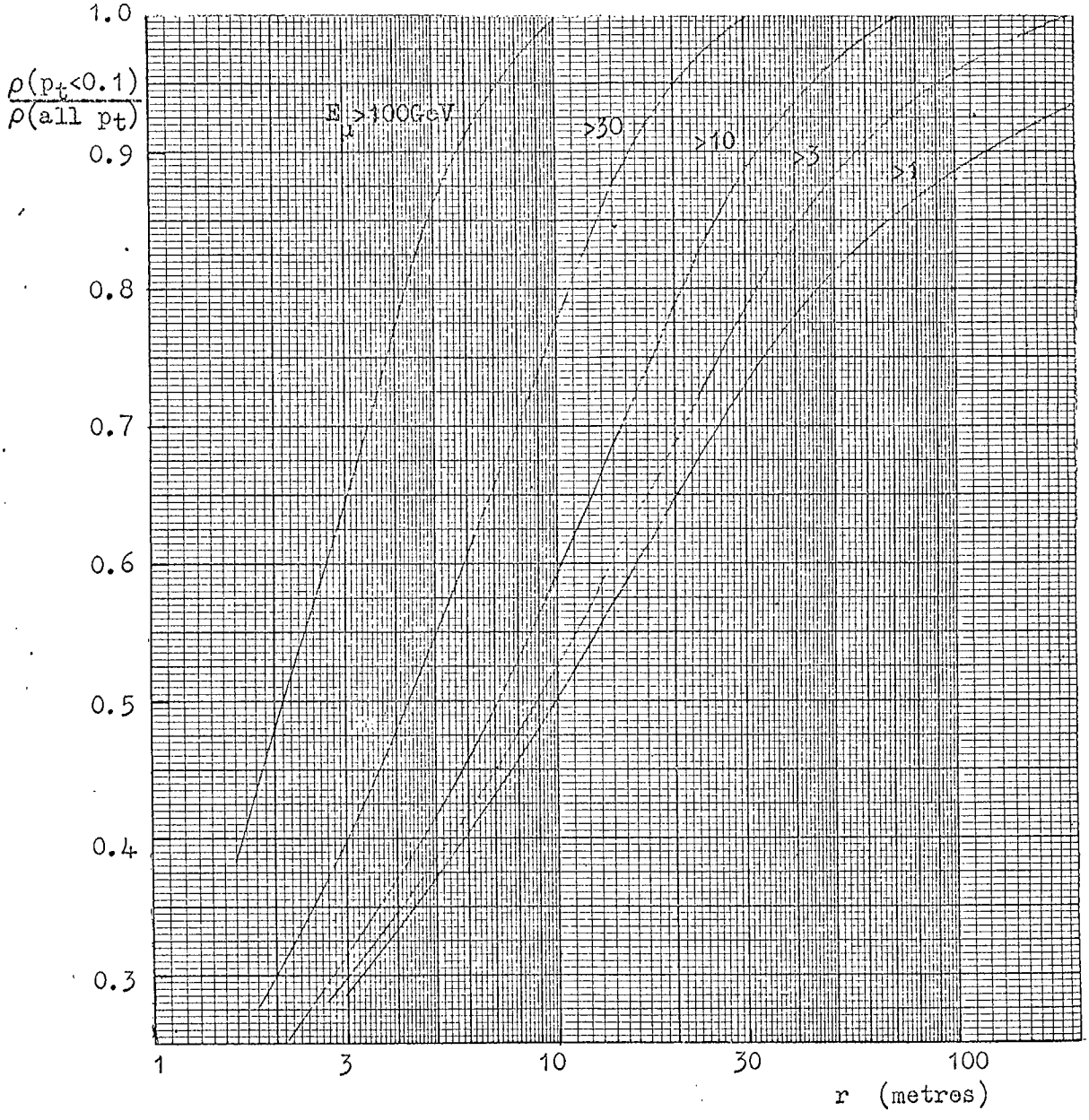

Fig. 6.15 The variation in the factor by which the lateral distribution derived using the C.K.P. transverse momentum distribution should be multiplied to allow for a cut-off below p_t=0.1GeV/c, as a function of radial distance.

iii) Tomaszewski et al. (1966) using a multiple scattering method to derive the transverse momentum distribution from ultra-high energy interactions in nuclear emulsion, have present results which tend to suggest a deficit of low momentum events.

iv) The adopted distribution comes from the work of Cocconi et al. and refers to proton-C, Be and B nucleus collisions and a degree of confirmation fromp-p data. In the proton-, pion-, oxygen and nitrogen nucleus collisions which are predominant in E.A.S., the probability of a pion being scattered within the nucleus after production is higher and this would give rise to a reduction in the probability of small transverse momenta.

6.5.3 The Discrepancy at Larger Radial Distances

Prior to the recent work at Haverah Park it had been found that with the adopted transverse momentum distribution at $\langle p_t \rangle$ = 0.4 GeV/c quite good agreement could be obtained between theory and experiment for muon thresholds of 1 and 10 GeV after allowance had been made for errors in core location and a reduction in the frequency of transverse momentum transfers below 0.1 GeV/c. However, for muon energies in excess of 40 GeV/c the theoretical lateral distribution is steeper than the distribution indicated by the experimental results of Barnaveli et al. (1964).

More recent measurements by Earnshaw et al. (1967) however have considerably extended the limits of muon energy and lateral distance to the region where there is considerable sensitivity of the muon density to the mean transverse momentum. The results are shown in Figure 6.16, the points have been scaled down by a factor of 7.6 to convert from the mean measured size of 2×10^7 particles to the size expected for a primary of 10^7 GeV. The theoretical treatment is approximate in that it refers to a unique primary energy rather than an energy spectrum and it used fixed interaction points. The effect of using an energy spectrum for primaries would be to make the distribution slightly narrower. It is obvious that the experimental distributions are wider than predicted and that the discrepancy increases with rising muon energy. To interpret these differences in terms of increased $\langle p_t \rangle$ would require extremely high values as may be seen in Figure 6.16 where distributions which fit the observed lateral density distributions are shown. These values are indicated by crosses in Figure 6.17.

Other parameters affecting the lateral spread of a shower, and their importance in attempting to explain the discrepancy, are as follows.

i) Multiplicity

In an attempt to produce an increase in the number of muons at large distances from the shower core a

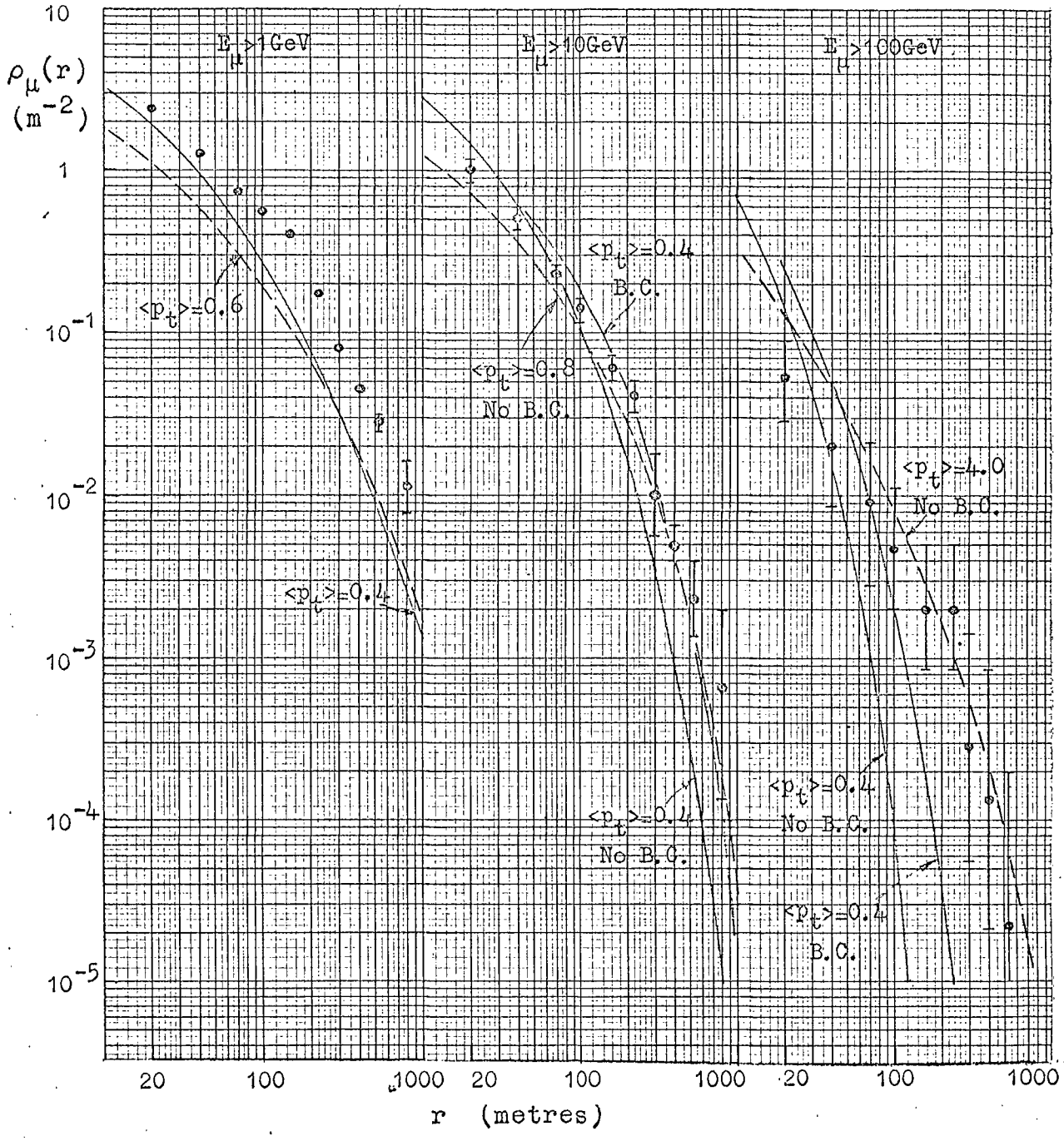

Fig. 6.16 Comparison of the experimental data of Earnshaw et al. (1967) on the lateral distribution of muons with various theoretical predictions, 'B.C.' denotes 'bias correction'.

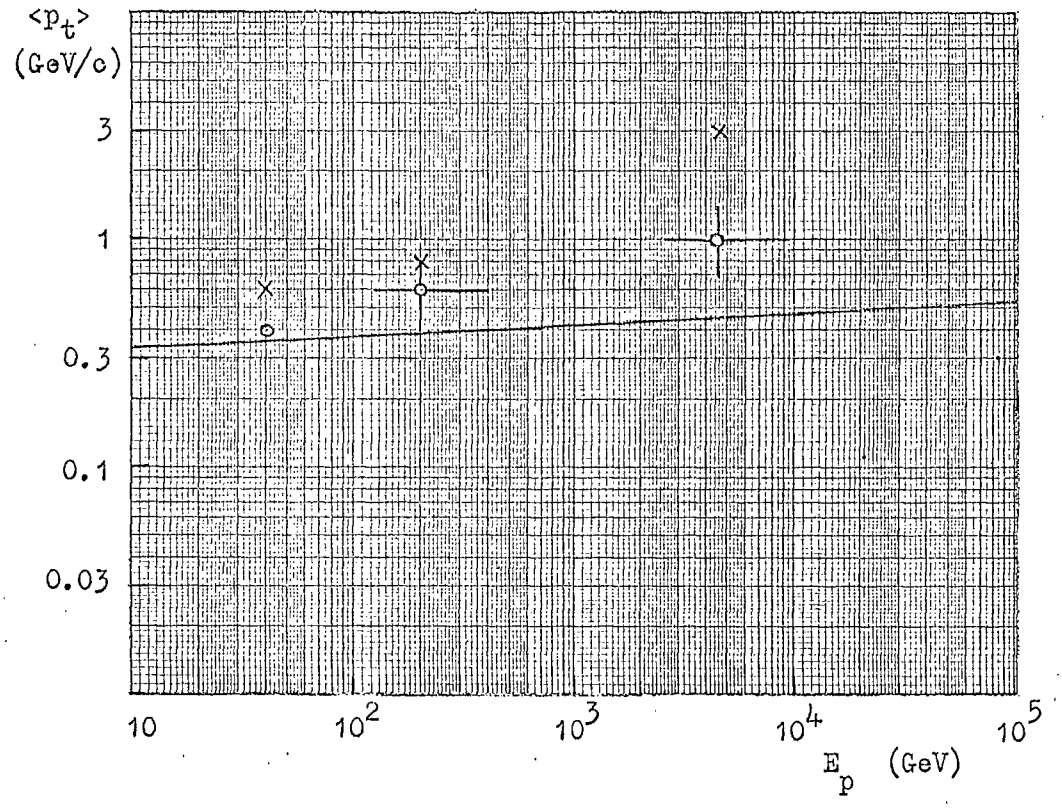

Fig. 6.17 Variation of the mean transverse momentum with primary energy. The line represents the best fit to the experimental results of Fig. 5.2, the crosses show the values of p_t necessary with no bias correction, and the open circles the values after correction.

model has been tried in which the multiplicity of secondary particles is allowed to increase substantially for incident particle energies in excess of 10^6 GeV, such that $n_s = 2.7\ E_p^{\frac{1}{4}} + 6.667\ 10^{-11}\ E_p^2$. This is rather a drastic step since Figure 6.11 shows the effect that model III has on the energy spectrum. The philosophy behind this investigation is to reduce the mean depth of muon production and this has been successful in that the most probable depth is now $\sim$320 g.cm^{-2} for $\theta = 0^o$ and $E_p = 2.10^7$ GeV whereas the most probable depth for model I is 640 g.cm^{-2}. As a consequence there is a reduction in the magnitude of the discrepancy between the predicted and observed lateral distributions, however, it is clear that the means of obtaining this improvement are untenable since it would destroy the agreement between the predicted and observed energy spectra.

ii) Divergence of the parent particles

The transverse momentum distribution has only been impressed on those pions which subsequently decay to muons. Thus the deviation of the primary particle from its initial path due to interactions has been neglected and the high energy pions which subsequently interact with an air nucleus are considered to travel along the shower axis. No accurate computation of the effect of these parameters has been made, however, simple calcula-

tions show that the lateral displacement of primaries and high energy pions will give only a small overall improvement because of the high longitudinal momenta of the particles involved.

iii) Errors in core location

Figures 6.12, 6.13 and 6.14 show that the importance of this effect is confined to small distances from the core. In the work of Earnshaw et al. (1967) several arrays were used to cover the range of lateral distances and the relative inaccuracy in each measurement of r was at the most 20%, this figure is given by de Beer et al. (1967); such a small inaccuracy means that its contribution to the solution of the discrepancy at large radial distances is negligible.

iv) Scattering and magnetic deflection

There should be a less than 2% effect for near-vertical showers.

v) Fluctuations in the lateral distribution of muons

The preceding work has shown that the major contribution to the fluctuations in N_μ and N_e comes from fluctuations in the interaction depths of the leading particle. As a first step a study was made of the effect of allowing the position and number of interactions of the primary to vary. The number of interactions en route to sea-level has a Poisson distribution with a mean of ~12.9 and the depth

between successive interactions has a distribution of the form $e^{-x/80}$.

The computer produced for each shower a set of interaction points for the primary particle, a typical set is illustrated in Figure 6.18. The secondary particles produced as a result of these interactions are allocated to pion production levels, the first of these, level '0', coinciding in depth with the first primary interaction level, at 31 g.cm^{-2} in this case, succeeding production levels being at 120 g.cm^{-2} intervals. Thus all of the pions produced by the first interaction of the primary will go to production level '0'. In order to explain the allocation of pions due to later primary interactions consider the pions produced at 489 g.cm^{-2}, these are allotted to production level '3' at 391 g.cm^{-2} and level '4' at 511 g.cm^{-2} as the inverse of the distance between interaction level and production level. Thus 18% of the pions will go to level '3' and 82% to level '4'. The method of computation of the shower formation from this stage is identical with that used in the non fluctuating case.

The extreme lateral distributions found for 124 such showers are shown in Figure 6.19; it is evident that the fluctuations are large and of particular im-

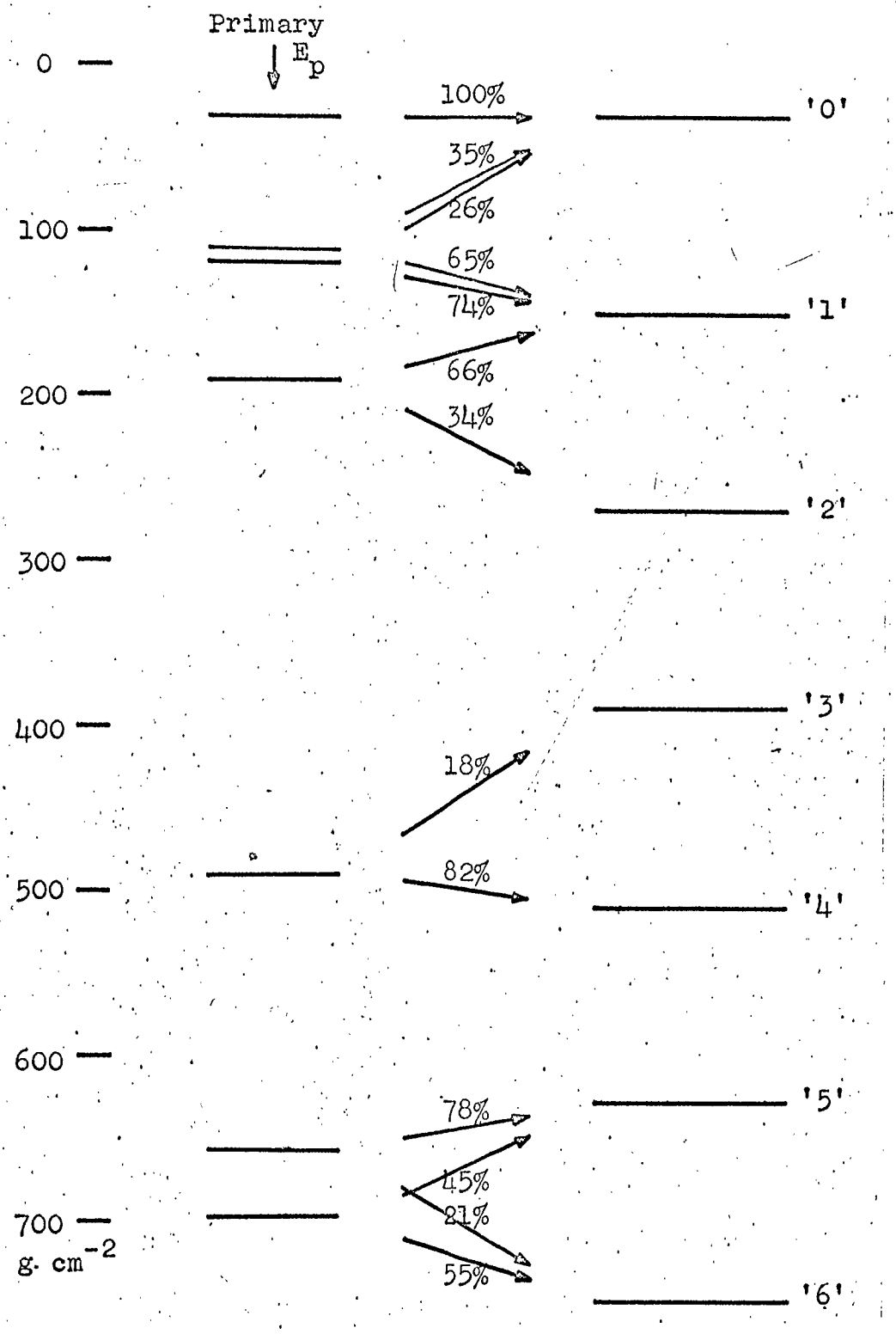

Fig. 6.18 The method of numerical calculation when fluctuations in the positions of the interaction points are allowed.

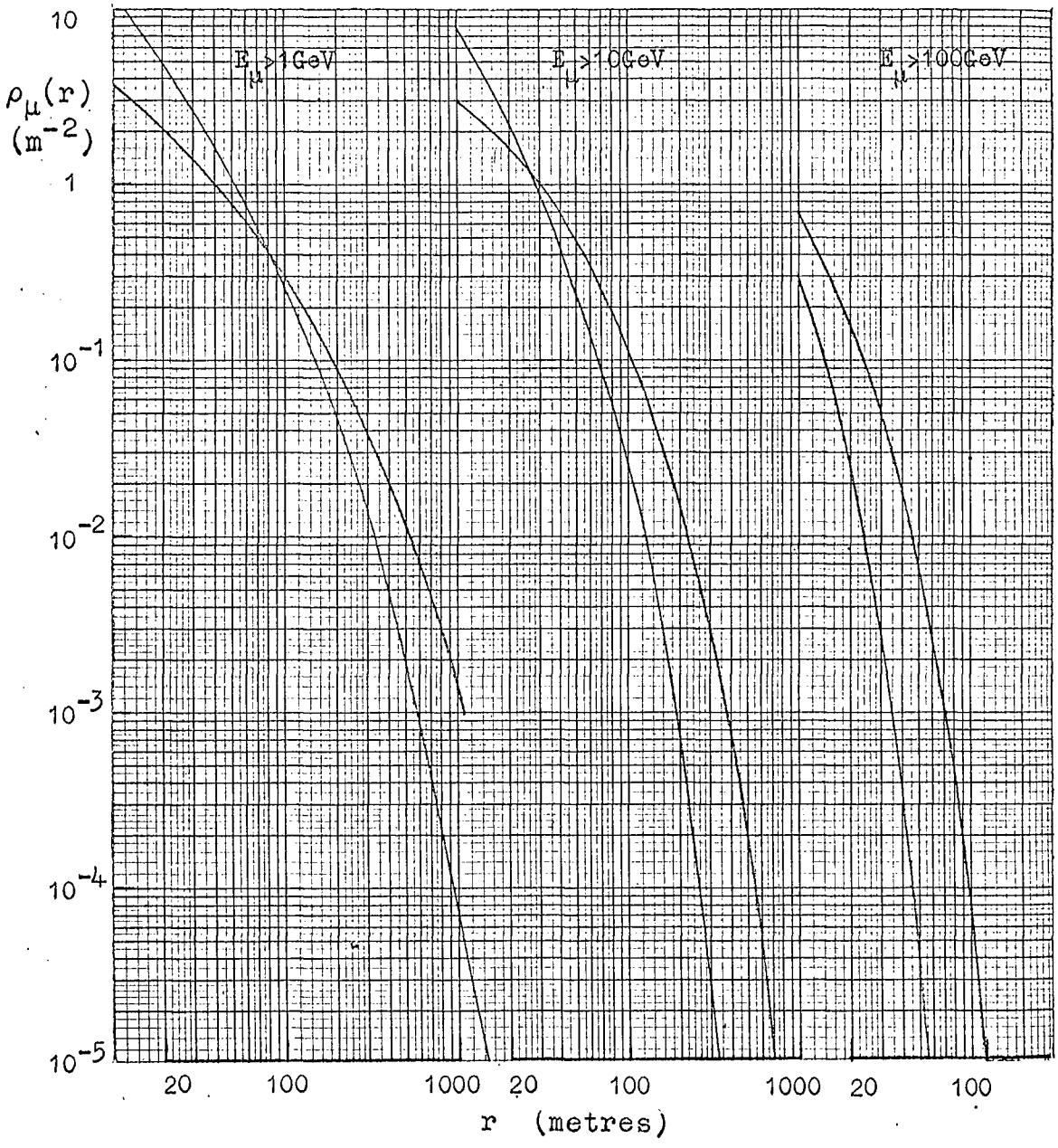

Fig. 6.19 The lateral distribution of muons produced by primary protons of 10^7GeV calculated using a Monte-Carlo method. The curves shown are the outer pairs from a set of 124 showers.

portance is the increase in spread as the muon threshold increases. If fluctuations in inelasticity and multiplicity were to be taken into account the spread would presumably be even larger.

It is interesting to note the correlation between various parameters of the muon shower, for example, N_e, N_μ, the mean height of muon production, h, and the shape of the lateral density distribution. As a starting point in this discussion take the interaction levels of the primary particle, if by chance there are several in the upper part of the atmosphere, say before 200 $g.cm^{-2}$, then the following generalisation may be made; N_μ will be high, N_e low, and the lateral distribution will be flatter than the mean. Conversely, if the first few interactions are later than usual the lateral distribution tends to be steeper, N_μ low and N_e higher than would be produced in a non-fluctuating model. Some of these statements are expressed quantitatively in Figure 6.20 which shows strong positive correlation between shower size and the mean radius of the muon distribution ($\bar{r}$) and also with the height of origin.

vi) Conclusions

It is concluded that corrections for parameters (i) to (iv) above do not bring about a significant improvement

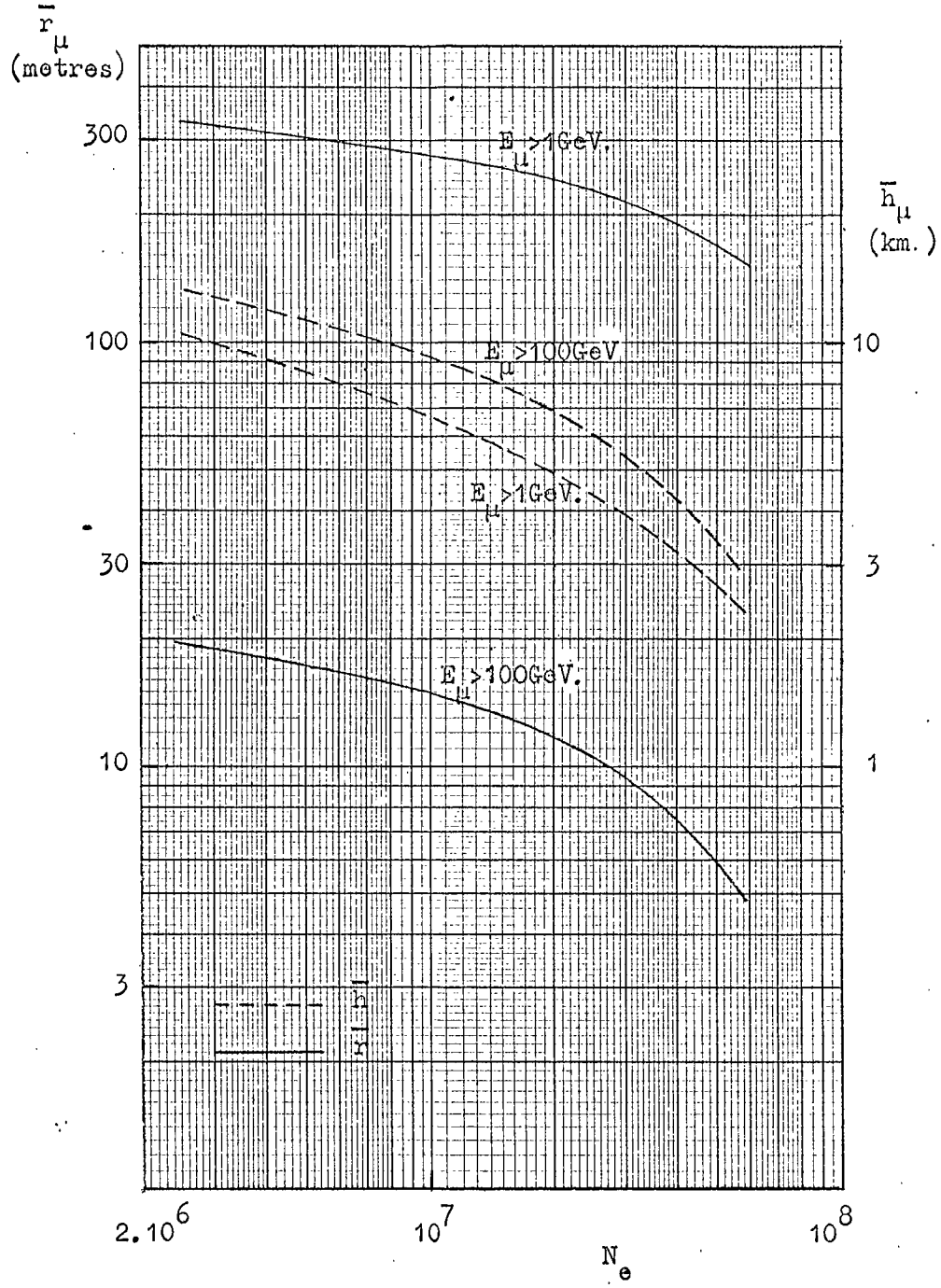

Fig. 6.20 Correlation between the mean radius and the mean height of origin of muons with shower size, for showers produced by primary protons of 10^8GeV.

in the fit between the predicted and observed lateral distributions.

The result of the study of fluctuations in the lateral distribution of muons, with regards to E.A.S. measurements, is that, where arrays have a few well spread detectors there will be a bias towards selecting the flatter showers, these being showers which by virtue of upward fluctuations have several early interactions. Such showers will have fewer electrons at sea-level but this loss will be more than offset by the increased muon density at large distances. The enhancement will be particularly marked in the case of the Haverah Park array since the use of Cerenkov detectors results in greater sensitivity to muons than electrons. When this bias effect has been allowed for it seems that any remaining discrepancy must be explained in terms of a change in $\langle p_t \rangle$.

6.5.4 Necessary Modifications to the Transverse Momentum Distribution

An attempt has been made to allow for the bias exposed in the preceeding section. With reference to the work of Earnshaw et al., an extrapolation has been made of the correlations between the lateral distributions found in fluctuation calculations for the three threshold energies. The predicted distributions are determined

for $E_\mu > 10$ GeV and $E_\mu > 100$ GeV which arise when a distribution is chosen for the $E_\mu > 1$ GeV case which reproduces the shape of the measured distribution for this energy threshold. This means that the $\langle p_t \rangle$ values are effectively normalised at their lowest mean energy point to 0.4 GeV/c; the resulting distributions for the other thresholds for $\langle p_t \rangle = 0.4$ GeV/c and after bias correction are shown in Figure 6.19. The open circles of Figure 6.18 show the values of mean transverse momentum which are necessary to give agreement with experiment, after bias correction. For $E_\mu > 10$ GeV, or pion interactions of mean energy ~200 GeV it is found to be necessary to raise $\langle p_t \rangle$ to 0.6 ± 0.2 GeV/c and a value of 1.0 ± 0.3 GeV/c is required to explain the discrepancy which exists after bias correction at $E_\mu > 100$ GeV or mean pion interaction energy of ~4000 GeV; even so the fit at small values of r is still not very good. A possible explanation of this poor fit is that the transverse momentum distribution does not in fact follow the C.K.P. distribution, but has a much longer tail.

It should be emphasised that these values of $\langle p_t \rangle$ are based on the assumption that the discrepancy between the bias corrected distribution and experimental results is solely a transverse momentum effect.

6.5.5 Other Models

The isobar model does not help since it leads to a decrease in the mean height of muon production which results in a steeper lateral distribution. The effects of using the persistent baryon model have been evaluated and this produces a similar shaped distribution to that given by the adopted model but the absolute magnitude of the densities is too low.

An alternative explanation has been put forward by Fowler (1967), this involves a rapid change in the characteristics of the nucleon-nucleon collision at high energies. Fowler postulates a second order phasetransition, possibly associated with the emission of quarks, which gives rise to high transverse momenta. On this hypothesis some of the energetic E.A.S. particles at large radial distances would then be expected to be quarks, if the quark interaction length is long. An experimental check of such a prediction should be possible.

Finally it should be noted that interpretation of the results in terms of excessive transverse momentum is limited by the assumptions adopted for the other model parameters. Thus it is possible to change interaction lengths so that the mean heights of origin are greater, and to account for the results in this way. However, the experimental data suggest a 'normal' height distri-

bution so that this explanation is unlikely.

Very recently Gierula (1967) has given evidence which suggests that the pion-air-nucleus interaction is not catastrophic but has $\overline{K} \sim 0.5$. The effect of this is to increase the width of the lateral distribution of muons somewhat (probably by ~20% - Wolfendale, private communication). Such an increase is not sufficient to explain the experimental data.

6.6 Summary of the Adopted Model

It is concluded that the transverse momentum distribution, the mean transverse momentum and the mass composition of the primary flux are the variables which require further study. The analysis of muons in large zenith angle showers will give further information about these parameters.

CHAPTER 7

Theoretical Studies at Large Zenith Angles

7.1 The Model

This is essentially the 'numerical' model previously used in the study of near-vertical showers. In view of the increased depth of atmosphere in which the shower may develop, the number of primary interaction levels is increased to sixteen, the primary particle is therefore considered until it has reached a depth of 1280 $g.cm^{-2}$, by which time its energy will be a factor of $\sim 10^4$ down on its initial value. Pion production levels extend to a depth of 2000 $g.cm^{-2}$. It has been found that this allocation has been over generous, consequently it is possible to say that no muons of ≥ 1 GeV at sea-level have been neglected in this analysis. Energy loss by the muons and loss of muons due to decay, Figure 7.1, are particularly important because of the increased muon path lengths to sea-level at the larger zenith angles. The widths of the energy cells considered now increase as 0.3 of the logarithm of the primary energy. The model deals quite well with the longitudinal development of the shower and evidence for this is provided by the comparison of the muon energy spectra with experimental results and other theoretical work.

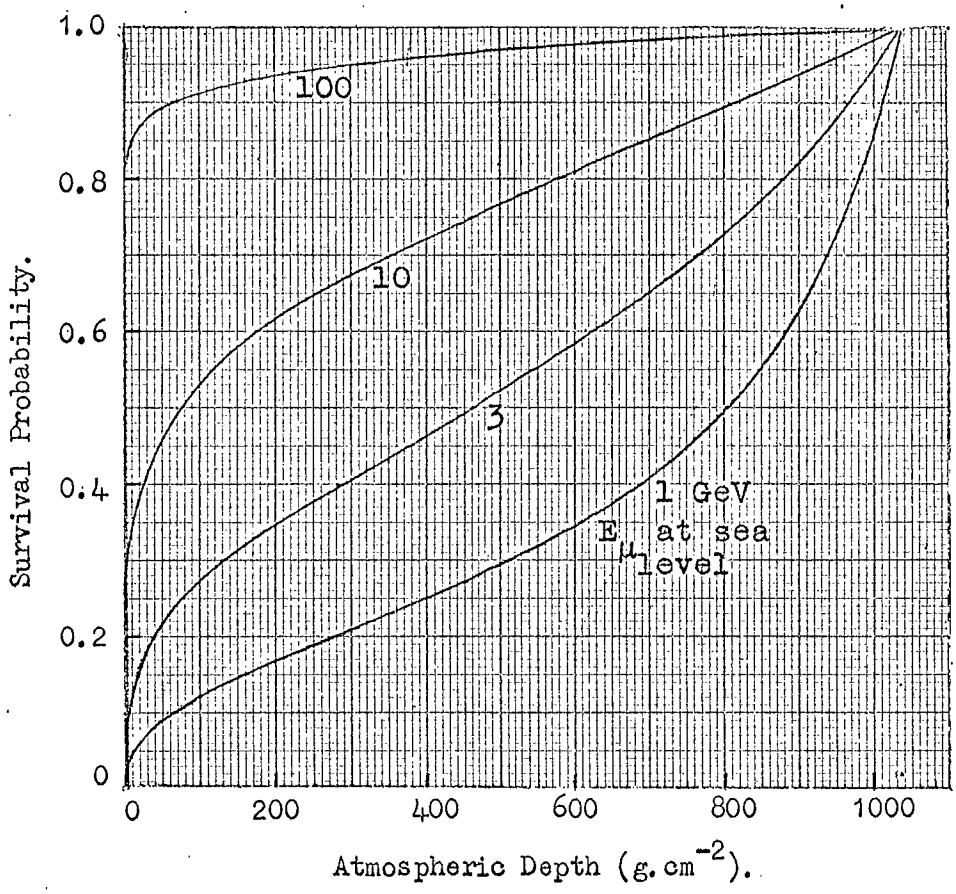

Fig. 7.1 Muon survival probability as a function of threshold energy and production depth for a zenith angle of 84°.

The effects of scattering and geomagnetic deflection are negligible at small zenith angles, however, the importance of these parameters increases with zenith angle due to the increasing path length. The effects of geomagnetic deflection are particularly difficult to study since the muon lateral distribution is no longer circularly symmetrical after the introduction of this parameter. It was hoped that a precise treatment would be possible by virtue of the computer being able to follow small groups of muons, originating at the same atmospheric depth and having similar energies, to an exact location at sea-level. However, this has not proved to be feasible because of the computing time which would be involved; it is hoped that by reducing the number of primary interaction levels and pion production levels a treatment of this nature might be possible in the future. In the present work a method is used which involves a compromise between accuracy and computing time, this will be discussed fully in section 7.7.1.

7.2 The Single Muon Energy Spectrum at Large Zenith Angles

During the computation the muon energies at production and the depths at which they are produced are extracted and are used as the basis of the data for this section of the analysis.

Initially the muon energy spectra for single showers initiated by primary protons having energies of 10^2, 10^3 10^4, ... 10^9 GeV are produced, an example at one of the zenith angles considered is given in Figure 7.2. The primary spectrum of Linsley (1964) is then folded in to give the predicted single muon energy spectra, the $\theta = 84^\circ$ spectrum may be compared with what is observed experimentally, and the comparison is made in Figure 7.3. The experimental results shown are those of MacKeown et al. (1966) and Ashton et al. (1966) for $\theta = 83.75^\circ$. Osborne (1966) takes the vertical muon energy spectrum at sea-level and works back through the atmosphere in order to obtain the parent pion spectrum. This spectrum is then applied at large zenith angles and the resulting sea-level muon spectra, with no scattering correction, at $\theta = 75^\circ$ and 84° are shown in Figure 7.3 for $E_\mu < 50$ GeV. Osborne gives the spectra for $E_\mu < 1000$ GeV and in the range $50 \text{ GeV} < E_\mu < 1000$ GeV the spectra predicted in the present work are coincident with those presented by Osborne. There is also good agreement when comparison is made with the results of Allen (1961); this suggests that the method of calculation is satisfactory.

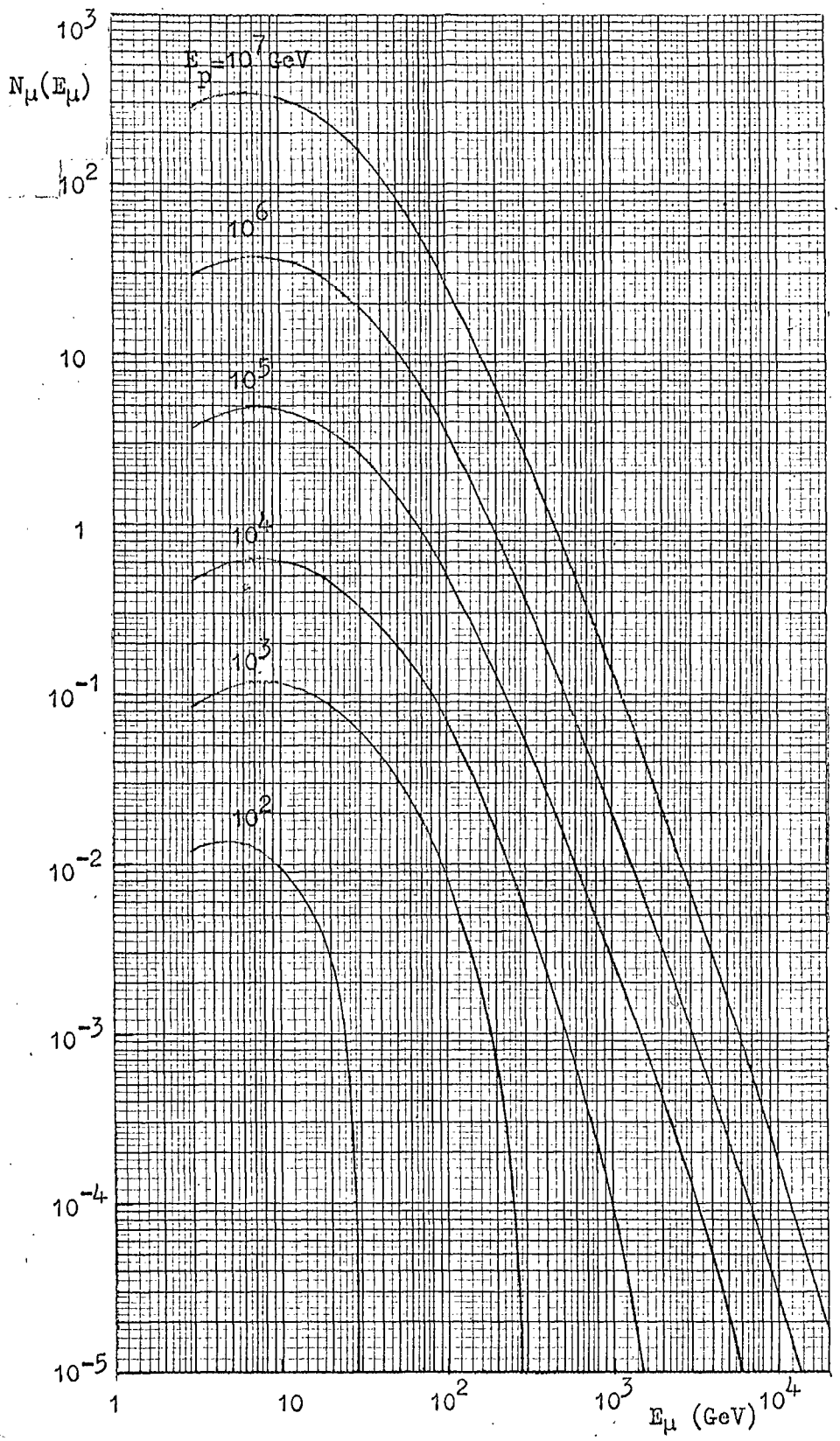

Fig. 7.2 Muon energy spectra for primary protons at a zenith angle of 75°.

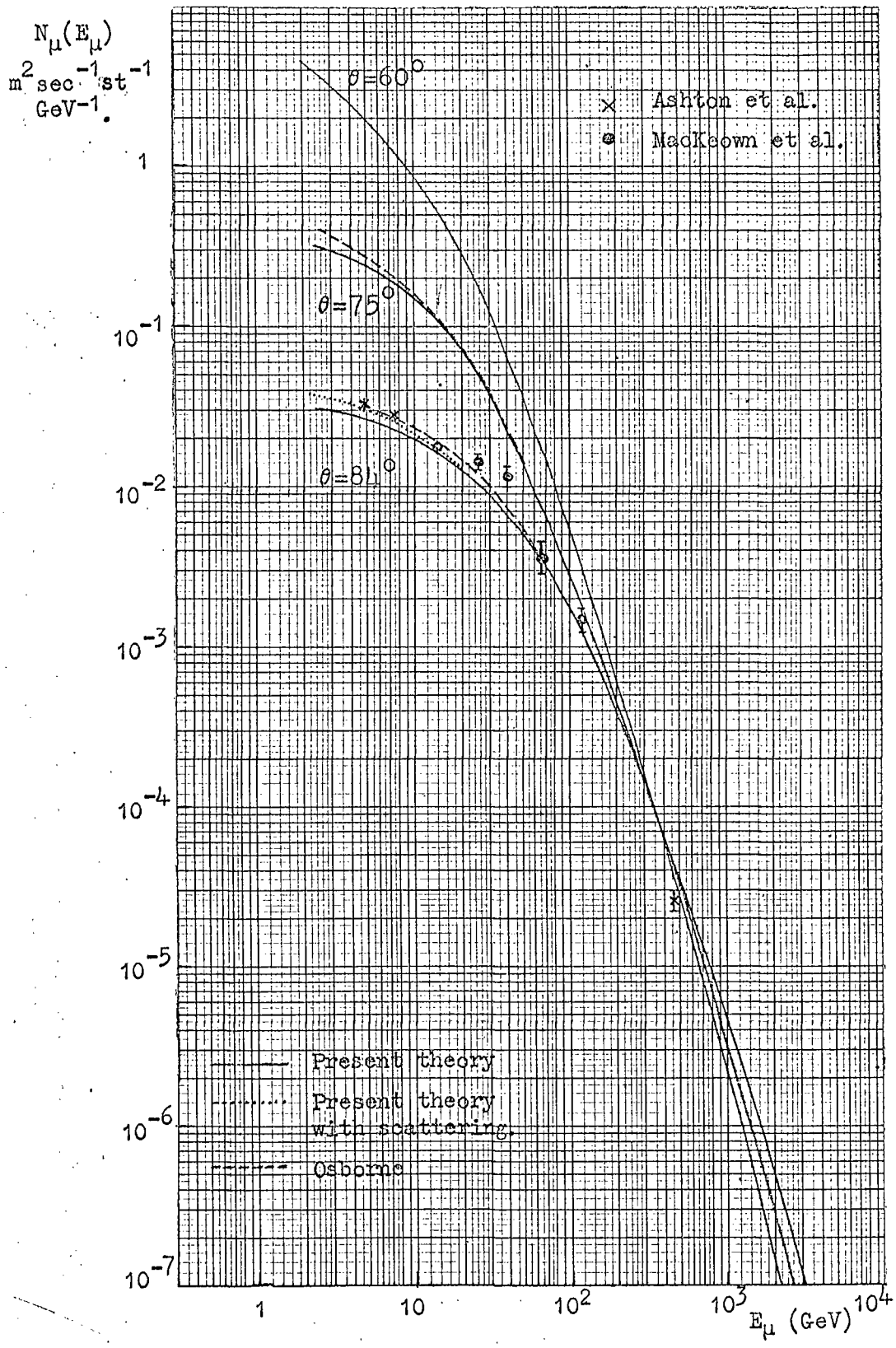

Fig. 7.3 Single muon energy spectra at sea-level.

Coulomb scattering of muons is of importance since at large zenith angles it can give rise to considerable variations in the length of the muon trajectory between production and sea-level. The net result is that the muon intensities at large zenith angles calculated taking scattering into account will be higher than in those neglecting scattering. Using the correction factors given by Osborne, the spectrum for $\theta = 84^{\circ}$ is elevated slightly at the lower muon energies thereby giving better agreement with experiment; there is no change in the muon intensities at $\theta = 60^{\circ}$ and 75° when scattering is included.

The conclusion to be made as a result of this analysis is that the model also predicts with good accuracy the longitudinal development of showers at large zenith angles.

From these energy spectra it is possible to determine the mean sea-level muon energy as a function of zenith angle, the resulting values are given in Table 7.1.

Table 7.1

The mean muon energy at sea-level for various zenith angles

θ	$\overline{E_{\mu}}$ s.l. GeV
60°	15.6
75°	26.8
84°	60.5

7.3 The Number of Muons at Sea-Level as a Function of Primary Energy

In Figure 7.4 the relationship between N_μ (>1 GeV) and E_p is shown for three zenith angles. It may be seen that there is an almost linear relationship for $E_p \gtrsim 10^4$ GeV and that $N_\mu \propto E_p^{0.9}$. Below $E_p \approx 10^4$ GeV the value of N_μ falls rapidly with decreasing primary energy, especially at the larger zenith angles; this is a consequence of the increasing muon path length with zenith angle since the muon energy at production must be relatively low and a large fraction of this energy will be lost in traversing the atmosphere, therefore the muon decay probability will be high and few muons will be seen at sea-level.

7.4 The Number of Muons at Sea-Level as a Function of their Height of Production

Figure 7.5 shows that the mean depth of muon production, for muons reaching sea-level with energies >1 GeV, is a function of both primary energy and zenith angle. Figure 7.6 may be used to convert from the muon production depth to height above sea-level along the trajectory. It should be remembered that the muon production depth is approximately 60 g.cm^{-2} lower (in the present model) than the parent pion production level. As an example, a primary proton of 10^7 GeV would give rise to a shower in which the sea-level muons would have a most probable height of

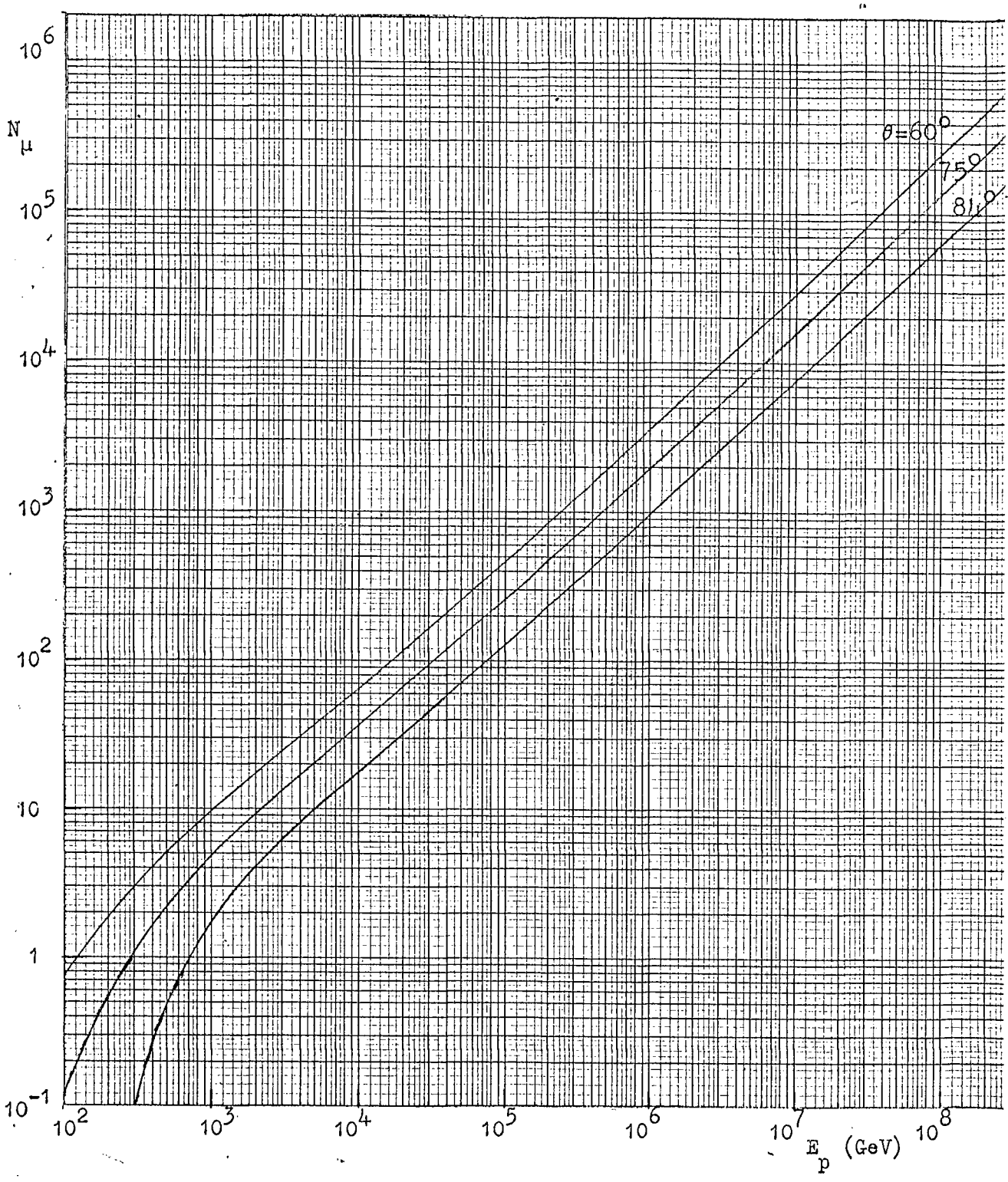

Fig. 7.4 The number of muons at sea-level with energy >1GeV as a function of the energy of the initiating proton.

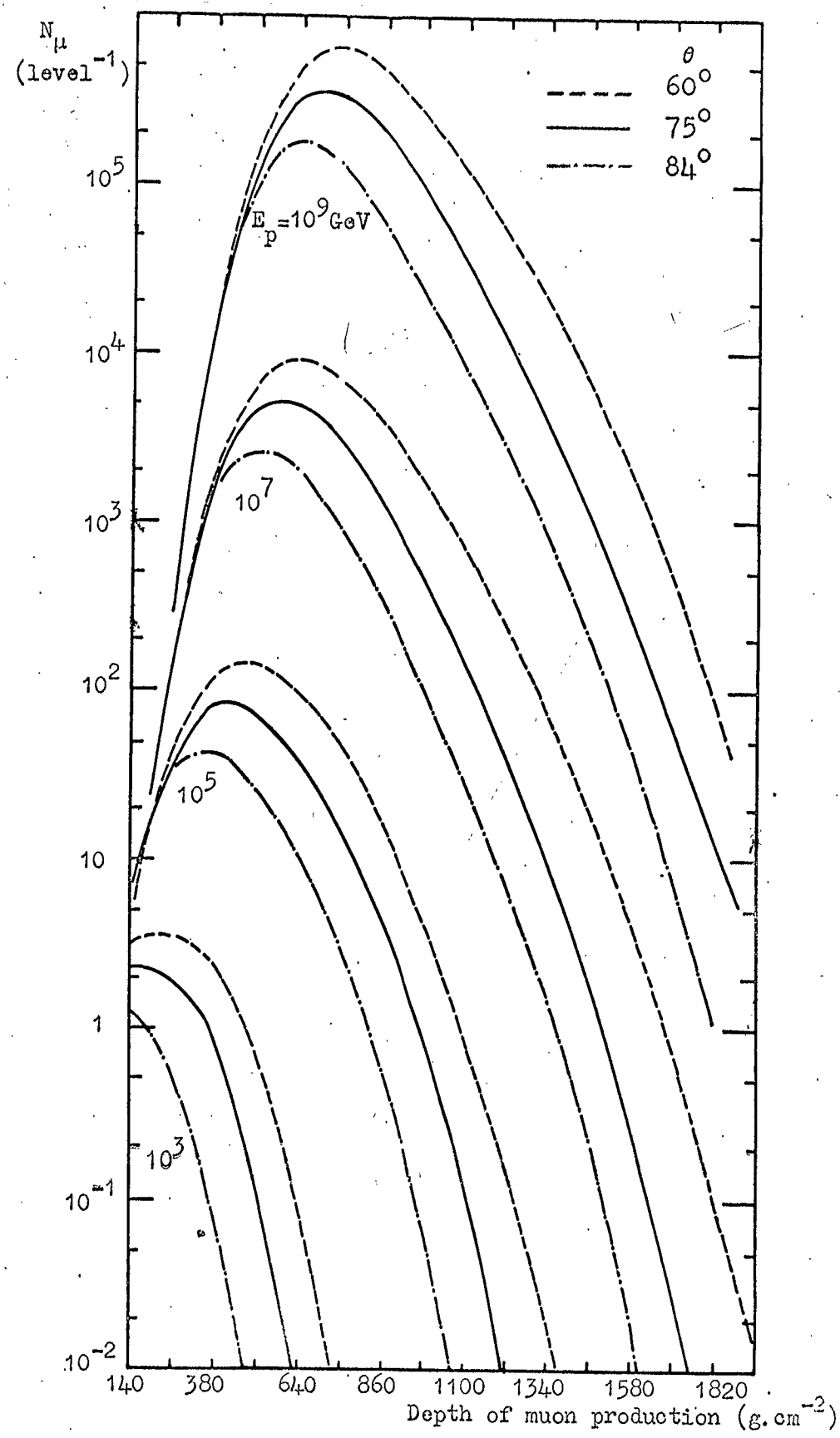

Fig. 7.5 The number of muons which survive to sea-level per production level.

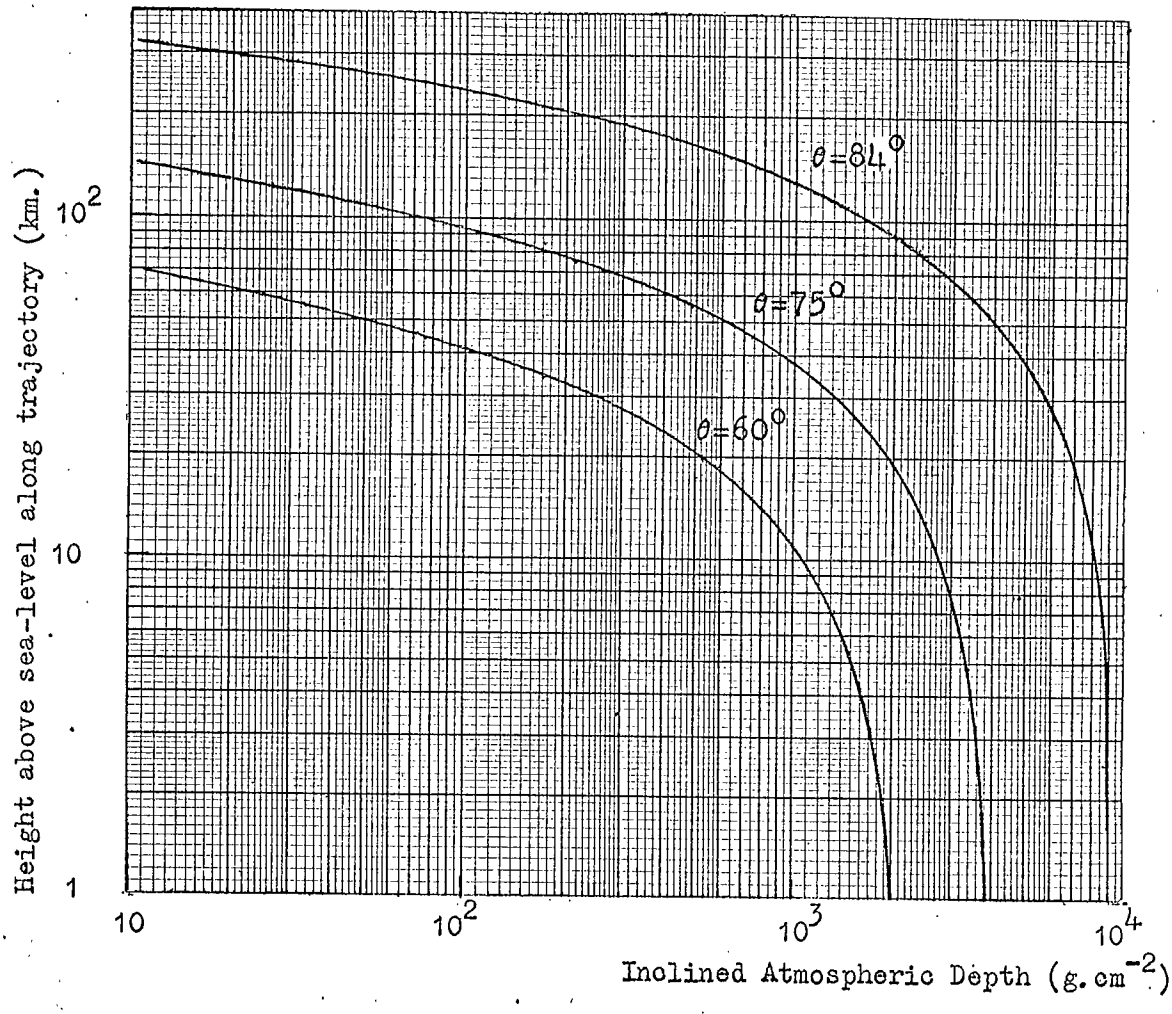

Fig. 7.6 The relationship between atmospheric depth and height above sea-level.

production of ~18.5 km at a zenith angle of 60°, ~52 km at $\theta = 75^{\circ}$ and ~155 km at $\theta = 84^{\circ}$.

7.5 The Lateral Distribution of Muons at Sea-Level

Initially the lateral spread of muons due to the introduction of the C.K.P. transverse momentum distribution is considered. The method of applying this to the muon energy spectra is identical to that used in the examination of the lateral spread of near vertical showers. In addition Coulomb scattering is considered.

7.5.1 Coulomb Scattering

The mean square value of the scattering is given for a cell of 12 g.cm^{-2} in depth in the following formula, which is derived in Appendix D.

$$\overline{\langle y^2 \rangle}_{12} = \frac{1.403\ 10^{-4}}{E_\mu{}^2} \left\{ h(\theta)^2 + \tfrac{1}{3}\left(\frac{0.12}{\rho(x)} \right)^2 \right\} \text{ metres}^2 \quad (7.1)$$

In order to calculate the total mean square displacement the mean square displacements for each 12 g.cm^{-2} cell between sea-level and the production depth are calculated and the linear sum of these evaluated.

If an annulus of mean radius r and width dr is considered, the probability of one particle which would have fallen within the annulus with no scattering, now falling on unit area at the centre of the annulus is given by:-

$$F(r)dr = \frac{1}{\pi\sigma_0^2} \exp\left(\frac{-r^2}{\sigma_0^2}\right) \qquad (7.2)$$

where σ_0 is the root mean square value of the total displacement; this expression is also derived in Appendix D.

The total number of particles falling in the annulus without scattering may be determined from the muon lateral density distributions for the case of transverse momentum only. Using this number with the formulae (7.1) and (7.2) the number falling on unit area at the centre of the annulus is calculable. Summing the results for annulii of increasing radius gives the resultant density of muons at a particular distance from the core of the shower. Repitition of this procedure for other distances from the core gives an overall picture of the lateral structure of the muon component of the shower after scattering has taken place.

7.5.2 Results of the Analysis

The muon lateral density distributions for showers initiated by primary protons of various energies are plotted for $\theta = 60^\circ$ and $\theta = 84^\circ$ in Figures 7.7 and 7.8. One effect of increasing zenith angle is, as mentioned earlier, that there is a more rapid decrease in muon number at sea-level as the energy of the primary particle falls below 10^4 GeV. This effect appears in these figures

Fig. 7.7 Muon lateral density distributions at sea-level and a zenith angle of 60°.

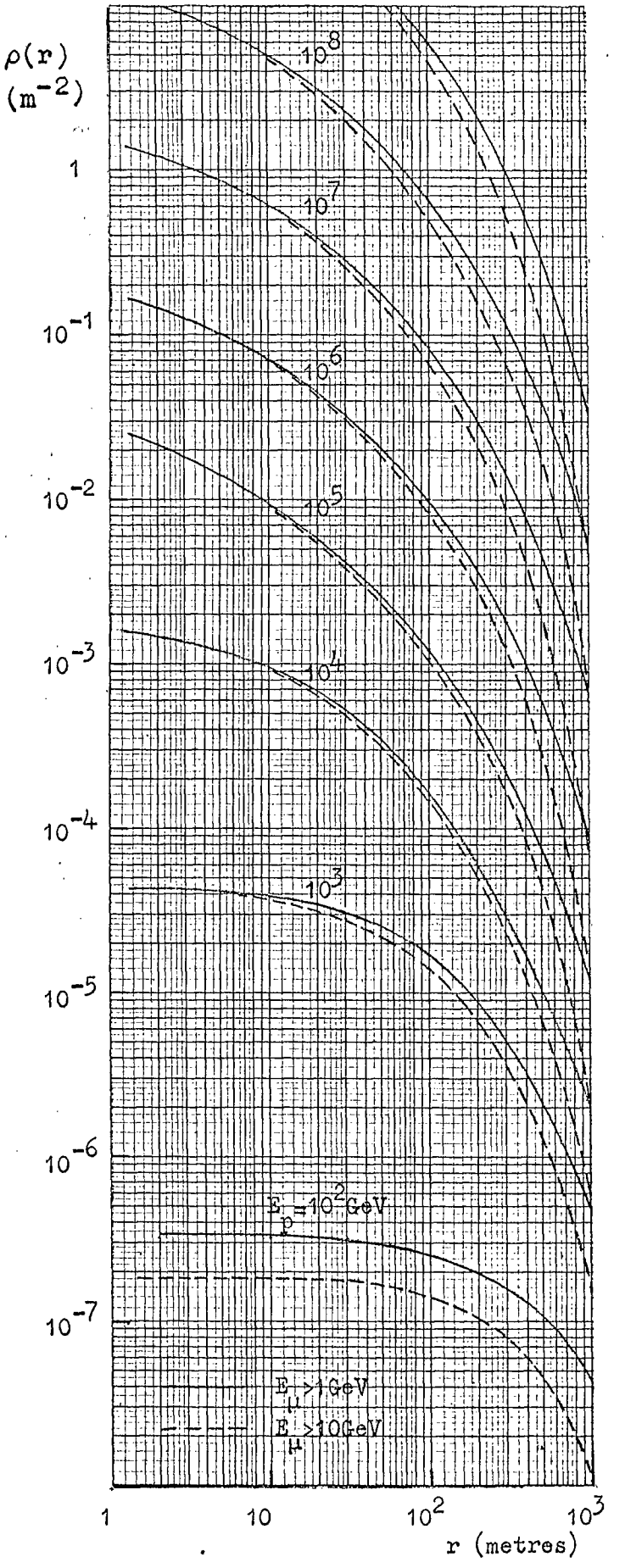

Fig. 7.8 Muon lateral density distributions at sea-level and a zenith angle of 84°.

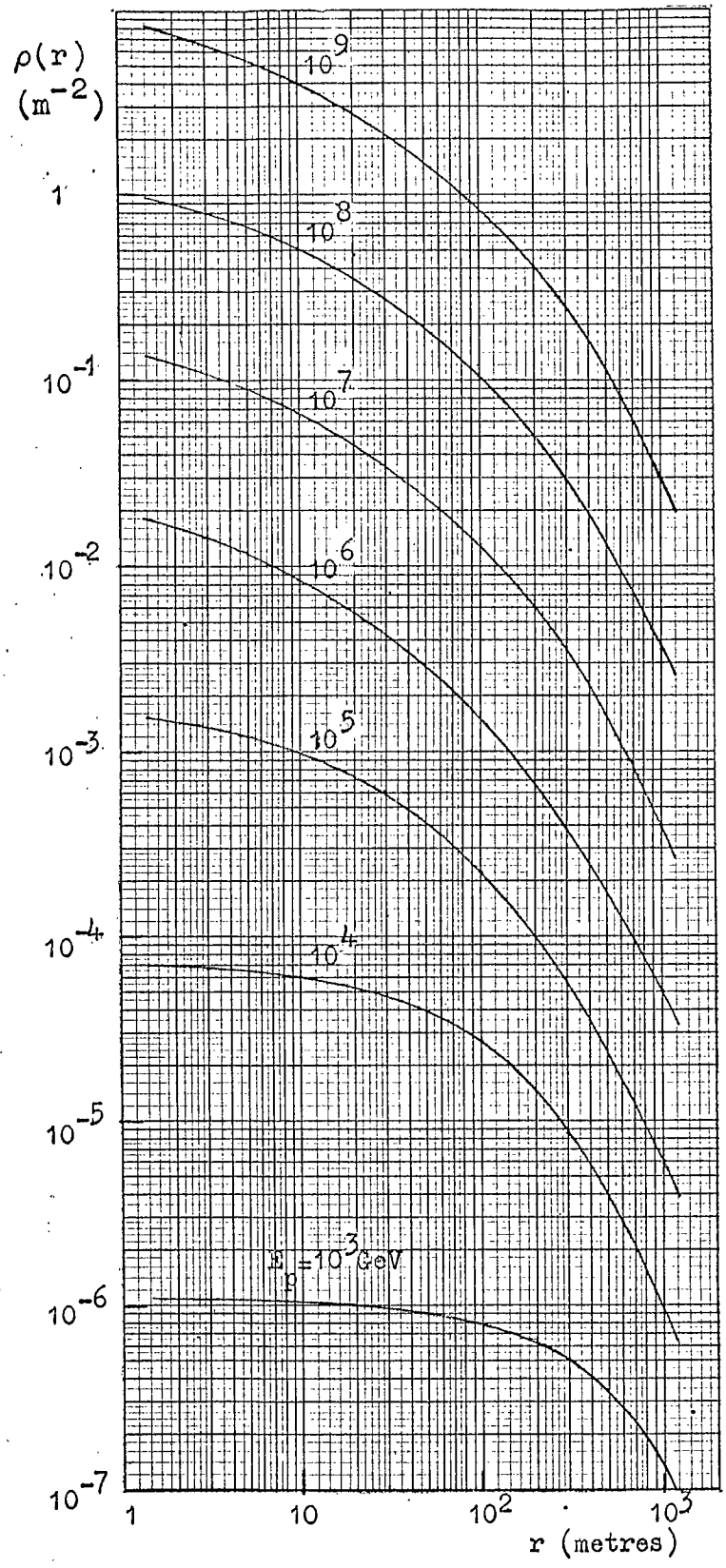

as a faster decrease in muon density, at specific distances from the core, as the primary energy falls below 10^4 GeV. The rate of decrease is again higher for the larger zenith angle.

It may also be seen that at $\theta = 84^\circ$ the distributions are considerably flatter than those for $\theta = 60^\circ$; this is again a consequence of increasing muon path length with zenith angle. All muons, especially those with low energies, will as a result of their transverse momentum and scattering fall at greater distances from the core at the larger zenith angles.

At a zenith angle of 60° it has been shown that the mean sea-level muon energy is ~16 GeV, therefore if the muon threshold energy is raised from 1 GeV to 10 GeV a significant change in the lateral distribution would be expected, this is shown in Figure 7.7. The result of a deficit of low energy muons is a steepening of the distribution since it is these low energy muons which suffer the greatest deflection and therefore arrive at large distances from the core. This steepening is not nearly as marked at $\theta = 84^\circ$ since the mean muon energy is much higher, ~60 GeV, and the fraction of muons having energies <10 GeV is considerably less than in the case of $\theta = 60^\circ$.

7.6 The Muon Density Spectrum

In order to predict a density spectrum of sea-level muons a primary energy spectrum should be folded into the muon lateral density distributions, initially the spectrum of Linsley (1964) was used. The resulting spectra for threshold energies of 1 GeV and 10 GeV for $\theta = 60^{\circ}$ and for 1 GeV at $\theta = 75^{\circ}$ and 84° are shown in integral form in Figure 7.9. The slope of the $\theta = 84^{\circ}$ spectrum increases from -1.8 at a density of 10^{-4} particles. m^{-2} to -2.2 at 10^{-2} particles m^{-2}; the effect of increasing the threshold energy at $\theta = 60^{\circ}$ may be seen to be a significant reduction in the frequency of occurrence of low density showers.

7.7 Comparison of the Zenith Angle Distribution with Experiment

The predicted rate for the observation of muon showers at a particular zenith angle may be obtained by applying the triggering conditions for the apparatus involved to the density spectrum to give an effective density spectrum and integration is carried out under this spectrum. In addition, allowance is made for the effect of the earth's magnetic field at the location of the apparatus.

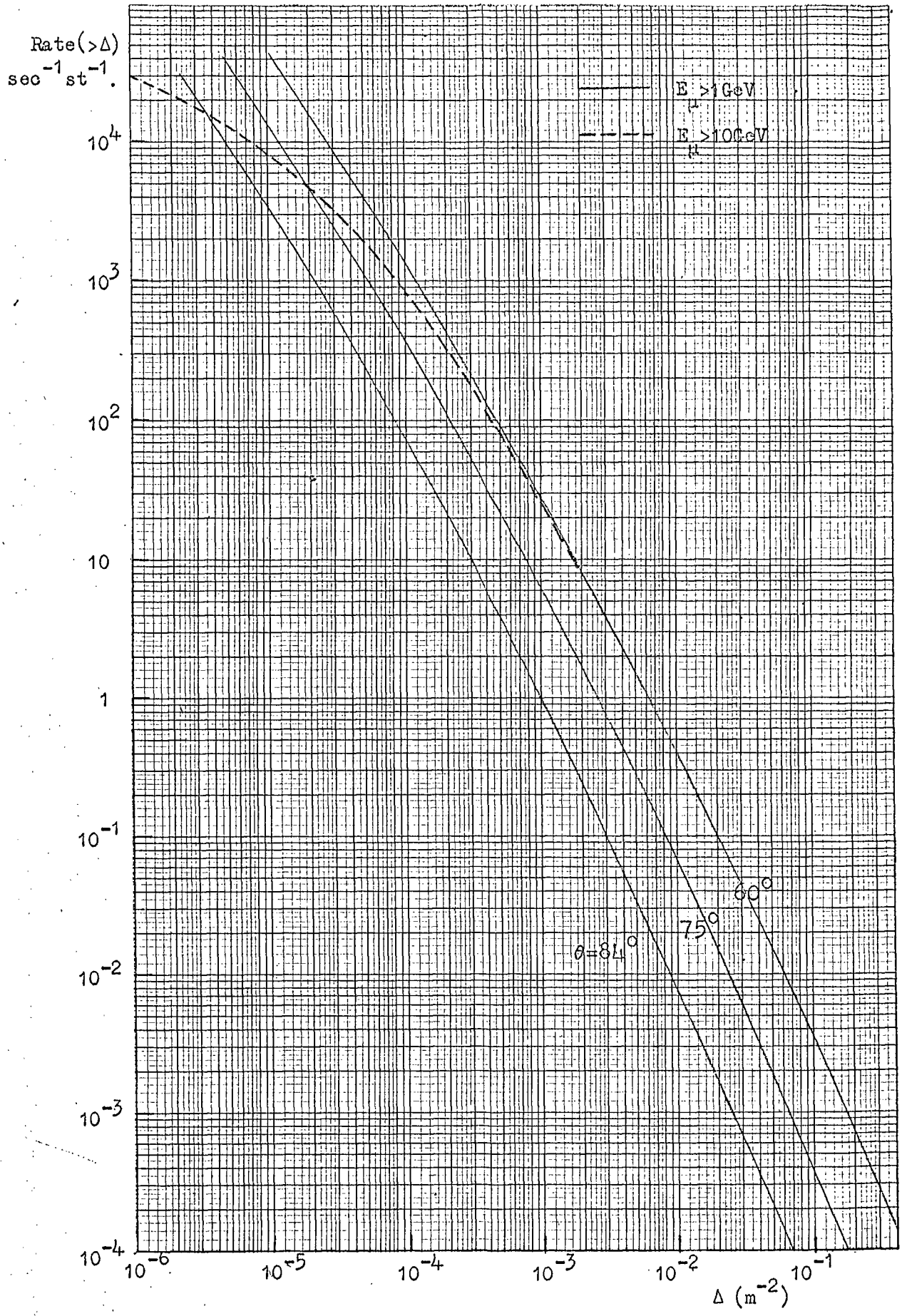

Fig. 7.9 The integral sea-level muon density spectra.

7.7.1 The Correction for the Earth's Magnetic Field

Precise calculations have been made at a zenith angle of 75° in order to obtain the root mean square distance $(\overline{r^2})$ of muons in showers under the following conditions.

i) with transverse momentum and scattering incorporated $(\overline{r_i^2})$

ii) with geomagnetic deflection only $(\overline{r_{ii}^2})$

The method of calculation of geomagnetic displacement for a single particle is to divide the muon trajectory into steps of 12 $g.cm^{-2}$ and to use the expression derived in Appendix E for the root mean square displacement in such a cell, which is:-

$$\sigma_{12mag} = \left[\frac{5.4\ 10^{-6} \times (h(\theta) + 0.06/\rho(x))}{3\rho(x)\ E_{\mu}}\right]^{\frac{1}{2}} \text{ metres} \qquad (7.3)$$

These are added in quadrature to give the total root mean square displacement for a single particle.

The result is that $\overline{r_{ii}^2} = 1.5\ \overline{r_i^2}$ for the magnetic field prevailing in Durham where the total magnetic intensity is 0.48 gauss and the angle of inclination is 67°, declination being 9° W of N.

The geomagnetic correction factor at $\theta = 75^{\circ}$ is defined to be:-

$$F_{75} = \sqrt{1^2 + (1.5)^2} \qquad (7.4)$$

That is, instead of considering the shower to be within the circular limits which arise when transverse momentum and scattering only are considered, or within an ellipse like boundary as in reality with geomagnetic deflection incorporated, the shower is considered to be circularly symmetrical with a radius which lies between that of the original circle and the semi-major axis of the ellipse. The first term inside the square root of (7.4) represents a mean transverse momentum of 0.4 GeV/c; the projection of this on the major axis of the ellipse should in fact be taken when combining with the geomagnetic deflection correction factor. To compensate for this the arithmetic mean is taken of the zenith angle distributions with and without geomagnetic correction.

The correction factor is dependent on the muon path length; geomagnetic deflection is proportional to path length, (l_θ), squared and the deflection due to transverse momentum is proportional to l_θ. In addition the angle (δ_θ) between the particle trajectory and the magnetic field direction must be considered. For other locations the correction factor also contains a term R which represents the ratio between the total magnetic field intensity at the location and the value in Durham. Thus the factor becomes:-

$$F_\theta = \sqrt{1^2 + \left(1.5\ R\ \frac{l_\theta}{l_{75}}\ \sin\delta_\theta\right)^2} \qquad (7.5)$$

The method of applying this correction factor is to move each point of the differential incident density spectrum to the left by F_θ^2 to allow for the increase of the area on which the shower falls, then up by F_θ^2 to allow for change in cell width and up by a further F_θ^2 because of the increased number of showers which will be capable of triggering the array.

7.7.2 Comparison with Durham Zenith Angle Distribution

The array triggering probability is given by:-

$$\text{A.T.P.} = (1 - e^{-\Delta S})^2\ e^{-\Delta S},\ S = 1\ m^2.$$

in this case and those following S will be the area presented by the triggering detectors to particles incident normally on the apparatus. The variation of effective area with zenith and azimuthal angle is not required since it is incorporated in the experimental points.

When this triggering function is folded into the appropriate density spectrum it is found that the integration to obtain the rate at a particular zenith angle is not convergent. That is to say, when integrating back to smaller densities the contributions from each cell do not become negligible with respect to the total. The solution to this problem has been to integrate under the energy

spectrum (Figure 7.3) for that angle in order to obtain the rate of single muons, the second stage being to find the lower limit for integration over the incident density spectrum which will give the same rate. This lower limit is then applied to the integration under the effective density spectrum. This procedure is used for all three zenith angles and the resultant zenith angle distribution without geomagnetic correction is shown as the broken line of Figure 7.10, which also shows the experimental points. This figure also gives the curve obtained when geomagnetic deflection is incorporated with mean transverse momenta of 0.4, 0.65 and 0.8 GeV/c.

If the discrepancy between the theory with the 'normal' mean transverse momentum of 0.4 GeV/c and experiment is solely a transverse momentum effect then this figure implies that the mean transverse momentum of particles released in high energy interactions is in the order of 0.8 GeV/c. It may be seen that the zenith angle distribution is extremely sensitive to the mean transverse momentum and that a two-fold increase in $\langle p_t \rangle$ leads to a ~~ten~~ four-fold reduction in the rate observed by the array.

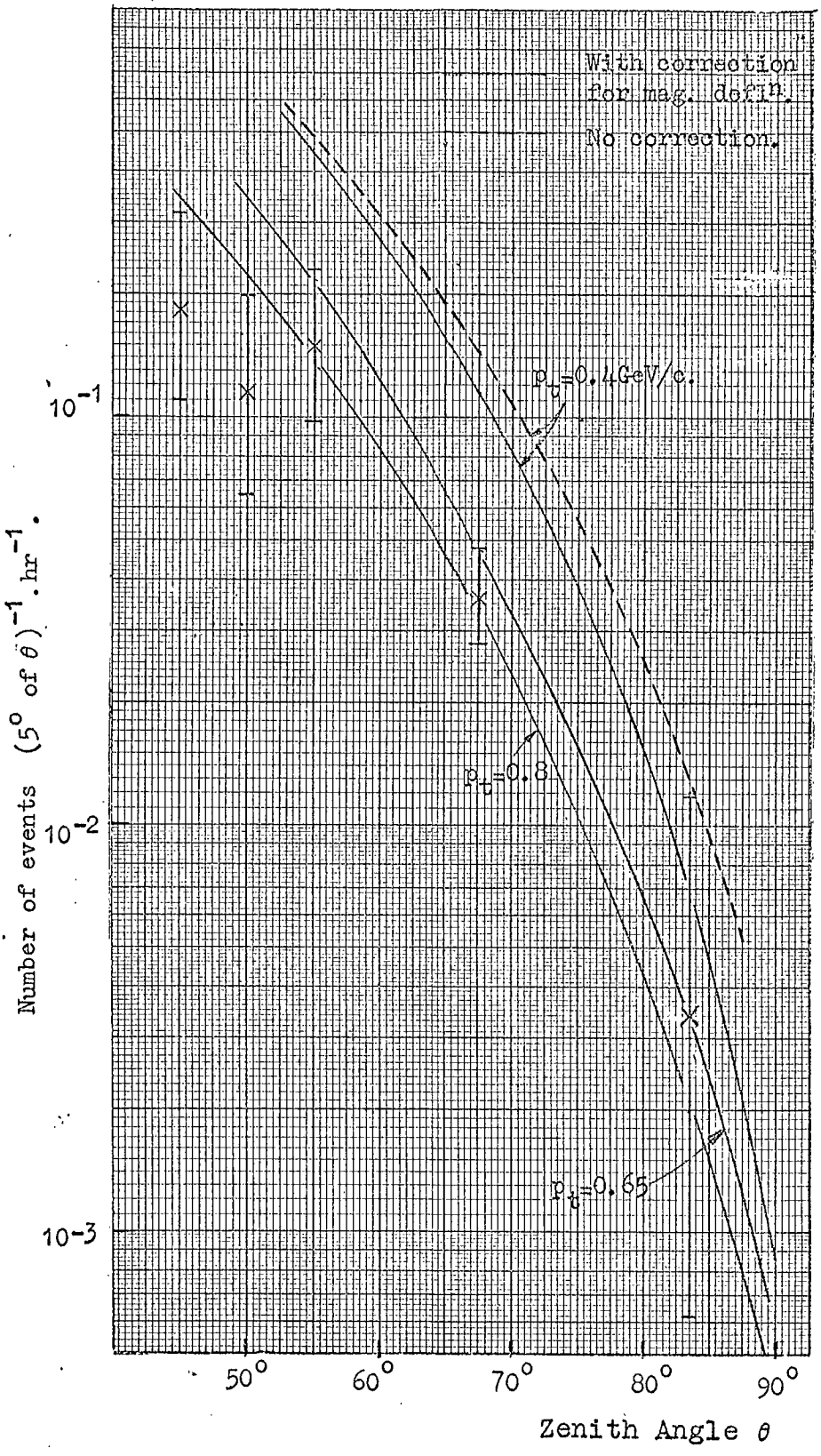

Fig. 7.10 Comparison of the predicted muon zenith angle distribution with the distribution determined from the Durham array data.

Although the correction for geomagnetic correction might be considered somewhat crude in itself, it should be borne in mind that a 100% change in effect of this correction on the zenith angle distribution will only make an approximately 15% change in the derived value of $\langle p_t \rangle$. Thus errors due to the inaccuracy of this correction are not thought to be important, at this stage, in comparison with the errors on the experimental points.

The N_μ-E_p dependence (Figure 7.4) in the energy region giving the maximum contribution to the rate is such that in going from proton to heavy primaries there is an increase in number of muons observed. This leads to an elevation of all lateral distributions which in turn gives rise to an enhanced rate. This is slightly offset by the slight flattening of the lateral distributions, which will lead to a reduction in the rate. The net result is however a slight increase in the predicted rate and it must be concluded that the introduction of heavy primary particles will not improve the fit between theory and experiment.

7.7.3 Comparison with the Utah Zenith Angle Distribution

The earth's magnetic field at Utah has a total intensity of 0.55 Gauss and the angle of inclination is $\sim 72^\circ$.

Apart from the array triggering probability being:-

$$A.T.P. = \frac{(S\Delta)^2}{2} e^{-\Delta S}, \quad S = 20 \text{ m}^2$$

the method is the same as that detailed in the preceding section.

A comparison is made with the experimental results of Parker in Figure 7.11 and it may be seen that to obtain a reasonable fit a mean transverse momentum of 1.2 GeV/c is required.

7.7.4 Comparison with the Nagoya Zenith Angle Distribution

At Nagoya the total geomagnetic intensity is 0.4 Gauss and the inclination is $\sim 50^{\circ}$.

$$A.T.P. = (1 - e^{-\Delta S})^2, \quad S = 10 \text{ m}^2$$

In this comparison it is necessary to allow for the fact that the muon threshold energy is reported to be ~10 GeV. Two lines are drawn on Figure 7.12 showing zenith angle distributions uncorrected for geomagnetic deflection, one for $E \gtrsim 1$ GeV, the other for $E \gtrsim 10$ GeV; the difference in slope and magnitude is small. This is because the maximum contribution to the rate is made by showers having a density of $\sim 4\ 10^{-3}$ particles m^{-2} at the array whereas the decrease in the incident density spectrum caused by an increase in the muon threshold energy

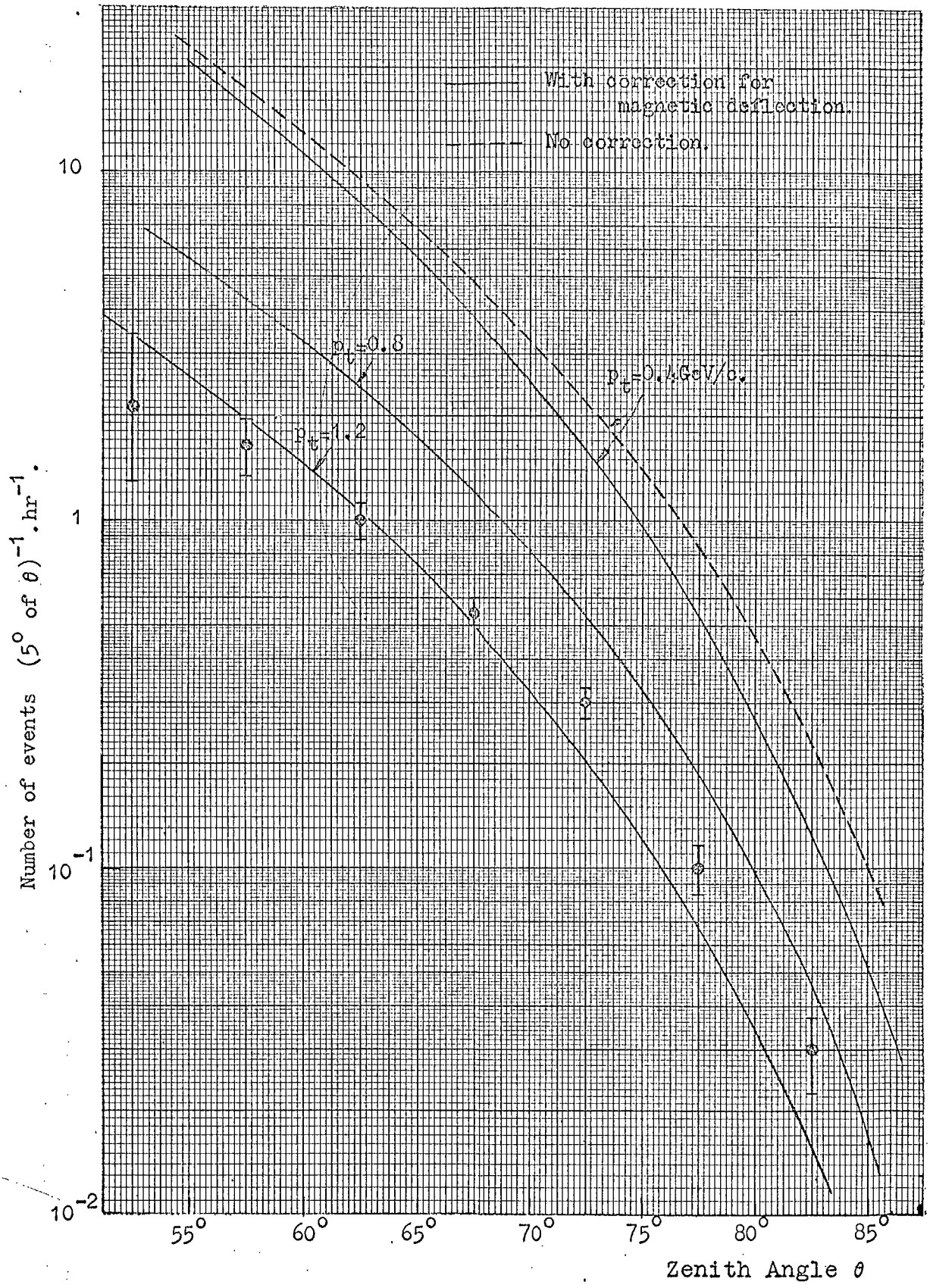

Fig. 7.11 Comparison of the predicted muon zenith angle distribution with the Utah distribution.

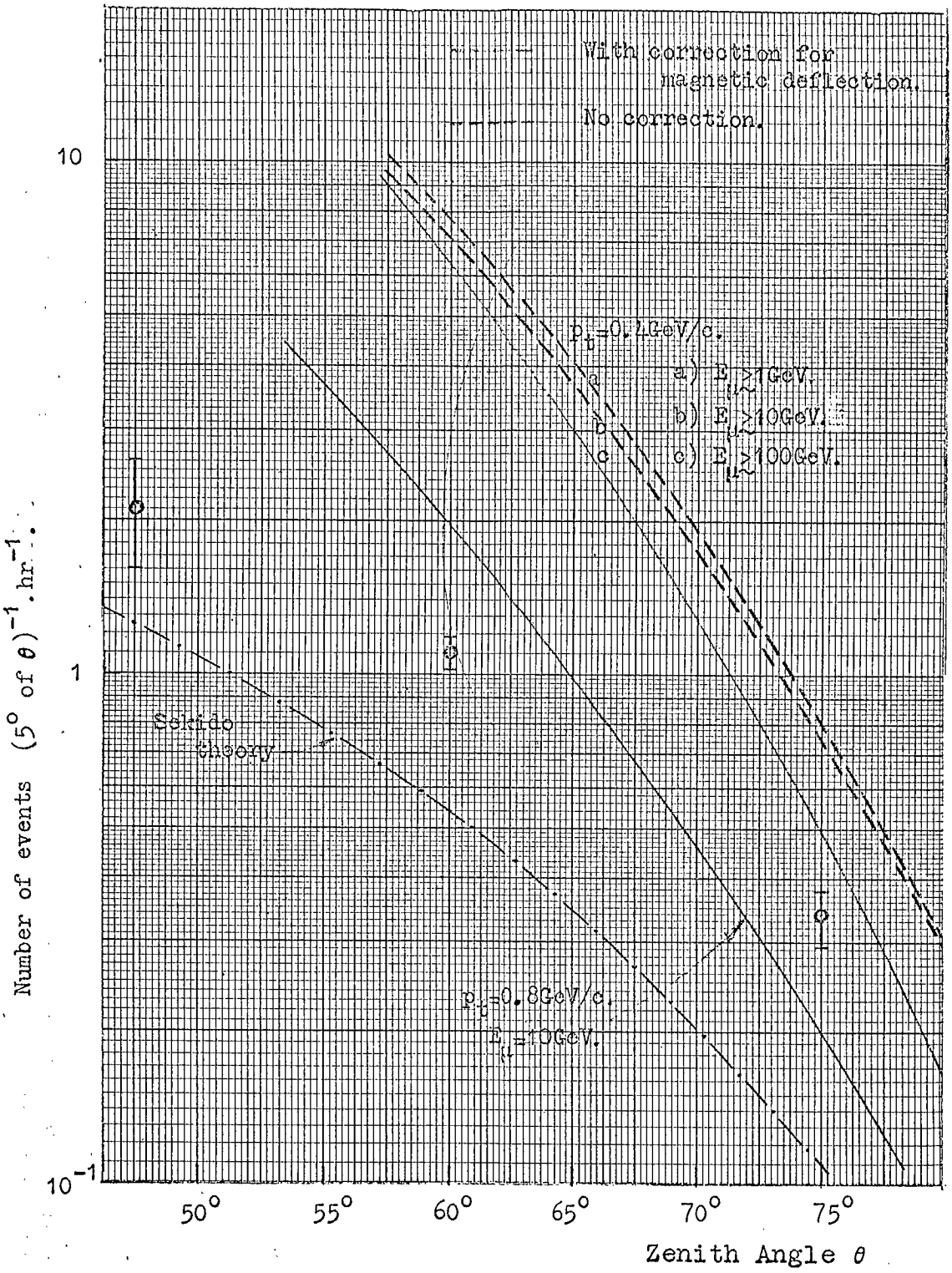

Fig. 7.12 Comparison of the predicted muon zenith angle distribution with the Nagoya distribution.

occurs at densities of $\lesssim 10^{-4}$ particles m^{-2}.

The conclusion is that it is extremely difficult to explain the Nagoya results in terms of the present theory.

It will also be noticed that there is a great discrepancy between the present theory and that of Sekido et al. which uses a $\langle p_t \rangle$ of 0.4 GeV/c. Analysis has shown the discrepancy to be mainly due to the different lateral structure function used by Sekido et al.; these authors assumed that $\Delta_\mu(r) \propto r^{-\frac{1}{2}}$ which is very much flatter than that predicted by the present theory. This flattening of the muon lateral density distribution is in fact comparable to that which would be produced by a considerable increase in the mean transverse momentum, and as already observed this would lead to a reduction in the predicted rate.

However, the fact still remains that the experimental points of Sekido et al. are not in agreement with the shape of the zenith angle distribution predicted by either of the theories.

7.7.5 Comparison with the Durham Number Spectrum

The incident density spectrum is converted to an effective density spectrum by the introduction of the array triggering probability. The number spectrum may

be obtained from the effective density spectrum by taking a cell of the latter having a certain median density and allowing Poissonian fluctuations in the number of particles crossing the flash tube trays as accompaniment of the triggering particles. This procedure is carried out for each cell of the effective density spectrum and the resultant frequency distributions are summed to give the number spectrum.

Several models of the primary flux have been used in this analysis.

i) Proton composition throughout with an energy spectrum as given by Linsley (1964), (equations 1.1 and 1 .2). This model of the primary flux is identical to that predicted by Hillas (1967), the background to this having been mentioned in §1.1.

The predicted number spectra for three values of $\langle p_t \rangle$ are shown in Figure 7.13 where comparison is made with the experimental points. This figure implies that a $\langle p_t \rangle$ of 0.8 GeV/c is required for the two-particle events whereas a value of 0.4 GeV/c would be satisfactory for the denser events. Figures 7.13 and 7.10 are not inconsistent since the experimental points on the latter are for 'Sekido type' events only, that is, for two-particle events, and the required $\langle p_t \rangle$ in this case

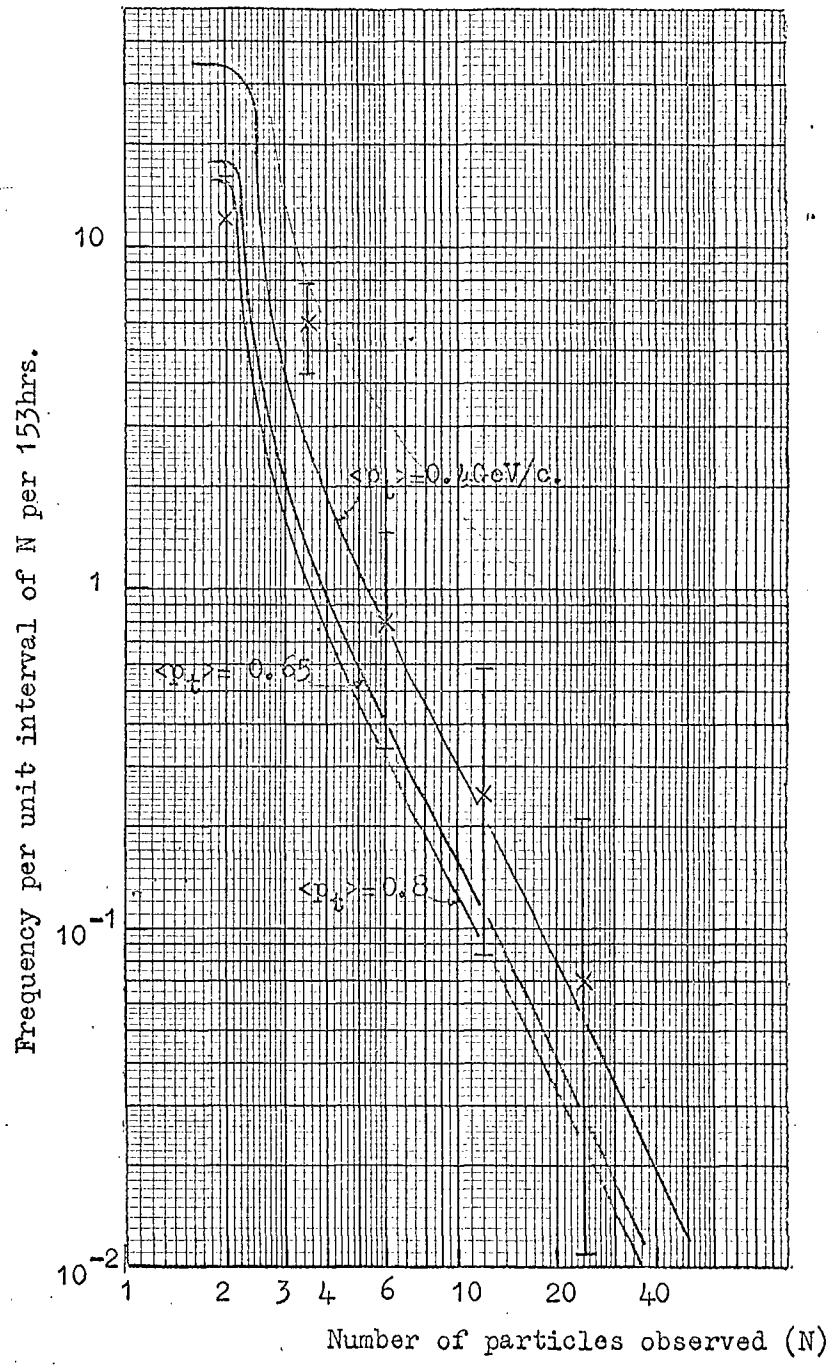

Fig. 7.13 Comparison of the predicted muon number spectrum with that determined from the Durham array data, in the angular range $57.5^{\circ} < \theta < 90^{\circ}$, $E_{\mu} \geq 1$GeV.

agrees well with that required for the two-particle events of the number spectrum.

It has been shown (§7.7.2) that the introduction of heavy primary nuclei into the model will not improve the fit between the predicted zenith angle distribution and that observed experimentally; but further evidence, to be presented later in this section, indicates that the deterioration in the fit will be only slight. Thus in the next phase of the analysis a mean transverse momentum of 0.8 GeV/c will be used and heavy primary nuclei will be introduced in an effort to reduce the discrepancy between theory and experiment for the >2 particle events of Figure 7.13.

ii) The modulated energy spectra of the various components of the primary flux adopted for this section of the analysis are shown in Figure 7.14, heavy nuclei becoming increasingly important for primary energies $\gtrsim 3.10^{15}$ eV. The result of using this model to predict the number spectrum is shown in Figure 7.15 denoted by (ii). As suggested previously the change to the rate of two particle events in changing from the protons only composition of the previous model, (i), is only small. This may be attributed to the fact that the two particle events arise from the lower energy primary particles which, as Figure 7.14 shows, are predominantly protons

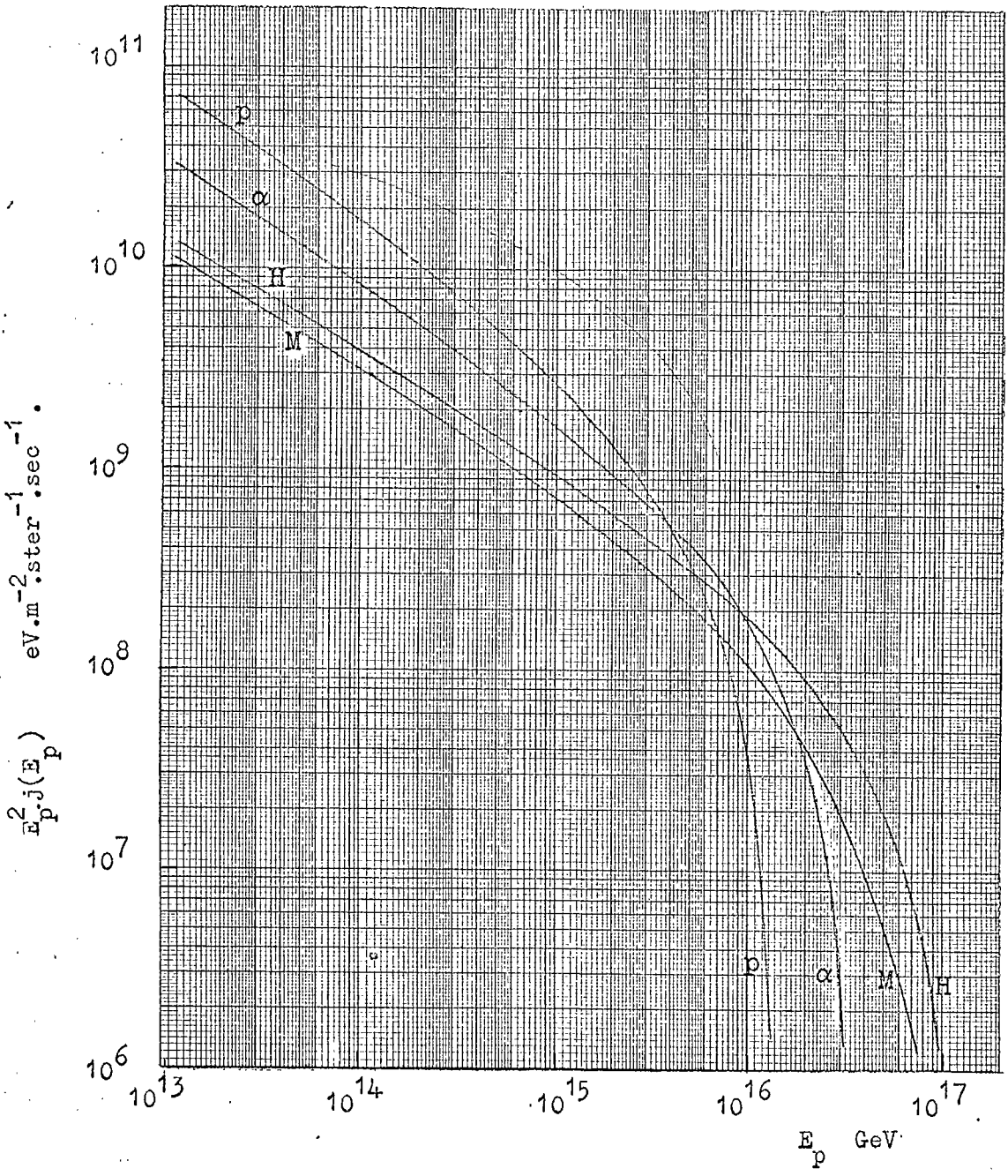

Fig. 7.14 The form of the primary flux adopted in model (ii). Ep is the energy per nucleus

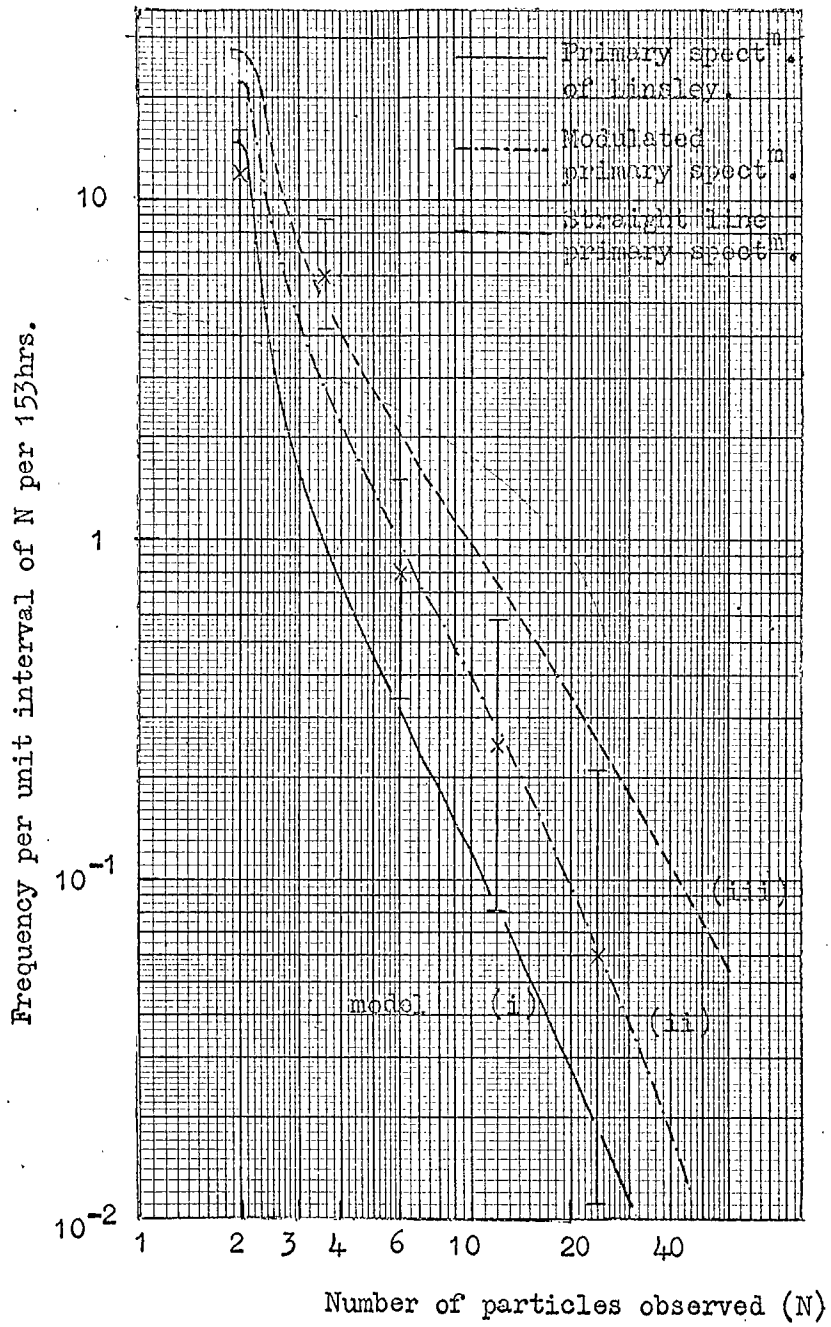

Fig. 7.15 Comparison of the predicted muon number spectrum for various models of the primary flux and $\langle p_t \rangle = 0.8$GeV/c, with the Durham data, $E_\mu \gtrsim 1$GeV.

anyway. The role played by the heavier nuclei increases when the primary energy exceeds a few times 10^{15} eV, and this is reflected in the increase in frequency of >2 particle events with respect to the spectrum predicted by model (i) which is shown in Figure 7.15 for $\langle p_t \rangle$ = 0.8 GeV/c for reference.

It may be concluded that model (ii) gives satisfactory agreement with the experimental results as they stand at the moment; it is hoped that the statistical errors on the experimental points will be reduced in the near future thus making a more conclusive statement possible.

iii) The third model of the primary flux considered has a straight line energy spectrum with protons throughout; the number spectrum which this predicts is shown as (iii) in Figure 7.15.

The adopted primary spectrum is that given by Adcock et al. (1967). In order to preserve the shape of the sea-level size spectrum it is necessary to make some change in the nature of high energy interactions. Adcock et al. suggest either a change in the multiplicity law at a few times 10^{15} eV, or a decrease in the nucleon interaction length in the same region of energy.

The result of this model is that the predicted frequency of two particle events and >2 particle events is increased to such an extent that the theoretical line now lies above the experimental points. A possible way of improving the fit between model (iii) predictions and experiment would be to propose a reduction in the coefficient of the primary energy spectrum.

7.7.6 Comparison with the Utah Multiple Events

When analysis is made using a $\langle p_t \rangle$ of 0.8 GeV/c and the Utah triggering probability, for the three models of the primary flux, the following two-muon event to three-muon event ratios are predicted, Table 7.2.

Table 7.2

The predicted two-muon event to three-muon event ratios for the Utah apparatus

Model	Ratio
(i)	36:1
(ii)	19:1
(iii)	13:1

These are to be compared with the experimental ratio of (23 ± 7):1. It is seen that model (ii) gives a result which lies within the experimental errors and this gives more weight to the conclusion expressed in the previous

section. Parker (1967) also gives a two-muon event to four-muon event ratio of 250:1, but this is based on only one four-muon event.

7.7.7 Summary

This analysis of muons in large zenith angle showers has provided further substantial evidence for an increase in the mean transverse momentum of secondary particles in high energy interactions, and the value required is in accord with the values given in §6.5.4.

Furthermore, evidence has been presented in §7.7.5 and §7.7.6 in favour of the second model for the primary flux, that is, a modulated flux as illustrated in Figure 7.14, and the analysis discriminates against the two models in which there is proton composition throughout.

7.8 The Role of Fluctuations in Large Zenith Angle Showers

Although calculations involving fluctuations have not been carried out at large zenith angles it is thought that their inclusion would have little effect on the results presented for muons because of the great depth of atmosphere in which shower development may take place.

However it is imperative that any proposed electron calculations should take fluctuations into account since an electron shower is formed and dies away over a relatively small thickness of atmosphere. Consequently a nucleon or charged pion which survived interaction or a neutral pion which survived decay until it had almost reached sea level could give rise to an electron shower which would not be seen with a non-fluctuating model. The results of the present model show at $\theta = 60^{\circ}$ a very low mean number of electrons compared with what is observed experimentally. This could be due to the neglect of fluctuations or because electrons produced as knock-ons by muons and those resulting indirectly from Bremsstrahlung have not been considered.

CHAPTER 8

Conclusions and Future Work

8.1 Conclusions

It has been shown that the adopted model will at all zenith angles accurately predict the sea-level energy spectrum of single muons, that is to say, it satisfactorily explains the longitudinal development of the muon component of E.A.S. This does not of course mean that the correct values for the model parameters and shapes of spectra have been determined, however, it does imply that when these are taken in conjunction with each other they form a satisfactory model.

When predictions for the lateral spread of near vertical showers are compared with experimental determinations for various muon threshold energies, two facts are immediately obvious. The first is an overestimate of muon densities at small radial distances for all threshold energies and secondly there is an underestimate of the muon density at large radial distances and at the higher threshold energies. The former has been explained in terms of a reduction in the probability of transverse momentum transfers below 0.1 GeV/c. Several explanations are put forward for the second phenomenon which does seem to be a real effect and not a consequence of experimental

biasses. This second discrepancy has also been noted very recently by Murthy et al. (1967) who compare the results of a simple theoretical treatment with experimental results. If the explanation is made solely in terms of a change in mean transverse momentum, then the present analysis indicates that for $E_\mu > 10$ GeV a value of $\langle p_t \rangle$ of 0.6 GeV/c is necessary and for $E_\mu > 100$ GeV/c, $\langle p_t \rangle \approx 1$ GeV/c is required.

With regards to the discussion of the merits of one centre and two centre models for the energy distribution of secondary particles (§5.4); it was stated that a two centre model would give rise to a steeper lateral distribution of muons, thus the choice of the C.K.P. one centre model seems to have been justified.

The introduction of the passive baryon and isobar theories decreases the accuracy of fit of the predictions of the model, consequently their introduction into a shower model cannot be advocated on the present evidence.

The study of fluctuations in the muon lateral distribution has shown the importance of experimental bias towards the selection of flatter showers, that is, those showers in which the primary particle has made several early interactions. Investigations into the fluctuations of the total number of electrons in near-vertical

E.A.S. have shown that the choice of this parameter as the datum for shower selection is unfortunate in view of the large fluctuations in N_e compared with the quite small fluctuations in N_μ.

Further evidence for an increase in the mean transverse momentum arises from a study of the muon component at large zenith angles. When comparison is made between the present theory and the results of the Durham array a value of $\langle p_t \rangle$ of 0.8 GeV/c is found to satisfy both the measured zenith angle distribution and the number spectrum. Both the value of $\langle p_t \rangle$ and the energy of parent particles making the major contribution are in good agreement with the range of values determined in the analysis of near vertical showers.

The results of analyses of both vertical and large zenith angle showers provide evidence for a change in the primary composition from predominantly protons to a higher effective mass at a primary energy of a few times 10^{15} eV. The evidence from the Durham number spectrum seems to be emphatically in favour of this model of the primary flux, provided that the assumed features of the interaction model are correct, and it discriminates against those models of the primary flux in which there is proton composition throughout. Comparison with the Utah multiple event ratios does not

provide conclusive evidence but it does tend to confirm the above statement. The comparisons are not dependent on the very high energy primary flux, consequently nothing can be deduced from the present work with regards to the 'ankle' in the primary energy spectrum at $\sim 10^{17}$ eV.

8.2 Modifications to the Array

The conclusion with regards to the array is that it has been satisfactory in operation so far; however, modifications have been made which will make the analysis easier and should provide further information about highly inclined muon showers. It would be advantageous to have a run of a few thousand hours in order that the statistical errors on the present experimental points may be reduced significantly. Chapter 7 showed that the zenith angle distribution is extremely sensitive to the assumed value for the mean transverse momentum and it is hoped that as the experimental errors are reduced so the value of $\langle p_t \rangle$ may be specified with increased certainty. When the number spectrum has been evaluated from the data of a longer experimental run a more precise statement concerning the model of the primary flux should be possible.

The major modifications to the array concern the triggering system; instead of a two-fold trigger on single scintillation counters S_1 and S_4, these are replaced by two-element telescopes; it will also be possible to trigger from a 120 GeV m.d.m. horizontal spectrograph which is in line with the 'east' telescope.

A schematic side view of one of the telescopes is shown in Figure 8.1, these are situated such that scintillation counters S_1 and S_4, as shown in Figure 2.1, form the first elements of the west and east telescopes respectively; the triggering elements of the east telescope are shown in the figure as S_4 and S_{4a}. Triggering particles from the north have to be capable of penetrating a total of approximately 5.75" iron, that is ~8.6 radiation lengths, there is in addition a 3" thick wall of barytes laded concrete which contributes a further two radiation lengths of absorber. This should be quite sufficient to rule out all possibility of a north triggering particle being anything other than a muon.

Near vertical showers of electrons will be eliminated by two means, first of all there is the anti-coincidence counter $\overline{S}_5$ and in addition at least four radiation lengths of absorber will be located above each telescope.

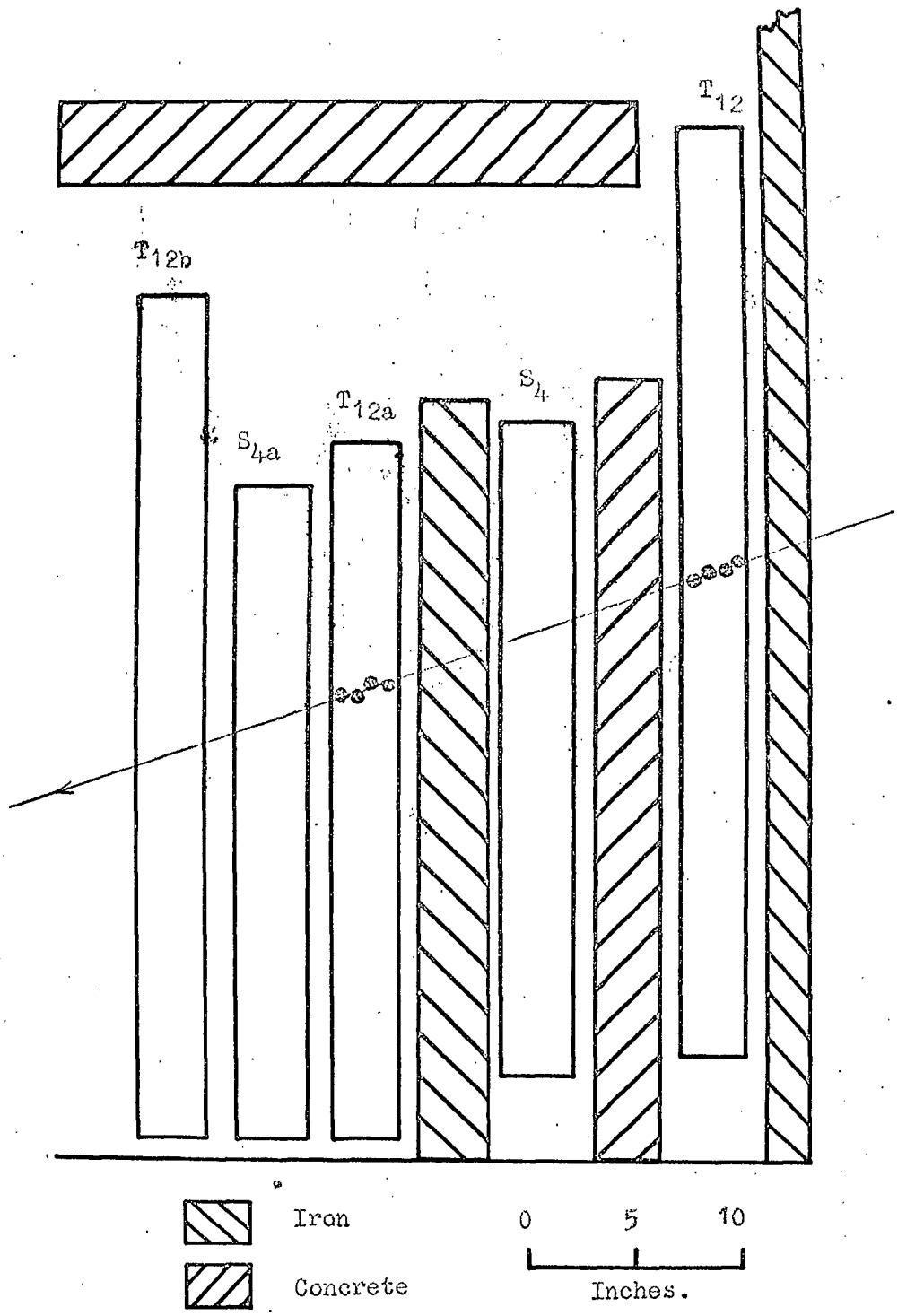

Fig. 8.1 A telescope of the modified Durham Horizontal Extensive Air Shower Array.

The zenith angle of the shower will be calculated from the tracks of the two triggering particles in two flash tube trays, for example, in the east telescope system, T_{12} and T_{12a} which are situated 48 cms apart. Tracks in the remainder of the flash tube trays will have to have a tube configuration consistent with this angle in order to be counted as a constituent of the muon shower. Flash tube tray T_{12b} in which the tubes are vertical will be used to measure the azimuthal angle of the shower. Thus the determination of shower direction can be made with greater accuracy, this means that the effective area of the array and hence the muon density may be determined more precisely. Each telescope will accept muons from the north in the zenith angle range $\sim 30^{\circ}$ to 90°.

ACKNOWLEDGMENTS

The author is grateful to Professor G.D. Rochester, F.R.S., for the provision of facilities for this work and for his continued support.

He is indebted to his Supervisor, Professor A.W. Wolfendale for his advice and guidance at all stages of the work and Dr. M.G. Thompson is thanked for his co-operation and help at all times.

The valuable discussions with Professor J.F. de Beer and Dr. J. Wdowczyk are acknowledged with gratitude, as are those with past and present members of the Durham Cosmic Ray Group, in particular Mr. M.J.L. Turner.

The Durham Computing Unit and the Atlas Computer Laboratory, Chilton are thanked for the provision of facilities.

Mrs. P. Brooke is thanked for her typing of this thesis.

The author is indebted to the Science Research Council for the provision of a Research Studentship during the period of this work.

REFERENCES

ABRAHAM, F., KIDD, J., KOSHIBA, M., LEVI-SETTI, R., TSAO, C.H., WOLTER, W., 1963, Nuovo Cim., 28, 221.

ABROSIMOV, A.T., BASILEVSKAYA, G.A., SOLOV'EVA, V.I., KHRISTIANSEN, G.B., 1960, Zh. Eksper. Teor. Fiz., 38, 100.

ABROSIMOV, A.T., GORIUNOV, N.N., DMITRIEV, V.A., SOLOV'EVA, V.I., KHRENOV, B.A., KHRISTIANSEN, G.B., 1958, Zh. Eksper. Teor. Fiz., 34, 1077.

ADCOCK, C., ODA, H., WOLFENDALE, A.W., 1967, Proc. Int. Conf. on Cosmic Rays, Calgary, E.A.S. 50.

AKASHI, M. et al. (Japanese and Brazilian Emulsion Groups), 1966, Proc. Int. Conf. on Cosmic Rays, London, 1965, 2, 835.

ALEXANDER, D., HOLYOAK, B., THOMPSON, M.G., TURNER, M.J.L., 1967, Proc. Int. Conf. on Cosmic Rays, Calgary, E.A.S. 77.

ALLEN, J.E., 1961, Ph.D. Thesis, Univ. of Durham.

ALY, H.H., DUTHIE, J.G.M., FISHER, C.M., 1959, Phil. Mag., 4, 993.

ALY, H.H., DUTHIE, J.G.M., KADDOURA, A., PERKINS, D.H., FOWLER, P.H., 1960, Proc. Rochester Conf. on High Energy Physics, 829.

ALY, H.H., KAPLON, M.F., SHEN, M.L., 1964, Nuovo Cim., 32, 905.

ANDERSON, C.D. and NEDDERMEYER, S.H., 1936, Phys. Rev., 50, 263.

ASHTON, F., COATS, R.B., HOLYOAK, B., SIMPSON, D.A., THOMPSON, M.G., 1965, Nuc. Inst. and Methods, 37, 181.

ASHTON, F., KAMIYA, Y., MACKEOWN, P.K., OSBORNE, J.L., PATTISON, J.B.M., RAMANA MURTHY, P.V., WOLFENDALE, A.W., 1966, Proc. Phys. Soc., 87, 79.

ASHTON, F., KISDNASWAMY, S., WOLFENDALE, A.W., 1958, Nuovo Cim., 8, 615.

AWUNOR-RENNOR, E.R.T., BLASKOVITCH, L., FRENCH, B.R., GHESQUIERE, C., DE MINVIELLE-DEVAUX, I.B., NEALE, W.W., PELLETIER, C., RIVET, P., SAHIAR, A.B., SKILLICORN, I.O., 1960, Nuovo Cim., 17, 134.

BARNAVELI, T.T., BIBILASHVILI, M.F., GRUBELASHVILI, G.A., DZHAVNSHVILI, A.K., KAZAROV, R.V., KHALDEEVA, I.V., 1964, Izv. Akad. Nauk. SSSR Ser. Fiz., 28, 1782.

DE BEER, J.F., HOLYOAK, B., WDOWCZYK, J., WOLFENDALE,A.W., 1966, Proc. Phys. Soc., 89, 567.

DE BEER, J.F., HOLYOAK, B., ODA, H., WDOWCZYK, J., WOLFENDALE, A.W., 1967a, Proc. Int. Conf. on Cosmic Rays, Calgary, E.A.S. 51.

DE BEER, J.F., HOLYOAK, B., ODA, H., WDOWCZYK, J., WOLFENDALE, A.W., 1967b, Proc. Int. Conf. on Cosmic Rays, Calgary, H.E. 45.

BENNETT, S.K. and GREISEN, K., 1961, Phys. Rev., 124, 1982.

BLUE, M.H., LORD, J.J., PARKS, J.G., TSAO, C.H., 1960, Nuovo Cim., 20, 274.

BOZOKI, G., FENYVES, E., JANOSSY, L., 1962, Nucl. Phys., 33, 236.

BRADT, H., LA POINTE, M., RAPPAPORT, S., 1966, Proc. Int. Conf. on Cosmic Rays, London, 1965, 2, 651.

BRADT, H. and RAPPAPORT, S., 1967, Proc. Int. Conf. on Cosmic Rays, Calgary, E.A.S. 41.

BRINI, D., PELI, L., RIMONDO, O., VERONESI, P., 1955, Nuovo Cim. (Suppl. 2), 1048.

BRISBOUT, F.A., GAULD, C.F., LEHANE, J., McCUSKER, C.B.A., MALOS, J., NISHIKAWA, K., VAN LOON, L.G., 1961, Nucl. Phys., 26, 634.

BROOKE, G., HAYMAN, P.J., KAMIYA, Y., WOLFENDALE, A.W., 1964, Proc. Phys. Soc., 83, 853.

CHATTERJEE, B.K., MURTHY, G.T., NARANAN, S., SREEKANTAN, B.V., SRINIVASA RAO, M.V., TONWAR, S.C., VATCH, R.H., 1966, Proc. Int. Conf. on Cosmic Rays, London, 1965, 2, 627.

CIOK, P., DANYSZ, M., GIERULA, J., JURAK, A., MIESOWICZ, M., PERNEGR, J., 1957, Nuovo Cim., 6, 1409.

COCCONI, G., 1961, Int. Conf. on Theoretical Aspects of Very High Energy Phenomena (Geneva: CERN), 128.

COCCONI, G., KOESTER, L.G., PERKINS, D.H., 1961, Lawrence Radiation Laboratory High Energy Physics Study Seminars, no. 28, part 2, UCID-1444, pp. 1-36.

CONVERSI, M. and GOZZINI, A., 1955, Nuovo Cim., 2, 189.

COWSIK, R., 1966, Proc. Int. Conf. on Cosmic Rays, London, 1965, 2, 656.

COXELL, H. and WOLFENDALE, A.W., 1960, Proc. Phys. Soc., 75, 378.

CRAWFORD, D.F. and MESSEL, H., 1965, Nucl. Phys., 61, no.1, 145.

VON DARDEL, G., 1962, CERN Internal Report NP62-17.

DEBENEDETTI, A., GARELLI, C.M., TALLONE, E., VIGONE, M., 1956, Nuovo Cim., 4, 1142.

DEDENKO, L.G., 1964, Soviet Physics-JETP, 19, No. 5, 1251.

DEDENKO, L.G., ZATSEPIN, G.T., 1959, Proc. Int. Conf. on Cosmic Rays, Moscow, 1959, 2, 201.

DOBROTIN, N.A., GUSEVA, V.V., KOTELNIKOV, K.A., LEBEDEV,A.M., RYABIKOV, S.V., SLAVATINSKY, S.A., ZELEVINSKAYA,N.G., 1962, J. Phys. Soc. Japan (Suppl. AIII), 17, 395.

EARL, J.A., 1959, M.I.T. Tech. Rep. no.70, 1-90.

EARNSHAW, J.C., ORFORD, K.J., ROCHESTER, G.D., SOMOGYI, A.J., TURVER, K.E., WALTON, A.B., 1967, Proc.Phys.Soc., 90, 91.

EDWARDS, B., 1958, Phil. Mag., 3, 237.

ERLYKIN, A.D., KULICHENKO, A.K., NAM, R.A., NIKOLSKII, S.I., YAKOVLEV, V.I., 1967, Proc. Int. Conf. on Cosmic Rays, Calgary, H.E. 27.

FOWLER, G.N., 1967, Private Communication.

FOWLER, P.H. and PERKINS, D.H., 1964, Proc.Roy.Soc., A278, 401.

FUJIOKA, G., 1961, J. Phys. Soc. Japan, 16, 1107.

GARDENER, M., KISDNASWAMY, S., RÖSSLE, E., WOLFENDALE, A.W., 1957, Proc. Phys. Soc., 70, 687.

GARWIN, R.L., 1952, Rev. Sci. Inst., 23, 755.

GAWIN, J., HIBNER, J., WDOWCZYK, J., ZAWADSKI, A., MAZE, R., 1966, Proc. Int. Conf. on Cosmic Rays, London, 1965, 2, 639.

GIERULA, J., 1967, Private Communication.

GINZBURG, V.L. and SYROVATSKY, S.I., 1964, The Origin of Cosmic Rays (Oxford: Pergamon Press).

GOODY, R.M., 1954, The Physics of the Stratosphere (Cambridge University Press).

GOULD, R.J. and SCHREDER, G., 1966, Phys. Rev. Letts., 16, 252.

GREISEN, K., 1960, Ann. Rev. Nuc. Sci., 10, 63.

GREISEN, K., 1966, Phys. Rev. Lett., 16, 748.

GRIGOROV, N.L., SOBINYAKOV, V.A., TRETYAKOVA, Ch.A., SHESTEPEROV, V.Yu., BABIAN, Ch.P., DULYAN, G.G., 1966a, Proc. Int. Conf. on Cosmic Rays, London, 1965, 2, 860.

GRIGOROV, N.L., SHESTEPEROV, V.Yu., BRIKKER, S.I., PODGURSKAYA, A.V., POPERYEKOVA, L.M., PLEKHOVA, A.I., SAVELYEVA, A.I., SOBINYAKOV, V.A., 1966b, Proc. Int. Conf. on Cosmic Rays, London, 1965, 2, 851.

GROTE, L.C., KRECKER, U., KUNDT, U., LANIUS, K., MANSKE, G., MEIER, H.W., 1961, Nuc. Phys., 24, 300.

HANSEN, L. and FRETTER, W., 1960, Phys. Rev., 118, 812.

HASEGAWA, H., NARANAN, S., MATANO, T., MIURA, I., ODA, M., TANAHASHI, G., TANAKA, Y., 1962, Proc. Int. Conf. on Cosmic Rays, Kyoto, 1961.

HASEGAWA, H., NOMA, M., SUGA, K., TOYODA, Y., 1966, Proc. Int. Conf. on Cosmic Rays, London, 1965, 2 642.

HASEGAWA, S., 1959, Nuovo Cim., 14, 909.

HILLAS, A.M., 1966, Proc. Int. Conf. on Cosmic Rays, London, 1965, 2, 758.

HILLAS, A.M., 1967, Phys. Lett., 24a, no. 12, 677.

HOLYOAK, B., THOMPSON, M.G., WDOWCZYK, J., 1966, Proc. Int. Conf. on Cosmic Rays, London, 1965, 2, 754.

HUGGETT, R.W., 1966, Proc. Int. Conf. on Cosmic Rays, London, 1965, 2, 898.

I.C.E.F., 1963, Nuovo Cim. (Suppl. 1), 1, 1039.

IMAEDA, K., 1967, to be published in Nuovo Cimento.

KAZUNO, M., 1962, Nuovo Cim., 24, 1013.

KHRENOV, B.A., 1965, Soviet J. Nucl. Phys., 1, 540.

KHRISTIANSEN, G.B., ATRASHKEVITCH, V.B., KALMYKOV, N.N., FOMIN, Yu.A., 1966, Proc. Int. Conf. on Cosmic Rays, London, 1965, 2, 774.

KOSHIBA, M., NOZAKI, T., TOTSUKA, Y., YAMADA, S., 1967, Proc. Int. Conf. on Cosmic Rays, Calgary, H.E.11.

LAL, S., PAL, Y., RAGHAVEN, R., SREEKANTAN, B.V., SUBRAMANIAN, A., VERMA, S.D., 1962, Proc. Int. Conf. on Cosmic Rays, Kyoto, 1961, 3, 390.

LEHANE, J.A., MILLAR, D.D., RATHBERGER, M.H., 1958, Nature, 182, 1699.

LINDENBAUM, S.J. and STERNHEIMER, R.M., 1962, Brookhaven Rep. BNL772 (T290), 32.

VON LINDERN, 1961, Ph.D. Thesis, Ludwigs Maximilians University.

LINSLEY, J., 1964, Proc. Int. Conf. on Cosmic Rays, Jaipur, 1963, 4, 77.

LLOYD, J.L., 1960, Proc. Phys. Soc., 75, 387.

LOHRMAN, E., TEUCHER, H.W., SCHEIN, H., 1961, Phys.Rev., 122, 672.

LUKIN, Yu.T., TAKIBAEV, Zh.S., SHALAGINA, E.V., 1960, Zh. Eksper. Teor. Fiz., 38, 1074.

MacKEOWN, P.K., SAID, S.S., WDOWCZYK, J., WOLFENDALE, A.W., 1966, Proc. Int. Conf. on Cosmic Rays, London, 1965, 2, 964.

MALHOTRA, P.K., 1964, Nucl. Phys. (Netherlands), 59, 551.

MALHOTRA, P.K., SHUKLA, P.G., STEPHENS, S.A., VIJAYALAKSHMI, B., BOUET, J., BOWLER, M.G., CLAPHAM, V.M., FOWLER, P.H., HACKFORTH, H.L., KEEREETAVEEP, J., TOVEY, S.N., 1966, Proc. Int. Conf. on Cosmic Rays, London, 1965, 2, 840.

MATANO, T., MIURA, I., NAGANO, M., SHIBATA, S., HASEGAWA, H., 1966, Proc. Int. Conf. on Cosmic Rays, London, 1965, 2, 637.

MATHIESEN, O., LONG, C.E., FREIER, P.S., WADDINGTON, C.J., 1967, Univ. of Minnesota Tech. Rep. CR100. Proc. Int. Conf. on Cosmic Rays, Calgary, O.G. 56.

MINAKAWA, O., NISHIMURA, Y., TSUZUKUI, M., YAMANOUCHI, H., AIZU, H., HASEGAWA, H., ISHII, Y., TOKUNAGA, S., FUJIMOTO, Y., HASEGAWA, H., NISHIMURA, J., NIU, K., NISHIKAWA, K., IMAEDA, K., KAZUNO, M., 1959, Nuovo Cim. (Suppl. 1), 11, 125.

MIYAKE, S., HINOTANI, K., ITO, N., KINO, S., SASAKI, H., HOSHII, H., 1966, Proc. Int. Conf. on Cosmic Rays, London, 1965, 2, 664.

MIYAKE, S., HINOTANI, K., KANEKO, T., ITO, N., 1963, J. Phys. Soc. Japan, 18, 465.

NIKOKSKII, S.I., 1963, Usp. Fiz. Nauk., 78, 365.

NISHIKAWA, K., 1959, J. Phys. Soc. Japan, 14, 879.

OSBORNE, J.L., 1966, Ph.D. Thesis, Univ. of Durham.

PAL, Y. and PETERS, B., 1964, K. Danske Vidensk. Selsk. Mat.-Fys. Medd. (Denmark), 33, No. 15, 54.

PARKER, T.L., 1967, Ph.D. Thesis, Univ. of Utah.

PENZIAS, A.A. and WILSON, R.W., 1965, Astrophys. J., 142, 419.

PETERS, B., 1962, Proc. Conf. High Energy Phys. (CERN), 623.

PORTER, N.A., CRANSHAW, T.E., GALBRAITH, W., 1957, Phil. Mag., 2, 900.

RAJOPADHYE, V.Y., 1960, Phil. Mag., 5, 537.

ROCHESTER, G.D., SOMOGYI, A.J., TURVER, K.E., WALTON, A.B., 1966, Proc. Int. Conf. on Cosmic Rays, London, 1965, 2, 765.

ROSSI, B., 1932, Nature, 130, 699.

SCHEIN, M., HASKIN, E.M., LOHRMAN, E., TEUCHER, M.W., 1959, Phys. Rev., 116, 1238.

SEKIDO, Y., KONDO, I., MURAYAMA, T., OKUDA, H., SAKAKIBARA, S., FUJIMOTO, K., 1966, Proc. Int. Conf. on Cosmic Rays, London, 1965, 2, 632.

SHIBATA, S., NAGANO, M., MATANO, T., SUGA, K., HASEGAWA, H., 1966, Proc. Int. Conf. on Cosmic Rays, London, 1965, 2, 672.

SMORODIN, Yu.A., 1967, Soviet Physics-JETP, 24, No.2, 290.

STREET, J.C. and STEVENSON, E.C., 1937, Phys.Rev., 52, 1003.

THIELHEIM, K.O. and KARIUS, S., 1966, Proc. Int. Conf. on Cosmic Rays, London, 1965, 2, 779.

TOMASZEWSKI, A., MICHALAK, W., SROKA, J., 1966, Nuovo Cim., 46, 760.

TOYADA, Y., SUGA, K., MURAKAMI, K., HASEGAWA, H., SHIBATA, S., DOMINGO, V., ESCOBAR, I., BRADT, H., CLARK, G., LA POINTE, M., 1966, Proc. Int. Conf. on Cosmic Rays, London, 1965, 2, 708.

UDGAONKAR, B.M. and GELL MANN, M., 1962, Phys. Rev. Letts., 8, 346.

VERNOV, S.N., KHRISTIANSEN, G.B., ABROSIMOV, A.I., BELYAEVA, I.F., DMITRIEV, V.A., KULIKOV, G.V., NETCHIN, Yu.A., SOLOV'EVA, V.I., KHRENOV, B.A., 1966, Proc, Int. Conf. on Cosmic Rays, London, 1965, 2, 769.

VERNOV, S.N., KHRISTIANSEN, G.B., ABROSIMOV, A.T., ATRASKEVITCH, V.B., BELYAEVA, I.F., VEDEENEV, O.V., KULIKOV, G.V., NETCHIN, Yu.A., SOLOV'EVA, V.I., FOMIN, Yu.A., KHRENOV, B.A., 1964, Izv. Akad.Nauk SSSR Ser. Fiz., 28, 1774.

VERNOV, S.N., LY-DON-KHVA, KHRENOV, B.A., KHRISTIANSEN, G.B., 1962, J. Phys. Soc. Japan (Suppl. AIII), 213.

WADDINGTON, C.J., 1960, Phil. Mag., 5, 311.

WALKER, W.D., WALKER, S.P., GREISEN, K., 1950, Phys. Rev., 80, 546.

WDOWCZYK, J., 1966, Proc. Int. Conf. on Cosmic Rays, London, 1965, 2, 691.

WILLIAMS, R.W., 1960, Nuovo Cim., 16, 762.

APPENDIX A

Properties of the Cosmic Ray Flux

i) The properties of the elementary particles

	Rest Energy MeV	Mean lifetime seconds
n	939.550 ± 0.005	$(1.01 \pm 0.3)\ 10^{3}$
p	938.256 ± 0.005	stable
$\pi^{\pm}$	139.580 ± 0.015	$(2.551 \pm 0.026)10^{-8}$
π^{o}	134.974 ± 0.015	$(1.78 \pm 0.26)\ 10^{1-6}$
$\mu^{\pm}$	105.659 ± 0.002	$(2.2001 \pm 0.0008)10^{-6}$
$e^{\pm}$	0.511006±0.000002	stable

ii) The relevant decay schemes

Decay mode	Relative abundance of alternative decay modes
$\pi^{+} \rightarrow \mu^{+} + \nu_{\mu}$	$1 - 10^{-4}$
$\rightarrow e^{+} + \nu_{e}$	10^{-4}
$\pi^{-} \rightarrow \mu^{-} + \overline{\nu_{\mu}}$	
$\pi^{o} \rightarrow 2\gamma$	98.8%
$\rightarrow \gamma + e^{+} + e^{-}$	1.2%
$\rightarrow 2e^{+} + 2e^{-}$	0.004%
$\mu^{\pm} \rightarrow e^{\pm} + \nu + \overline{\nu}$	

APPENDIX B

The Atmosphere

The atmosphere may be divided into two layers, the stratosphere and the troposphere, the boundary between these being known as the tropopause. From sea-level to the tropopause atmospheric temperature increases with height, above the tropopause, that is, in the stratosphere, the temperature remains at a constant value.

The relationships between pressure, x, density, ρ, and altitude, h, are derived below. Subscript 't' refers to values at the tropopause and 'o' to those at sea-level.

The density of the atmosphere at depth x $g.cm^{-2}$ is given by:-

$$\rho(x) = \frac{x\ g}{R\ T(h)}\ g.cm^{-3} \qquad (B1)$$

where T(h) is the absolute temperature at h kms. and the gas constant, $R = 2.888\ 10^6$ erg. $^oK^{-1}$ $g.cm^{-1}$.

We also have the relationship:-

$$dx = \rho\ dh\ \ g.cm^{-2} \qquad (B2)$$

Combining B1 and B2 and integrating

$$\frac{x}{x_o} = \exp\left[\frac{-g}{R}\int_o^h \frac{dh}{t(h)}\right] \qquad (B3)$$

For the tropopause, i.e. $x > x_t$, $T(h) = T_o - \Gamma h$, where Γ is the lapse rate; B3 becomes:-

$$x = x_o \left[1 - \frac{\Gamma h}{T_o}\right]^{g/\Gamma R} \qquad (B4)$$

For the stratosphere i.e. $x \leqslant x_t$, $T(h) = T_t$

$$x = x_t \exp\left[\frac{-g}{RT_t}(h-h_t)\right] \qquad (B5)$$

Goody (1954) gives the following values at the latitude of Durham (55°N)

$h_t = 10.3$ km

$T_t = 219^oK$

$T_o = 282^oK$

thus, $\Gamma = 6.078\ ^oK/km$

$x_o = 1034\ g.cm^{-2}$

Substitution in B2, B4, B5, gives:-

tropopause $x_t = 253.3\ g.cm^{-2}$

troposphere $x = 1034\ (1-0.02156\ h)^{5.587}\ g.cm^{-2}$ (B6)

$(h)x = 46.380-13.398\ x^{0.179}$ kms (B7)

$\rho(x) = 4.170\ 10^{-6}\ x^{0.821}\ g.cm^{-3}$ (B8)

stratosphere $x = 253.3\ \exp(-0.1549(h-10.3))\ g.cm^{-2}$ (B9)

$h(x) = 46.040-6.4576\ \ln(x)$ kms. (B10)

$\rho(x) = 1.548\ 10^{-6}x\ g.cm^{-3}$ (B11)

The preceeding statements are true for a vertical section through the atmosphere. Suppose that the depth in $g.cm^{-2}$ of point C in Figure B1 is known and the inclined height from C to the point of observation, $h(\theta)$, is required. Then equation (B7) or (B10) will give $h(x_v)$, the equivalent vertical height and $h(\theta)$ may be derived as follows.

The cosine rule on triangle ABC of Figure B1 gives:-

$$\left[R_E + h(x_v)\right]^2 = \left[h(\theta)\right]^2 + \left[R_E\right]^2 + 2h(\theta)R_E \cos\theta$$

$$\therefore \quad h(\theta) = -R_E\cos\theta + \left\{\left[R_E\cos\theta\right]^2 - \left[R_E\right]^2 + \left[R_E + h(x_v)\right]^2\right\}^{\frac{1}{2}} \qquad (B12)$$

where $R_E = 6370$ km.

$$\sec\theta^* = \left[1 - \frac{\sin^2\theta}{(1+h(x_v)/R_E)^2}\right]^{-\frac{1}{2}} \qquad (B13)$$

Figure B2 shows the height above sea-level (along the trajectory) as a function of equivalent vertical height for various zenith angles. The inclined depth is plotted as a function of equivalent vertical depth in Figure B3a and Figure B3b shows the relationship between vertical height and depth in the atmosphere at $\theta = 0^\circ$.

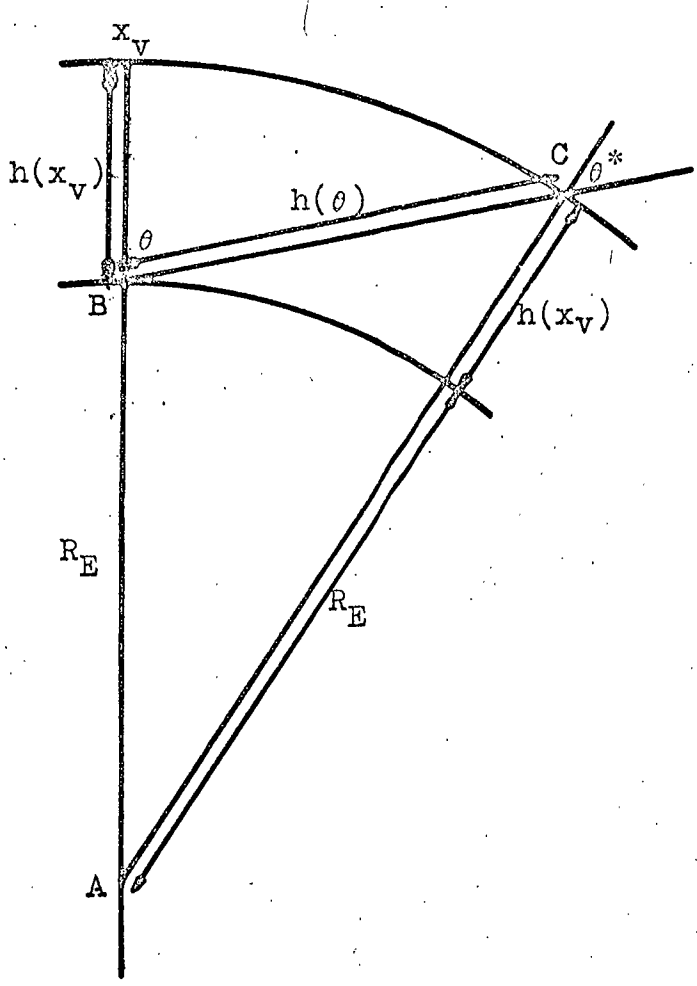

Figure B.1.

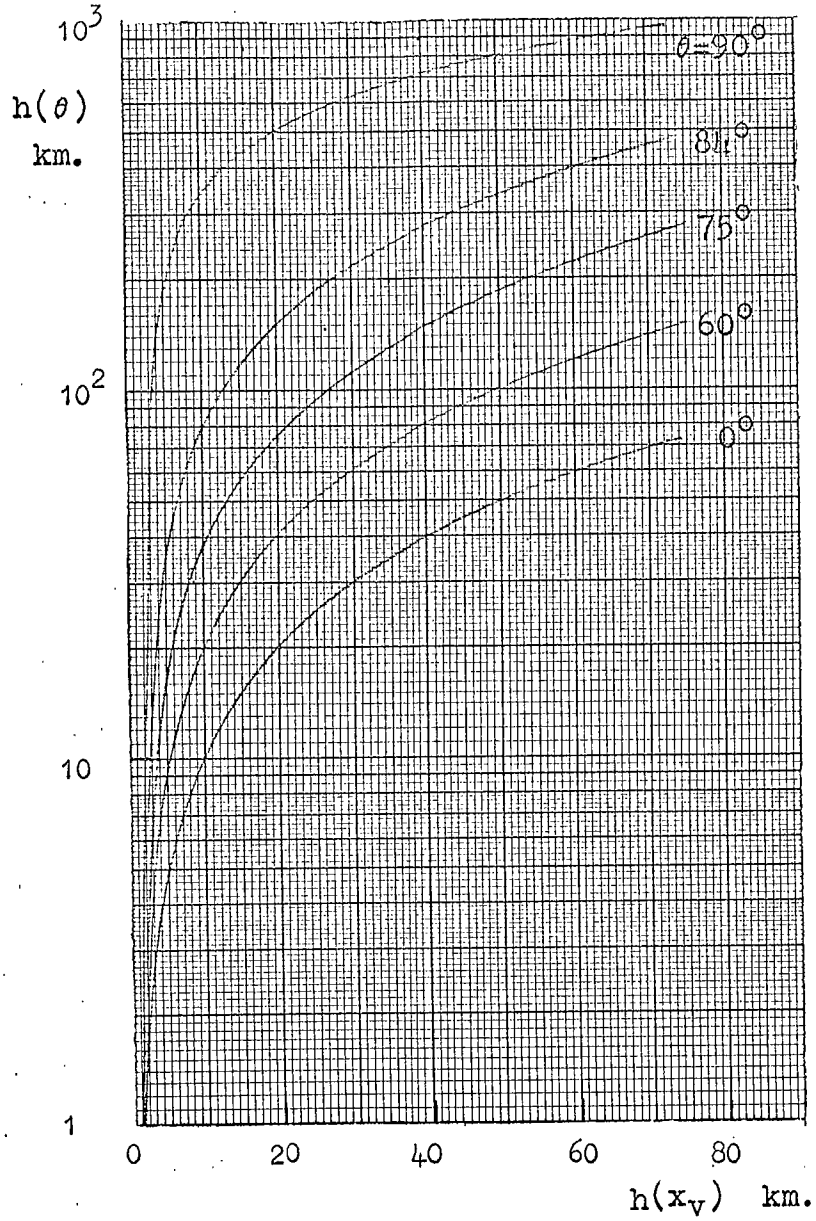

Fig. B.2 Inclined height above sea-level as a function of equivalent vertical height.

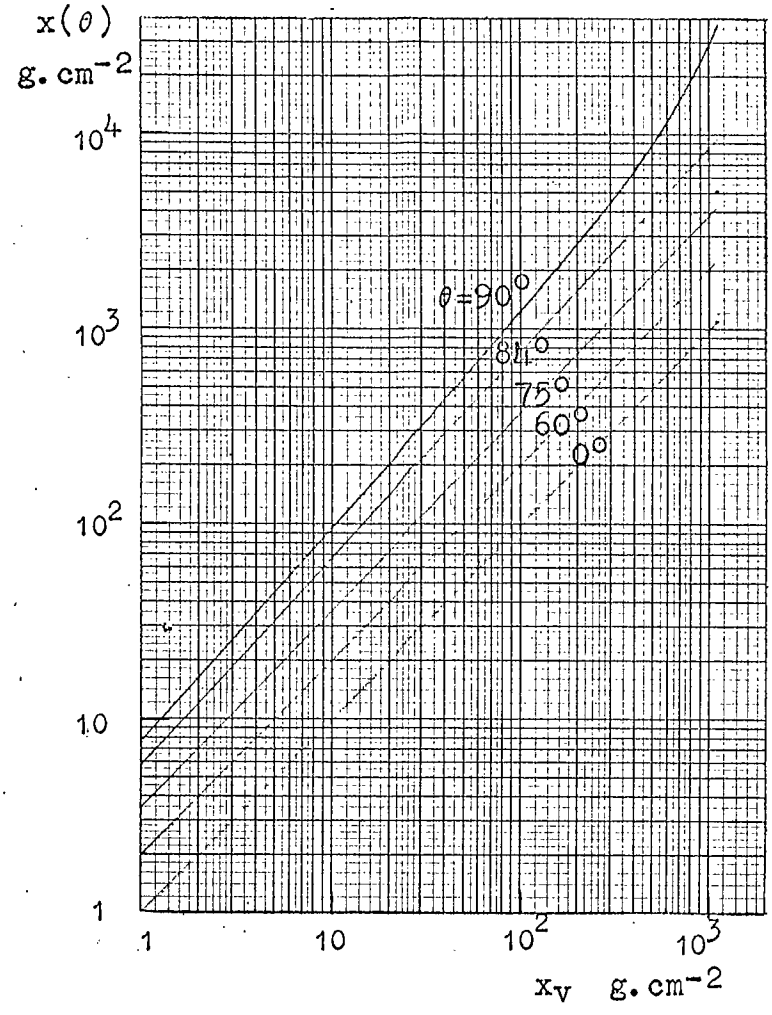

Figure B.3a.

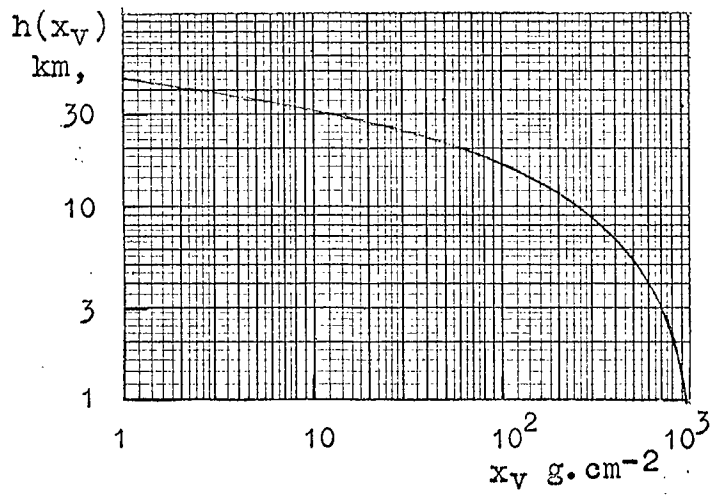

Figure B.3b.

APPENDIX C

Analytical Method of Calculation

The following diffusion equations are taken as the starting of the calculations.

$$\frac{\partial \Pi(E,x)}{\partial x} = -\left\{1 + \frac{B}{E(x+x_o)}\right\}\Pi(E,x) + \int_E^\infty S(E',E)\Pi(E',x)dE' \quad (C1)$$

This equation describes the pion cascades due to the interaction of the primary at depth x_o; it is solved using the method of successive generations.

The equations for successive generations, obtained from C1 are:-

$$\frac{\partial \Pi_1(E,x)}{\partial x} = -\left\{1 + \frac{B}{E(x+x_o)}\right\}\Pi_1(E,x)$$

$$\frac{\partial \Pi_n(E,x)}{\partial x} = -\left\{1 + \frac{B}{E(x+x_o)}\right\}\Pi_n(E,x) + \int_E^\infty S(E',E)\Pi_{n-1}(E',x)dE' \quad (C2)$$

for $n = 2,3,4, \ldots\ldots$

It is assumed that the shape of the distribution in depth of interaction of pions of a given generation is independent of energy. The reduction in the number of pions available for interaction, due to decay, is taken into account. In order to simplify the calculations, the muons are considered to originate at $\lambda_\pi/2$ below the depth at which the parent pion was produced.

Under these assumptions the function $\Pi_{n-1}(E',x)$ in equation C2 becomes

$$\Pi_{n-1}(E')\ P_{n-1}(E')\ f_{n-1}(x)$$

where $\Pi_{n-1}(E')$ is the energy spectrum of pions of the $(n-1)^{th}$ generation, $f(x)$ is their distribution in depth, neglecting decay, $P(E)$ is their interaction probability as a function of energy.

This simplification makes it possible to solve equation C2, as follows:-

$$\Pi_1(E,x) = \Pi(E,0)\left\{\frac{x+x_o}{x_o}\right\}^{-B/E} e^{-x}$$

$$\Pi_n(E,x) = \Pi_n(E)\left\{\frac{(x+x_o)^{n-1}}{n-1+B/E} - \binom{n-2}{1}\frac{(x+x_o)^{n-2}}{n-2+B/E}\,x_o + \cdots\cdots\right.$$

$$\left. + \frac{(-1)^{n-2}\binom{n-2}{n-2}x_o^{n-2}\,\frac{x+x_o}{1+B/E}}{} + \frac{(-1)^{n-1}\,(n-2)!\;x_o^{B/E+n-1}(x+x_o)^{-B/E}}{(n-1+B/E)\ \cdots\cdots\cdots\ (1+B/E)}\right\}\frac{e^{-x}}{(n-2)!} \qquad (C3)$$

for $n \geqslant 2$.

where
$$\Pi_n(E) = \int_E^\infty P(E')S(E',E)\Pi_{n-1}(E')dE' \qquad (C4)$$

$\mu(E,x)$, which represents the number of muons produced at a certain depth x from pions of energy E, is given by:-

$$\mu(E,x) = \frac{B\sum\Pi_n(E,x)}{E(x+x_o)} \qquad (C5)$$

Using this function the total number of muons arriving at sea-level is calculated from the following expression.

$$N\mu(E>E_t) = \int_{E_t}^{\infty} \int_{o}^{x_s} \mu(E,x)\ SP(E,E_t,x)\ dx\ dE \qquad (C6)$$

where $SP(E,E_t,\ x)$ gives the probability that a muon produced at depth x by a pion of energy E will arrive at sea-level with energy greater than E_t.

This function $SP(E,E_t,x)$ is calculated taking into account muon energy losses and their energy distribution resulting from π-μ decay.

The expression for the mean distance of muons from the axis is:-

$$\bar{r} = \frac{1}{N\mu(E>E_t)} \int_{E_t}^{\infty} \int_{o}^{x_s} \mu(E,x) SP(E,E_t,x) r_1(E,x) dr\ dE \qquad (C7)$$

where $r_1(E,x)$ represents the mean distance at which a muon with parameters E and x reaches sea-level.

APPENDIX D

Coulomb Scattering

From Figure D1 we have

$$\overline{\langle y_s^2 \rangle} = \overline{\phi^2}\, h(\theta)^2 + \frac{\overline{\phi^2}}{3} \Delta h^2 \qquad (D1)$$

For spatial angle of scattering, ϕ,

$$\overline{\phi^2} = \frac{(0.021)^2}{E_\mu^2} \frac{\Delta x}{X_o} \qquad (D2)$$

where E_μ is in GeV, Δx in $g.cm^{-2}$ and X_o is the radiation length for air in $g.cm^{-2}$.

Substituting $\Delta x = 12$ $g.cm^{-2}$ and $X_o = 37.7$ $g.cm^{-2}$ in equation D2

$$\overline{\phi^2} = \frac{1.403\ 10^{-4}}{E_\mu^2} \qquad (D3)$$

Thus D1 becomes

$$\overline{\langle y_s^2 \rangle}_{12} = \frac{1.403\ 10^{-4}}{E_\mu^2} \left[h(\theta)^2 + \frac{\Delta h^2}{3} \right] \qquad (D4)$$

If Δx in $g.cm^{-2}$ and $\rho(x)$ in $g.cm^{-3}$ then

$$\Delta h = \frac{\Delta x}{\rho(x)} \text{ cm} \qquad (D5)$$

$$\text{or} \quad \Delta h = \frac{\Delta x\ 10^{-2}}{\rho(x)} \text{ m} \qquad (D6)$$

Therefore

$$\overline{\langle y_s^2 \rangle}_{12} = \frac{1.403\ 10^{-4}}{E_\mu^2} \left[h(\theta)^2 + \tfrac{1}{3}\left\{\frac{0.12}{\rho(x)}\right\}^2 \right] \qquad (D7)$$

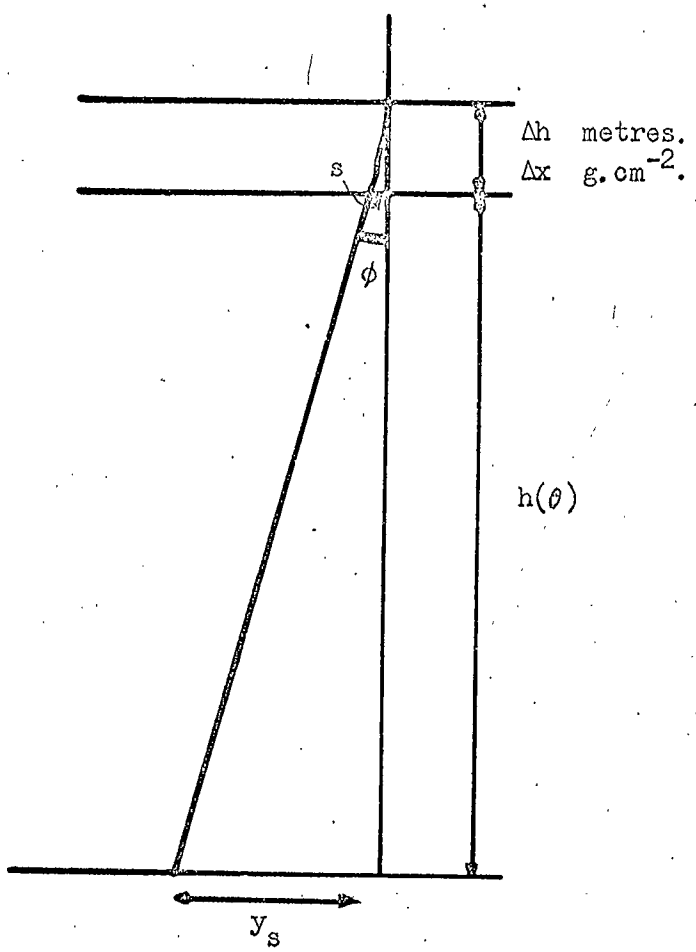

Figure D.1.

The factor $\frac{1}{3}$ in the second term of (D1) occurs because ϕ is the angle of the particle trajectory on leaving cell relative to trajectory on entry, and it is not the mean angle which is required in this calculation.

Table D1

The root mean square value of scattering (σ_o)

i) $E_\mu \approx 1$ GeV at sea-level

Depth of muon production g.cm^{-2}	σ_o metres $\theta = 60^\circ$	75°	84°
2060	8.71	$4.12\ 10^2$	$9.85\ 10^2$
1580	$1.24\ 10^2$	$5.10\ 10^2$	$1.05\ 10^3$
1100	$2.50\ 10^2$	$6.13\ 10^2$	$1.13\ 10^3$
620	$3.86\ 10^2$	$7.30\ 10^2$	$1.22\ 10^3$
140	$5.83\ 10^2$	$9.08\ 10^2$	$1.36\ 10^3$

ii) $\theta = 75^\circ$ Depth of production = 620 g.cm^{-2}

E_μ at production GeV	σ_o metres
8.69	$7.30\ 10^2$
10.2	$6.02\ 10^2$
12.6	$4.59\ 10^2$
17.0	$3.21\ 10^2$
41.7	$1.20\ 10^2$
264	1.82 10

The probability of a particle which would have fallen in the shaded area of Figure D2a without scattering arriving in unit area at the centre when scattering is included, is given by:-

$$F(r)dr = G(x)dx\ G(y)dy \qquad (D8)$$

where $x^2 + y^2 = r^2$.

Referring to Figures D2b and D2c which show the Gaussian distributions in the xz and yz planes formed by the scattered particles; equation (D8) may be rewritten as follows

$$F(r)dr = G(x)\,\Delta s\ G(0)\,\Delta t \qquad (D9)$$

$\Delta s . \Delta t = 1$

$$\therefore \qquad F(r)dr = G(x)\ G(0) \qquad (D10)$$

Now,

$$G(x) = \frac{1}{\sigma\sqrt{2\pi}} \exp\left(\frac{-x^2}{2\sigma^2}\right) \qquad (D11)$$

If $\sigma_o = \sigma\sqrt{2}$ is the root mean square value for spatial distribution, then,

$$G(x) = \frac{1}{\sigma_o\sqrt{\pi}} \exp\left(\frac{-x^2}{\sigma_o^2}\right) \qquad (D12)$$

and

$$G(0) = \frac{1}{\sigma_o\sqrt{\pi}} \qquad (D13)$$

$\therefore$ The probability of one particle which would have fallen in the annulus, arriving on unit area at centre when scattered is,

$$F(r)dr = \frac{1}{\pi\sigma_o^2} \exp\left(\frac{-r^2}{\sigma_o^2}\right) \qquad \text{(D14)}$$

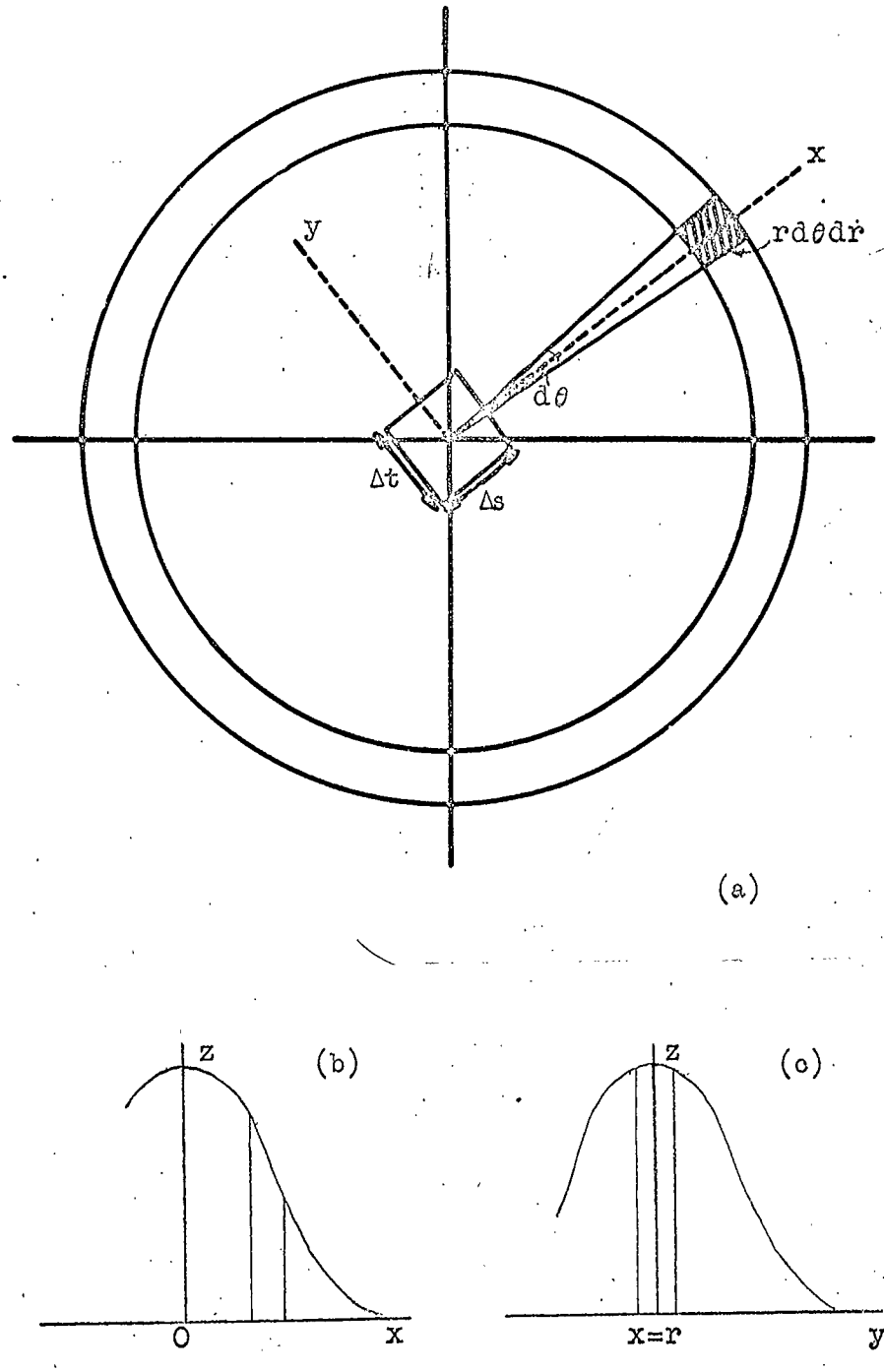

Figure D.2.

APPENDIX E

Geomagnetic Deflection

From Figure E1,

$$y_m = \alpha . h(\theta) \qquad (E1)$$

and $$\alpha = \frac{\Delta h}{R} \qquad (E2)$$

where R is the radius of curvature of the muon trajectory in the earth's magnetic field.

$$R_{(cm)} = \frac{E_\mu(eV)}{B_{(Gauss)}} \frac{1}{300} \qquad (E3)$$

$$\Delta h = \frac{\Delta x}{\rho(x)} \qquad (E4)$$

Substitution of E2, E3 and E4 in E1 gives

$$y_m = h(\theta) \frac{\Delta x}{\rho(x)} \frac{300}{E_\mu} B \qquad (E5)$$

Thus,

$$y_m = \frac{1.8\ 10^{-6}}{\rho(x)\ E_\mu} (h(\theta) + 0.06/\rho(x)) \text{ metres} \qquad (E6)$$

for E_μ in GeV.

The term $0.06/\rho(x)$ is to allow for the fact that Δh is not negligible with respect to $h(\theta)$.

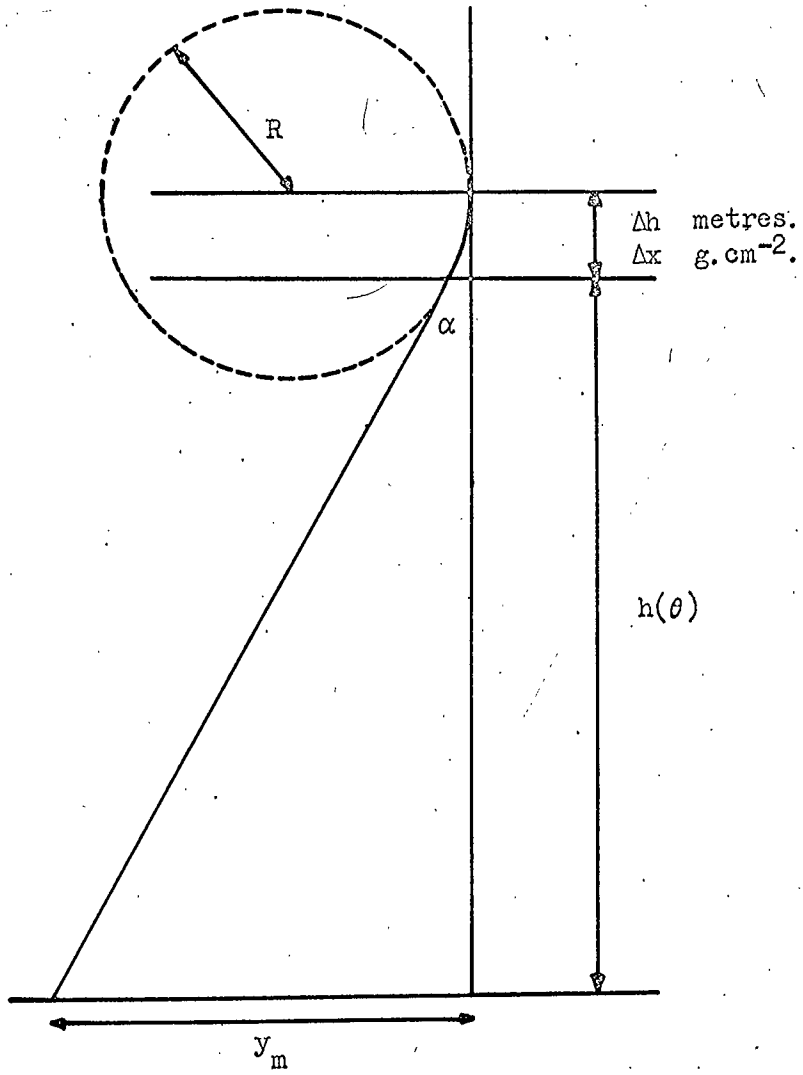

Figure E.1.

Table E1

Geomagnetic displacement at sea-level

i) $E_\mu \approx$ 1 GeV at sea-level

Depth of muon production g.cm^{-2}	Σy_m metres $\theta = 60^\circ$	75°	84°
2060	2.61	$8.08\ 10^2$	$4.76\ 10^3$
1580	$1.11\ 10^2$	$1.25\ 10^3$	$5.80\ 10^3$
1100	$3.64\ 10^2$	$1.90\ 10^3$	$7.36\ 10^3$
620	$8.79\ 10^2$	$3.09\ 10^3$	$1.02\ 10^4$
140	$3.44\ 10^3$	$8.47\ 10^3$	$2.14\ 10^4$

ii) $\theta = 75^\circ$, Depth of production = 620 g.cm^{-2}

E_μ at production GeV	Σy_m metres
8.96	$3.09\ 10^3$
10.2	$2.56\ 10^3$
12.6	$1.96\ 10^3$
17.0	$1.37\ 10^3$
41.7	$5.12\ 10^2$
264	$7.73\ 10^1$